Load Analysis of Ankle Foot Orthoses during Gait

by

Graham Henderson

Bioengineering Unit

University of Strathclyde

Glasgow

2011

This thesis is submitted in partial fulfilment of the requirements of Master of Science in Bioengineering

This thesis is the result of the author's original research. It has been composed by the author and has not been previously submitted for examination which has led to the award of a degree.

Signed: Date:

Abstract

The loads acting on ankle foot orthoses (AFOs) during gait have rarely been quantified. Orthotists prescribe AFOs for a wide range of gait deficiencies that can result from neurological disorders such as stroke, multiple sclerosis and cerebral palsy. Knowledge of the loads acting on an AFO during gait, would be valuable information for an orthotist, as it could help them to more effectively design AFOs that meet individual's biomechanical requirements. Therefore the aim of the thesis was to develop a validated Finite Element (FE) model, which could be used to quantify and analyse the loads acting on an AFO during gait. In this thesis the pressures acting on an AFO worn by a normal subject (with no neurological disorders) during gait, were recorded by two different types of pressure transducers. Pressures were found to be low on the calf section of the AFO in comparison to the foot section. A digital scan of an AFO was taken and inserted into Finite Element Analysis (FEA) software to create an FE model. The pressures and the assumed boundary conditions at toe off, were then inserted into the FE model. The analyses were conducted in an iterative process using different AFO thicknesses, different material properties, linear geometry and non-linear geometry. A validation was conducted, which found the most accurate analysis had an error of 33%. At toe off the total forces in the y-direction (the vertical direction) transmitted by the AFO were shown to be minimal (2.2% of the total forces). At the same point in the gait cycle the moment around the ankle generated by the AFO (in the sagittal plane) was shown to be a 40Nm dorsiflexion moment. Consequently the AFO was not assisting the limb but on the contrary wasting muscle power at toe off. This indicates that an AFO makes it more difficult to walk for a normal subject. Useful clinical data could potentially be found by completing a similar study using a subject with a gait abnormality.

Acknowledgements

I would like to thank my supervisor Stephan Solomondis for all his time, valuable advice and expertise. My gratitude also goes out to my co-supervisor from the DMEM department Nicola Cairns who provided great advice and helped a lot with numerous aspects of the thesis. I would like to thank Enrica Papi for providing data for the validation of the FEA. I also extend my thanks to Stephen Murray who helped to prepare the AFO for the pressure measuring experiments.

I would like to thank Duncan Lindsay for his help with using the DMEM facilities including the digital scanner and Ansys software. From the DMEM department I would also like to thank David Cunningham and Barrie Hunter for their advice. From the mechanical engineering department I would like to thank Magnus Gislason for his advice on the FEA.

The help of Arjan Buis and Daniel Rafferty was very much appreciated who are from the National centre of Prosthetics and Orthotics and the University of Caledonian respectively. The use of their equipment was key to this project.

I would like to thank Roy Bowers from the National centre of Prosthetics and Orthotics for making the AFO that was used in this study.

I am extremely grateful to NHS Lothian who provided funding for my MSc; I would also like to thank David Gow and the team at the SMART centre in Edinburgh for their support.

Finally I would like to thank my subject for being a willing volunteer!

Contents

List of tables

List of figures

Chapter 1. Introduction

1.1. Background

An orthosis is a device that is externally applied to the body and is designed to alter the structural and functional features of the neuromuscular and skeletal systems [**1**]. More precisely an orthosis can support body weight, control joint motion (direction, range and strength) and can change the shape of body tissues [**2**]. A lower limb orthosis is designed to assist gait, reduce pain, decrease weight bearing, control movement and minimise the worsening of a deformity [**3**].

An ankle foot orthosis (AFO) is a particular type of orthosis that fits around an individual's foot and shank, which aims to provide direct control of the motion and alignment of the ankle and foot [**4**]. AFOs can be prescribed to individuals with neurological disorders such as stroke [**5,6,7,8,9**] multiple sclerosis [**5**] and cerebral palsy [**10,11,12,13,14**]. The aim of prescribing an AFO is to minimise gait deviations and to improve functional outcomes [**4**]. This is generally done by improving mediolateral stability during stance phase, increasing toe clearance during the swing phase and promoting heel strike [**15**].

Since 1970 plastics such as polypropylene have superseded metals as the preferred material for constructing AFOs [**16**]; as they are lighter and more cosmetic [**17**]. AFOs can be custom made to fit an individual or they can be prefabricated [**4**].

The design of an AFO is determined by an orthotist's assessment of a patient. To help the orthotist design the AFO efficiently, it would be useful to know and analyse the loads acting on the AFO. If these loads are determined then the percentage of the load acting on the orthosis can be calculated and compared to the load acting on the leg and orthosis. With more precise knowledge of the loads acting on an AFO the orthotist could use the information to design an AFO that met the exact needs of an individual patient. However, several studies [**5,18,19**] have reported that there is very little experimental data about the mechanical characteristics of AFOs available in the scientific literature. Consequently there is currently a lack of information to aid the orthotist in the design of AFOs.

For the orthotist in a clinical practice it would be an inefficient use of time to make an AFO and then subsequently calculate the loads acting on it. This is because the biomechanical characteristics are being found out after the AFO is made and

therefore it is too late to change the design. A computer aided design/finite element analysis system would allow the orthotist to quickly find out the biomechanical requirements for a particular AFO design. They could then adjust the design until the biomechanical characteristics are deemed to be sufficient to improve the patient's functional outcome. After the design has been finalised computationally they could then fabricate the AFO. Using computers to aid orthotists to design AFOs has the potential advantages of increasing the flexibility of the design, improving the speed of production, increasing the consistency of quality and improving standardisation [**20**]. Previous attempts to construct a finite element (FE) model of an AFO have been made [**21,22,23,24**]. However, these studies either do not validate their work or do not validate their work using the exact same AFO as used in their FE models. Therefore the validity of their findings has not been verified.

1.2. Aims and objectives

It would be potentially useful for orthotists to have a better understanding of the loads being applied to an AFO and for them to use AFO FE models to establish design criteria before their fabrication. With this knowledge and considering the limitations of experimental and FE AFO studies to date, the aim of this study was to develop a validated FE model of an AFO which could be used to analyse the loads applied during gait.

This aim was achieved through the following specific objectives:

- Measure the pressures acting on an AFO during normal gait using two pressure measurement systems
- Calculate the position and magnitude of the pressures acting on the AFO using the experimental data
- Make an accurate 3D digital surface model of the AFO and export it into FEA software
- Develop an FEA model of the AFO and predict the stresses, strains and loads acting on the AFO.
- Validate the results of the FEA analysis using experimental strain data
- Analyse the stresses, strains and loads acting on the AFO using the results from the FEA.

1.3. Layout of thesis

Chapter 2 presents a literature review of the gait cycle and gait analysis. In chapter 3 there is a summary of the clinical conditions that can result in gait deviations and might lead to the prescription of an AFO. Chapter 4 reviews the different types of AFOs, their main functions, the materials they are made from and details the biomechanics of AFOs. In chapter 5 there is an overview of FE method and an introduction into the software Ansys (Ansys, USA). Chapter 6 presents a literature review of the loads, both experimental and theoretical that act on AFOs. After chapter 6 the experimental part of the thesis begins. In chapter 7 information about two different pressure measurement experiments is detailed and the results are then analysed and discussed. Chapter 8 explains how the geometry of the AFO was digitally scanned and exported to the FEA software. In chapter 9 information from the two previous chapters is used to develop an FE model. The results are compared to a validation study and iterative steps are taken to improve the accuracy of the analyses. Chapter 10 discusses the results from chapter 9 and also links to the results from chapters 7 and 8. Finally chapter 11 concludes the thesis by summarising what was done, listing the main conclusions and suggesting future work.

Chapter 2. Gait and Gait Analysis Background

2.1. Introduction to gait and gait analysis

Human gait is bipedal and it is a sequence of motions by the lower limbs that provides forwards propulsion. Gait requires interaction between the central nervous system, the peripheral nervous system and the musculoskeletal effector system [**25**]. Muscles are activated and develop tension which generates forces and moments in the lower limbs [**25**].

Gait analysis can be used to study the loads acting on the body during walking and running. It can provide useful information that can assist in the clinical diagnosis of skeletal and muscular abnormalities, and in the assessment of treatment [**26**].

This chapter introduces normal gait and explains the biomechanics that are involved with it. This is important information for orthotists because AFOs are prescribed to minimise gait deviations [**4**] and therefore help the patient to walk with the most efficient biomechanics, which are described in this chapter. During this chapter and subsequent chapters anatomical terms such as planes (for example sagittal) positional terms (for example anterior, posterior etc), movement terms (for example abduction) and the names and positions of muscles and bones will be used, they can all be found and explained in a publication by Whittle [**27**].

2.2. The gait cycle

The following section is referenced from a study by Gage et. al [**28**]. The sequence of motions by the lower limbs that control human gait create a repeating pattern; this is known as the gait cycle. Figure 2-1 shows a schematic of the gait cycle for one leg, whilst this is happening the other leg also follows the same cycle but in a different phase. The gait cycle is split into two major parts; stance phase and swing phase. Stance phase occurs when the foot is in contact with the ground, it happens for approximately 60% of the cycle. There are two periods of approximately 10% of the cycle when both feet are in contact with the ground, which is known as double support. Swing phase results in the foot being clear of the ground and lasts for approximately 40% of the cycle.

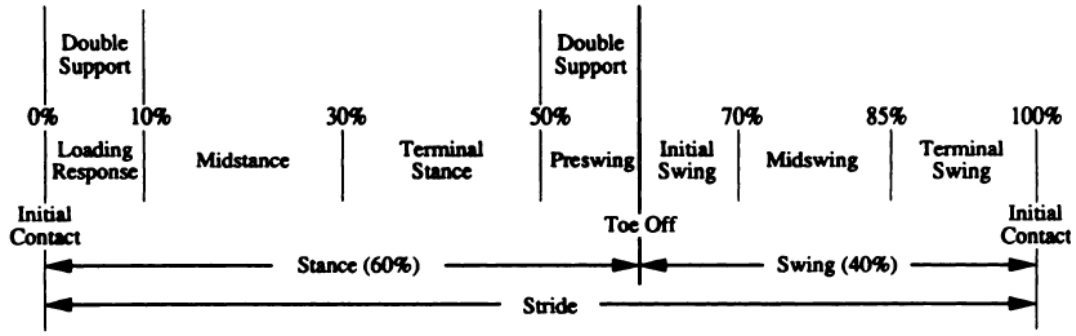

Figure 2-1 : Schematic representation of the gait cycle – reproduced from [28**]**

The stance and swing phases can be split into different stages as shown pictorially in Figure 2-2. Both initial contact and terminal stance are instantaneous events.

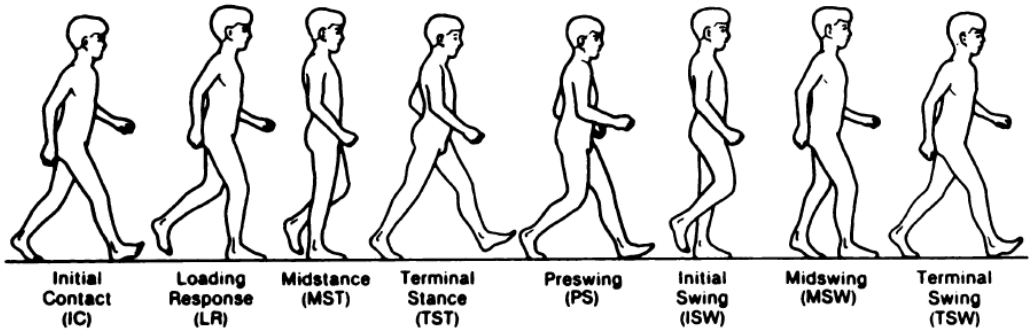

Figure 2-2: An artist's representation of a patient moving through the gait cycle – reproduced from [28**]**

2.3. The biomechanics of the lower limbs during gait

To allow normal gait to occur sufficient forces need to be created by the muscles in the body. These forces generate moments at the joints and this in turn leads to movement of the lower limbs. The analysis of the forces and the moments that act externally and internally on the body is known as biomechanics. For simplification it

is easier to study the motion of the ankle, knee and hip in the sagittal plane. The following biomechanics sections refer to work done by Perry [**29**].

2.3.1. Ankle biomechanics during gait

Figure 2-3 and Figure 2-4 show typical ankle moments and angles during the gait cycle for normal gait.

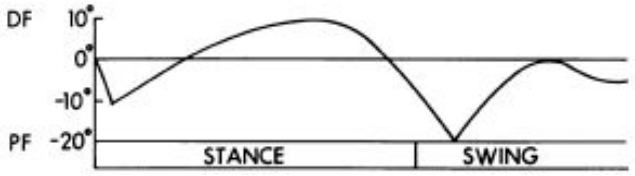

Figure 2-3: The ankle angle during gait – reproduced from [30**]**

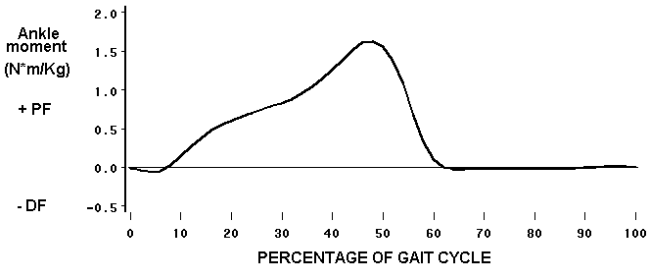

Figure 2-4: The ankle moment during gait – reproduced from [31**]**

Between the initial contact and mid stance phases of the gait cycle there is a moment tending to plantarflex the ankle. The primary dorsiflexors (tibialis anterior, extensor hallicus longus, and extensor digitorum longus) contract to resist this moment and provide controlled plantarflexion of the foot [**32**]. This is an eccentric contraction and is shown in Figure 2-5.

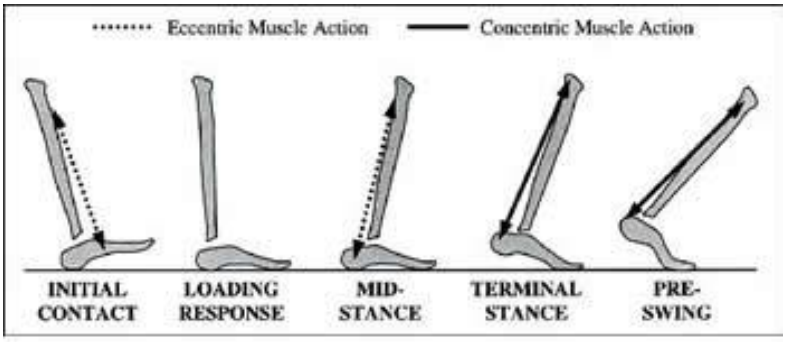

Figure 2-5: Motion and net muscle action of the foot-ankle complex during gait – reproduced from [32**]**

At the middle and the end of the stance phase the plantarflexors (soleus, gastrocnemius, flexor digitorum longus, flexor hallucis longus, and peroneus longus and brevis) contract and resist the large dorsiflexion moment. These muscles provide the power to initiate heel rise and propel the foot forwards [**32**]. During midswing the dorsiflexor muscles contract to prevent toe drag.

2.3.2. Knee biomechanics during gait

Figure 2-6 and Figure 2-7 show the typical angles and moments for the knee during the gait cycle for a normal gait. At initial contact the knee is in full extension, it then quickly flexes to approximately 15 degrees.

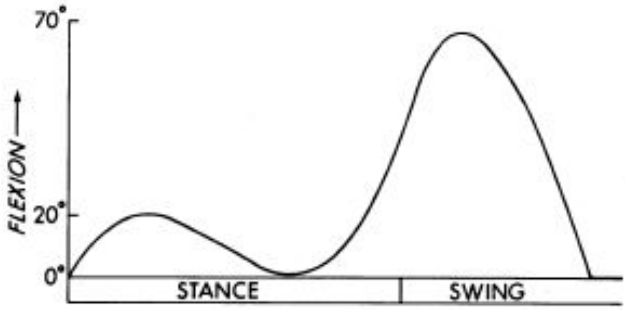

Figure 2-6: Knee angle during gait – reproduced from [30**]**

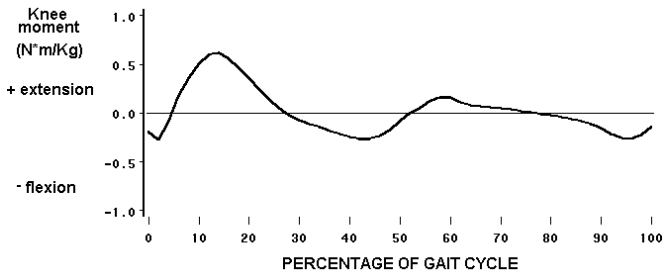

Figure 2-7: Knee moment during gait – reproduced from [31**]**

This flexion is caused by the contraction of the dorsiflexor muscles and this shifts the ground reaction force behind the knee as shown in Figure 2-8.

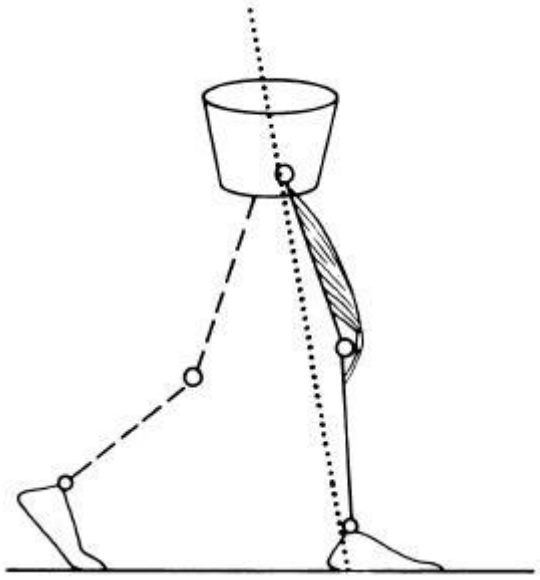

Figure 2-8: The ground reaction force falling posterior to the knee resulting in knee flexion – reproduced from [33**]**

To resist the moment created by the ground reaction force there is an internal extension moment. This moment is created by an increase in quadriceps activity. The knee then returns to a neutral position before starting to flex for a second time. This second period of flexion begins because the ground reaction force is behind the knee joint (Figure 2-9). As the swing phase commences the knee can flex up to approximately 70 degrees and this aids toe clearance.

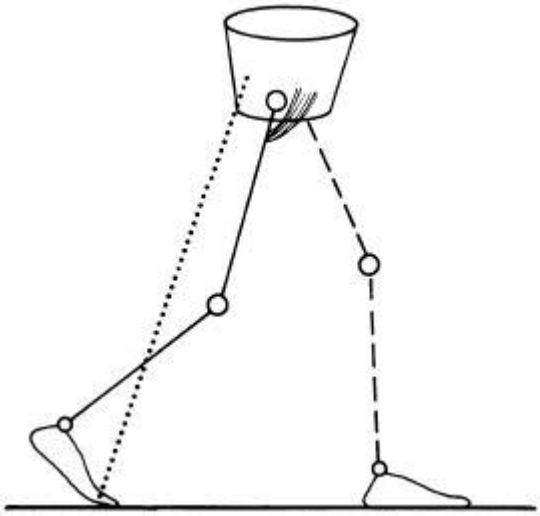

Figure 2-9: The ground reaction force falling posterior to the knee resulting in knee flexion – reproduced from [33**]**

2.3.3. Hip biomechanics during gait

The typical angles and moments for the hip during gait are shown in Figure 2-10 and Figure 2-11.

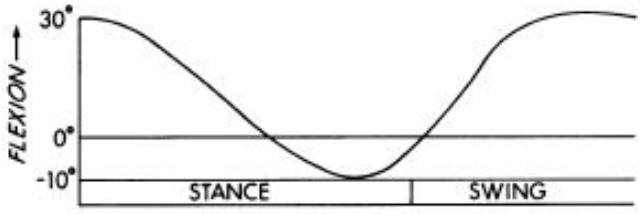

Figure 2-10: Hip angle during gait – reproduced from [30**]**

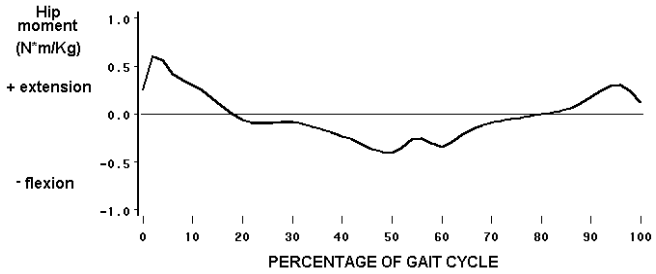

Figure 2-11: Hip moment during gait – reproduced from [31**]**

In contrast to the knee there is only one cycle of flexion and extension by the hip. As Figure 2-10 shows the hip is in approximately 30 degrees of flexion at initial contact. At this point in time the ground reaction force falls anterior of the hip joint (Figure 2-12) therefore creating an external flexion moment at the hip.

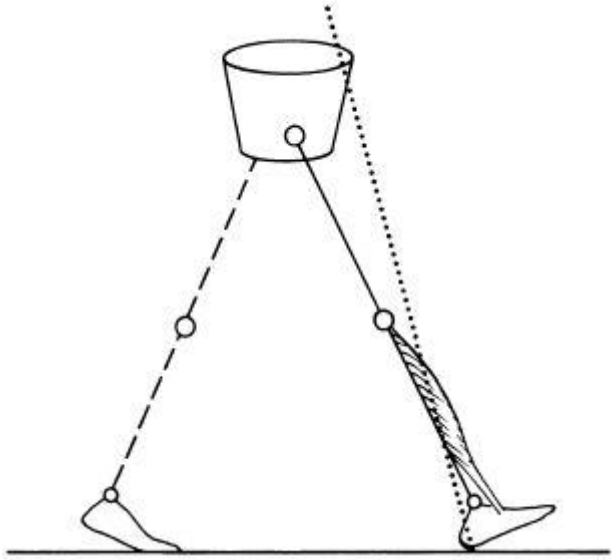

Figure 2-12: The ground reaction force falling anterior to the hip causing hip flexion – reproduced from [33**]**

Primarily the gluteus maximus and adductor magnus muscles resist this moment. The hip passively extends during mid stance and continues to do so until the swing phase. During the swing phase the iliacus is the main muscle that flexes the hip, this advances the thigh before the next stance phase.

2.4. Gait analysis equipment

To allow the precise analysis of the biomechanics of the body, technology has been developed to analyse the different parameters of gait. The systems developed can be split into three main categories; electromyography, kinematics and kinetics [**34,35,36**]. The data from these systems is useful for a range of different reasons including differentiating between normal and pathological gaits. Commonly motion capture technology is used to capture kinematic data and force plates are mainly used to capture kinetic data.

2.4.1. Motion Analysis Systems

In relation to gait analysis, motion analysis systems can be used to calculate joint angles, velocities, accelerations, temporal data and other kinematic characteristics [**37**]. An example of a motion analysis system is the Vicon system (Vicon, USA). The Vicon system works by placing reflective markers on the subject's limbs at predetermined locations [**38**]. These markers reflect the infrared light emitted from the cameras surrounding the subject. The cameras then receive the reflected light and send the information to a computer. The computer analyses the data so that the movement of all the markers can be determined in 3 dimensions. Prior to using the Vicon system it has to be calibrated [**39**]

One of the major problems with motion capture is that of marker movement due to skin movements over the underlying skeleton [**35**]. Current research is trying to overcome this problem.

2.4.2. Force measurement systems

One way to measure kinetic data is to use a force platform. A force platform produces electrical signals corresponding to the force and moments produced when a subject walks over the platform [**39**]. Figure 2-13 shows the 3-dimensional force and moment inputs that are outputted as electrical signals. These signals are sent to a computer where a piece of software analyses them and calculates the equivalent forces and moments generated at the platform.

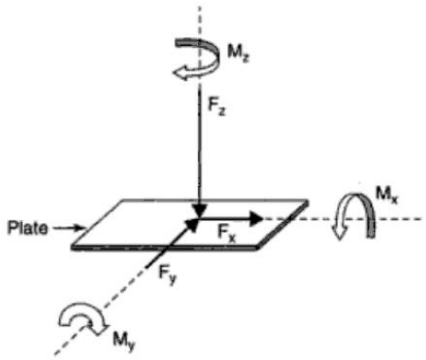

Figure 2-13: The 3D force and moment inputs measured by a force platform – reproduced from [39**]**

There are two main types of force plate; one that uses piezoelectric crystals as the transducer and one that uses strain gauges. The advantages of using the piezoelectric models are that they have a greater range and sensitivity; however they are more expensive [**40**].

2.4.3. Pressure mapping systems

Pressure mapping systems are frequently used to measure the pressures acting on the sole of the foot during gait. They are used to screen, treat and modify the behaviour of individuals who are experiencing a range of foot problems [**41**]. One transducer that can be used to measure the underfoot pressures is the force sensing resistor (FSR). FSRs consist of two mylar sheets; one sheet which has metal tracks imprinted on the surface and the other which has a conductive polymer impregnated into it [**42**]. As the thin sandwich is pressed together the conductive particles form a resistive path between the metal tracks [**41**]. If a high pressure is applied then this equates to a reduction in the resistance. The transducers can be arranged into a matrix and then can be inserted into a polymer insole for insertion into a shoe. Software correction means the output voltage has a linear relationship with the applied force.

An example of a FSR matrix system called the F-scan system (Tekscan, USA) (see Figure 2-14) has been tested for in-shoe pressure measurement [**43**]. It was found to have limitations because of the system's inaccurate calibration, poor

hysteresis and creep properties. There are examples of the F-scan pressure sensor equipment being used in studies that record the pressure distribution at the socket/stump interface for trans-tibial amputees [**44**] and at the skin/AFO interface [**45,46**]. Nowak et. al looked at the pressure distribution at the interface between an AFO and the skin for the purpose of reducing pressure sores on the lower leg and foot for diabetic patients. During normal gait they measured low pressures at the calf section of the AFO and high pressures at the foot section.

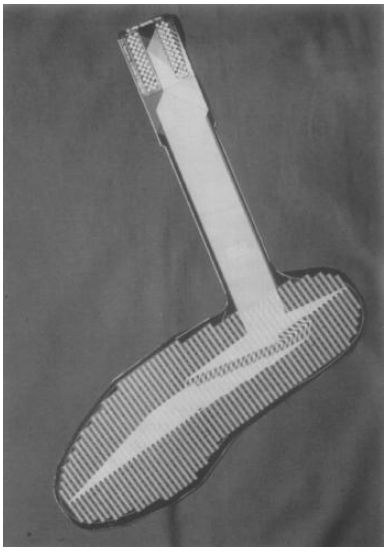

Figure 2-14: The F-scan pressuring mapping sensor – reproduced from [43**]**

In the study for this thesis FSR matrix technology will be used but the limitations will be noted and results will be checked with a more reliable transducer.

Gant et al. [**47**] also recorded pressures at the AFO body interface. They also found low pressures at the calf and high pressures on the foot section.

An alternative to FSR technology is to use capacitive sensors. These sensors have two conducting plates that are separated by an insulating layer (dielectric) [**41**]. If an external force pushes the plates closer together their capacitance will change [**48**]. Computers can record the capacitance and scale the result according to a calibration curve [**41**]. The Pedar pressure measurement system (Novel, Germany) is an example of a system that uses capacitive sensors. Several studies have shown the Pedar pressure system to give results that have good reliability [**49**], good

accuracy [**50**] and good repeatability [**50,51**]. One of these studies found that more accurate and reliable results were obtainable using the Pedar system than using the F-scan system [**50**].

Chapter 3. Clinical Conditions and Gait Deviations

3.1. Introduction to clinical conditions and gait deviations

There are a wide range of clinical conditions and injuries that can cause walking difficulty. The causes of a pathological gait can be grouped into four main catagories; structural impairment, motor unit insufficiency, peripheral sensory and motor impairment and central control dysfunction [**52**]. One or a multiple number of these factors will cause a deviation from the normal gait that was described in the previous chapter.

In this chapter the clinical condition is described initially and then gait deviations are detailed. The main gait deviations described are ones that can be treated with an AFO.

3.2. Upper motor neuron disorders

Upper motor neuron disorders include multiple sclerosis, cerebral vascular accidents, cerebral palsy, brain injuries and spinal cord injuries [**53**]. The cause of the disorder is a lesion or damage to the pathway of the upper motor neurons. This pathway runs from the cortex of the brain to the medulla or the spinal cord. The damage can result in various degrees of muscle spasticity. Spasticity is the resistance to passive muscle stretch which increases with the velocity of the stretch [**54**].

3.2.1. Cerebral vascular accidents

A cerebral vascular accident or a stroke typically causes damage to the motor cells and pathways of the central nervous system and is caused by haemorrhage or thrombus affecting the arterial supply of the brain [**55**]. More severe cases of stroke lead to impairment of body awareness, balance, muscle strength and coordination of both the upper and lower extremities [**56**]. Stroke can also lead to hemiplegia or hemiparesis, which is muscle paralysis or weakness on one side of the body.

The damage caused by a stroke can lead to the diminished strength of the ankle dorsiflexors. This can lead to drop foot where the plantarflexion of the foot during

initial contact is not controlled. It can also lead to the inadequate foot clearance during swing phase. Other gait deviations associated with hemiplegia and hemiparesis include circumduction of the leg, hyperextension of the knee, and equinovarus [**57**]. Equinovarus is a foot deformity that causes both equinus and varus of the foot. Equinus deformity of the foot is defined as the inability to dorsiflex the ankle to allow the heel to contact the ground without some compensation mechanism in the lower limb and foot [**58**]. In equinovarus it is the varus movement of the foot that allows the heel to contact the ground. A varus movement is when the foot is moved medially in relation to the ankle joint and therefore the sole of the foot turns inwards [**59**].

3.2.2. Cerebral palsy

Cerebral palsy refers to a central nervous system disorder; it is a group of persistent postural or movement dysfunctions secondary to a nonprogressive lesion in the developing brain [**58**]. The dysfunctions can manifest themselves as spasticity, athetosis, dystonia, ataxia, hypotonia or a combination of these factors. Cerebral palsy can be caused by prenatal trauma, drug exposure or a congenital defect [**60**].

The abnormalities that can occur from cerebral palsy that affect gait include; the loss of selective muscle control, abnormal muscle tone, muscle imbalance and deficient equilibrium reactions [**61**]. From these primary abnormalities resulting secondary problems can occur; for example abnormal bone and muscle growth. The gait deviations caused by these abnormalities can lead to further changes to normal gait which occur as coping mechanisms. For example spasticity of the rectus femoris and hamstrings can lead to a stiff knee in the swing phase of the gait cycle. This can cause problems with foot clearance and hence the affected individual will commonly circumduct and prevent their foot from hitting the floor. In this example the spasticity is the primary deviation and the circumduction is the coping mechanism.

Examples of gait deviations associated with cerebral palsy include; bilateral excessive hip and knee flexion (crouch gait) or knee hyperextension (genu recurvatum), excessive ankle plantarflexion and anterior pelvic tilt [**62**]. Cerebral palsy can also cause calcaneus, equinus, varus and valgus foot deformities [**62**]. A

valgus foot deformity is one where the foot moves laterally to the ankle joint and the sole of the foot points outwards [**59**]. A review of the literature concerning dynamic gait of children with cerebral palsy shows that varus is thought to be associated with increased activity of the tibialis posterior and valgus associated with decreased activity of the tibialis posterior [**63**].

3.2.3. Mutiple sclerosis

Multiple sclerosis is an inflammatory disease that destroys myelin sheaths that surround nerve cells [**60**]. The result of this is that it can affect motor control and cause muscle weakness as well as spasticity. Spasticity leads to simultaneous contraction of many muscles and this causes the tone to increase in all muscles [**64**]. The result is the affected limb feels tight and movements tend to be slower and less smooth.

3.3. Lower motor neuron disorders

Lower motor neuron disorders include poliomyelitis, cauda equina syndrome, spinal stenosis and polyradiculopathy [**65**]. Similar to upper motor neuron disorders the cause is a lesion or damage to a neural pathway. However, it is damage to the lower motor neuron pathway which runs from the spinal cord to the peripheral muscles. The damage can result in various degrees of flaccid paralysis of muscles [**65**].

3.3.1. Post-polio syndrome

Poliomyelitis (polio) is an acute viral infection that attacks the motor neurons and causes muscular paralysis and atrophy [**60**]. After being infected by polio, signs of a new weakness or increase in the weakness of previously affected or non-affected limbs, may indicate the development of post-polio syndrome (PPS) [**65**]. One problem that can occur in PPS is the weakness of the quadriceps muscles [**66**].

3.4. Muscular dystrophy

Muscular dystrophy refers to a group of inherited diseases in which various genes controlling muscle function are defective [**67**]. The diseases cause muscle weakness and wasting, the weakness is usually progressive but this depends on the type of disease. Figure 3-1 shows some of the different types of muscular dystrophy. One common type is the Duchenne Type, which is caused by the missing protein dystrophin. Symptoms shown in the affected individual's gait include clumsiness, impaired balance and a tiptoe gait [**68**].

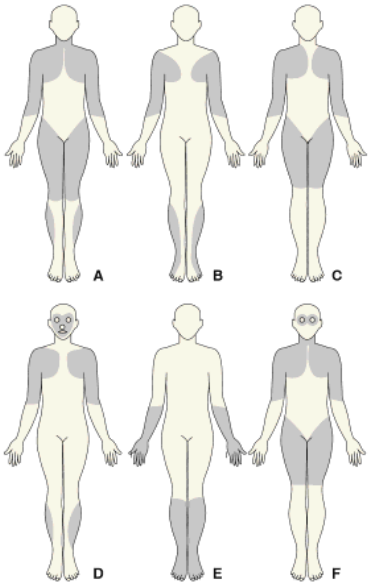

Figure 3-1: The general distribution of muscle dystrophies: a) Duchenne and Becker b) Emery-Dreyfuss c) Limb-girdle d) Fascio-scapulohumeral e) Distal f) Occulopharyngeal – reproduced from [68**]**

3.5. Congenital abnormality

A congenital abnormality is when an individual is born with an abnormality of structure, function or body metabolism and results in a physical or mental disability, or is fatal [**69**].

An example is spina bifada which is a condition resulting from the failure of the vertebral laminae to unite during development; commonly associated with the

development of abnormalities in the brain and spinal cord [**60**]. Abnormalities in certain sections of the spinal cord can lead to paralysis of muscles in the lower limbs which can affect gait.

An individual with myelomeningocele, which is certain type of spina bifida can have paralysis of the plantarflexor muscles. This can lead to increased knee flexion, increased anterior pelvic tilt, altered pelvic frontal and transverse movement and increased trunk rotation [**70**].

Chapter 4. Orthoses and Ankle Foot Orthoses

4.1. Introduction to orthoses

Building upon the previous definition of an orthosis, they should perform at least one of 3 basic functions [**2**]:

1. Support anatomical structures from weight bearing
2. Control joint motion (direction, range strength) by
    i. Limiting motion (partially or completely)
    ii. Restoring motion (partially or completely)
3. Change the shape of body tissues by
    i. Bending or twisting skeletal structures
    ii. Stretching soft tissues

By performing one or more of the above functions an orthosis can prevent joint collapse, maintain the position of a joint and protect damaged or weak soft tissue. An orthosis can also alleviate pain through external support of body weight, it can prevent or control unwanted motion, replace lost or reduced motion and correct or prevent deformities, including contractures [**2**]. An ideal orthosis controls only those motions that are abnormal or undesirable and permits motion where normal function can occur [**33**].

4.2. Introduction to ankle foot orthoses

The ankle and foot are vital mechanical structures in the body because they provide the link between the body and the ground. The significant mechanical structures in the ankle and foot are [**71**]:

- The skeleton – along with the ligaments and the arches provide the rigidity and lever arm mechanism required to maintain balance during standing as well as facilitating propulsion.
- The joints – allow mobility of the foot
- The muscles and tendons – control foot movement

It is the controlled and coordinated movements of the above structures that lead to the normal biomechanics of the lower limbs and thus a normal gait pattern.

An AFO is a device that is prescribed when the normal mechanical structures and mechanisms of the lower limbs are altered by a certain clinical condition or injury. The aim of the AFO is to adjust the biomechanics of the lower limbs so they resemble normal gait biomechanics as closely as possible. AFOs are one of the most frequently prescribed orthoses and in the USA 26% of orthoses that are prescribed are AFOs [**72**].

This chapter will detail different types of AFOs and then will give some examples of conditions they can be prescribed for. The final section explains the biomechanics of AFOs. For the explanation of any anatomical terms please refer to a publication by Whittle [**27**].

4.3. Materials and types of ankle foot orthoses

Prior to the 1970s all lower limb orthoses including AFOs were assembled from metal components with their body contact areas padded with felt and covered with leather [**73**]. This type of AFO was replaced because they were heavy and had a poor cosmetic appearance [**17**]. There are reasons however, why these traditional AFOs are still prescribed [**52**]:

1. Satisfied previous wearers
2. Unusually large or heavy individuals
3. When minimal contact with the leg is desirable

Thermoplastic AFOs were introduced in the 1970s and as materials for constructing AFOs they have many advantages including their clarity, flexibility, rigidity, faster processing times, localised adjustment by the use of heat, inert material and surface quality [**74**]. They are also easy to clean and have good force distributing properties and allow total contact between the skin and the orthosis [**17**]. One commonly used thermoplastic is polypropylene and it can be used for all lower limb orthoses, particularly where rigidity is required [**52**]. Polypropylene has a glass transition temperature of -18 degrees Celsius [**75**]. At room temperature polypropylene is above the glass transition temperature and behaves as a rubber, this means the relationship between stress and strain is non-linear [**76**].

Thermoplastic AFOs allow unlimited design potentials and allow the exact customising of the orthosis to match the biomechanical needs of the patient [**17**].

The following section is referenced from a publication called Orthotics: a comprehensive clinical approach [**77**]. To custom make an AFO for an individual the orthotist wraps the ankle and foot in plaster to form a negative model. Liquid plaster is then poured into the hollow model to create a positive model. The orthotist can then refine the model; they can add material to sensitive areas and take material away from load tolerant areas. The thermoplastic is then heated and pulled over the positive model to form the AFO. New techniques of fabrication include computer aided design and computer aided manufacture.

There are also prefabricated AFOs available; however these lack the intimacy of fit and the stiffness necessary to control complex deformity or instability of the foot and ankle [**4**]. There are many different types of AFOs and the main ones are detailed in the following sections. The types detailed below are custom made types.

4.3.1. Posterior leaf spring ankle foot orthosis

The posterior leaf spring AFO is shown in Figure 4-1. The AFO is trimmed postero-laterally and postero-medially at the supramalleolar area [**78**]. This allows ankle flexibility and passive dorsiflexion during stance phase.

Figure 4-1: A posterior leaf spring AFO – reproduced from [79**]**

It is usually prescribed for isolated dorsiflexor weakness and to prevent drop foot during swing phase. It is not suitable for any significant problem of high tone or spasticity, any significant medio-lateral instability of the foot or for orthotic influence on the knee and/or hip [**52**]. The title posterior leaf spring suggests that the AFO has an energy storage and return feature. This is assumed to mean that at heel strike the AFO absorbs energy and this energy is returned at the terminal stance phase to assist toe off.

A study with cerebral palsy children has shown that posterior leaf spring AFOs reduce excessive equinus in swing and allow ankle dorsiflexion in midstance [**12**]. The same study also concluded that the AFO did not augment power generation at the ankle.

4.3.2. Hinged or articulated ankle foot orthosis

In the design of a hinged AFO (see Figure 4-2) a mechanical joint can allow motion in one direction and prevent it in another. Typically hinged AFOs block plantarflexion at 90° and they allow a certain degree of dorsiflexion [**4**]. The hinged AFO may be unsuitable for individuals with moderate or severe medio-lateral instability (for example individuals with varus or valgus deformities).

Figure 4-2: A hinged/articulated AFO – reproduced from [80**]**

Hinged AFOs have been shown to improve some gait impairments in patients with stroke [**9**]. They have also been shown to be useful in controlling equinus deformity and reducing the energy expenditure of gait in children with hemiplegic spastic cerebral palsy [**11**].

4.3.3. Solid ankle foot orthosis

Solid AFOs (see Figure 4-3) prevent all motion at the foot and ankle. The design covers the back of the leg completely and extends from just below the fibular head to the metatarsal heads. An increase in the height of the sides provides better varus or valgus control [**78**].

Figure 4-3: A solid AFO – reproduced from [81**]**

They are designed for individuals with high tone or spasticity in the plantarflexors, a gastrocnemius contracture, significant medio-lateral instability of the foot and/or need for the AFO to influence the knee or hip [**52**]. The AFO enables heel strike during stance phase, toe clearance during swing phase and also control of varus or valgus deformities. Carbon fibre reinforcements may be added to the ankle section to increase the stiffness of the AFO.

Groups of subjects with cerebral palsy and hemiplegia (due to strokes) have shown that gait parameters can be improved with a solid AFO [**7,10**].

4.3.4. Ground reaction ankle foot orthosis

A ground reaction/floor reaction AFO (GRAFO/FRAFO) is shown in Figure 4-4; it is a type of solid AFO that is specifically designed to align the ground reaction force vector in front of the knee during mid to late stance phase (see Figure 4-5). This generates an external knee extension moment which prevents excessive knee flexion and aids stability. To have this effect on the knee the GRAFO must be very stiff and optimally aligned [**52**]. One notable design feature is the brace across the front of the tibia; this prevents any excessive tibia forward progression. The GRAFO prevents excessive dorsiflexion and crouch gait [**78**]. A study found the GRAFO to be effective in improving the extension of the knees and ankle [**13**].

Figure 4-4: A ground reaction AFO – reproduced from [82**]**

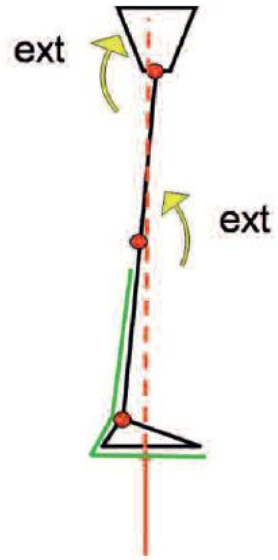

Figure 4-5: A diagram of the ground reaction force creating an extension moment at the knee – reproduced from [4]

4.3.5. Spiral AFO

A spiral AFO (see Figure 4-6) encircles the leg and consists of a shoe insert and a narrow proximal strip that is moulded into a 360-degree spiral. This strip arises from the medial aspect of the insert, wraps around the leg and terminates near the medial tibial condyle [**77**]. At initial heel contact the spiral uncurls slightly and this allows a degree of plantarflexion. The spiral returns to its original shape during midstance and compresses during terminal stance as the ankle dorsiflexes. The heel rise causes the limb to off-load and allows the spiral to uncoil slightly to assist plantarflexion. During swing phase the spiral returns to its original shape. The spiral AFO is useful for patients with complete flaccid paralysis of the foot which can be freely dorsiflexed or plantarflexed beyond the neutral position [**83**]. It is not designed for individuals with plantarflexion contractures because it is too flexible and will not provide the level of resistance needed for these individuals. A study has shown that spiral AFOs are more advantageous than solid AFOs for children with spastic cerebral palsy when balance control is required [**14**].

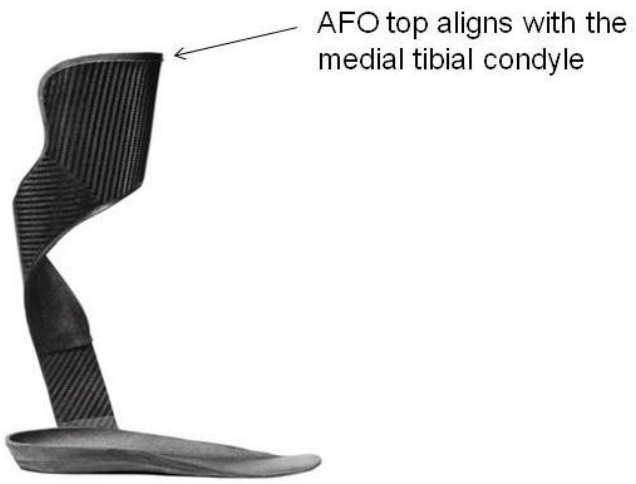

Figure 4-6: A spiral AFO – reproduced from [84**]**

4.4. Biomechanics of AFOs

The lower limbs of the body experience external loads during the gait cycle and it is the muscles that generate internal loads to counteract these external loads and provide a normal gait pattern. When there is muscle weakness or another pathological problem an AFO can be used to adjust and reduce the external loads acting on the limbs. It is important to note that the footwear worn with an AFO plays a crucial role in overall function [**85**] and therefore in this biomechanics section *the term AFO refers to the orthosis and footwear combination*. The following section is referenced from a publication by the American Association of Orthopaedic Surgeons [**52**].

AFOs can apply biomechanical effects to the lower limbs in two main ways; one is by using the three point force system and the other is to realign the ground reaction force. One of the differences between these two systems is that the three force system has a direct biomechanical effect on the ankle joint in contrast to the ground reaction system, which has indirect biomechanical effects on the proximal joints in the leg.

The three forces should maximise lever arms and the area of force application, they should also be applied in a way that respects the underlying anatomy. One way to do this is to ensure the area of the orthosis is shaped to match as closely as possible the contours of the underlying skeletal structures. An example of the three

point force system is shown in Figure 4-7. This is designed to prevent equinus and reduce problems with ground clearance. The three forces (applied by AFO on limb) are located to the posterior to the calf, at the plantar surface of the foot near the metatarsal heads and the dorsum of the foot near the ankle joint.

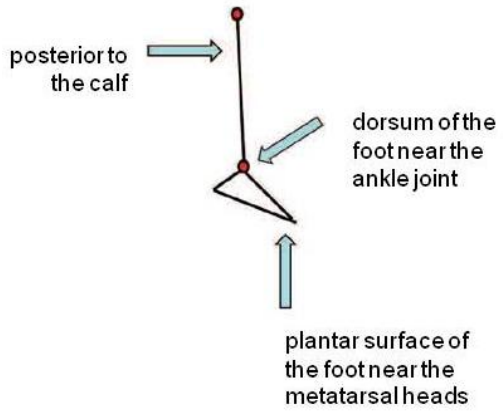

Figure 4-7: Schematic of the three point force system – reproduced from [4]

Another example is the force system needed to treat varus foot deformities. This involves two sets of three point force loads; one at the subtalar joint and one at the midtarsal joint. At the subtalar joint the forces are applied to the medial aspect of the heel, the area above the lateral malleolus and the medial aspect of the proximal calf. At the midtarsal joint the forces are applied to the medial heel, the lateral midfoot and along the first metatarsal joint. All these forces are shown in Figure 4-8.

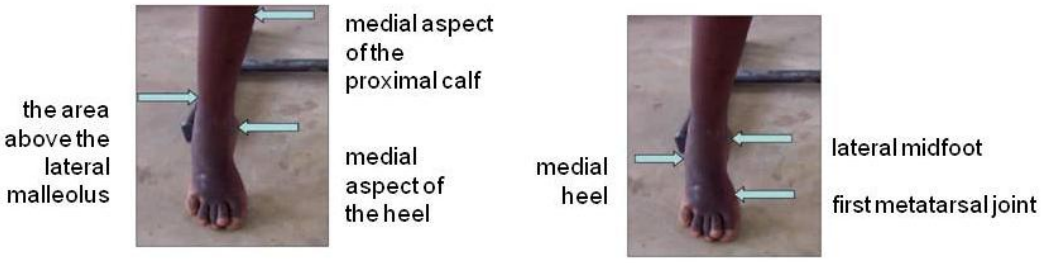

Figure 4-8: Example of the three point force system - reproduced from [4]

To control valgus deformities the forces are reversed so that the forces acting on the lateral side act on the medial side and vice versa.

By designing an AFO in specific ways the realignment of the ground reaction force can be achieved. This then modifies the external lever arms and moments at the ankle, knee and hip. An example of the use of the ground reaction force system is for individuals with knee hyperextension. This is caused by the ground reaction force being positioned too far anteriorly to the knee and therefore creating a large external extension moment. It also causes an external extension moment at the hip. A correctly fitted AFO can adjust the thigh so it is 10 degrees inclined anteriorly and it can move the ground reaction force posteriorly. It does this by allowing more of the plantar area of the foot to make contact with the ground as shown in Figure 4-9.

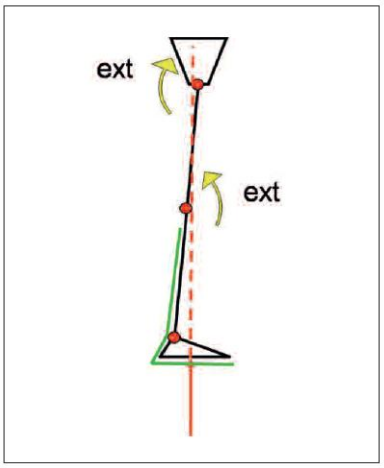

Figure 4-9: An example of an AFO realigning a ground reaction force - reproduced from [4]

There is still an external extension moment at the knee but it is reduced and therefore aids stability and facilitates knee flexion in the swing phase.

Tuning of an AFO is when height is either added to the heel or sole of an AFO. This can be beneficial because it can adjust the angle of the shank and therefore move the knee and hip joints towards or past the ground reaction force which can aid stability.

Chapter 5. Finite Element Method

5.1. Introduction to finite element analysis

Finite element method (FEM) is a numerical analysis that permits the formulation of equations using the basic principles of mechanics [**86**]. Finite element analysis (FEA) is the term used for the application of FEM. FEA is mostly done by a computer and it enables the simulation and analysis of real world physical systems. Common FEA commercial software packages include Ansys, IDEAS and Abaqus.

5.2. Background and theory

The creation of the FEM is credited to the mathematician Richard L. Courant, he first published his work on FEM in 1942 [**87**]. However, it was not until computers became widely available in the 1960s and 1970s that FEA started to be used by engineers. The first use of FEM in an engineering application was as a method of stress analysis in the design of aircrafts [**88**]. In the present day FEM is used in the analysis of solid mechanics, fluid flow, heat transfer, electric and magnetic fields and many others. The following section is referenced from a publication by Bhavikati [**88**].

The steps involved in FEA are:

1. Select suitable field variables and the elements
2. Discritise the continua
3. Select the interpolation functions
4. Find the element properties
5. Assemble the element properties to get global properties
6. Impose the boundary conditions
7. Solve the system equations to get the nodal unknowns
8. Make the additional calculations to get the required values

The field variables are the unknown factors in the analysis and in stress analysis problems they are the displacements of the structure. These unknowns are split into smaller sections known as elements. There are different types of elements that can be chosen depending on the analysis; each type is represented by a different

interpolating function. The interpolating functions are derived using polynomials. These interpolating functions are defined by nodal points (nodes), which can vary in number depending on the type of element. FEA allows the unknowns at the different nodes to be estimated by using the interpolating functions. The next stage in FEA is to determine the element properties; this is done by defining the stiffness characteristics of each element. For stress analysis, Equation 1 relates the nodal displacements and nodal forces:

$$\{F_e\} = [k_e]\{u_e\} \qquad \text{Equation 1}$$

Where F_e is the nodal force vector, k_e is the element stiffness matrix and u_e is the nodal displacement vector of the element. Each element stiffness matrix needs to be placed into a global stiffness matrix. Any boundary conditions need to be taken into account. An example boundary condition is zero displacement at one end of a model. The boundary conditions also include applying values for the forces being applied to the model. The simultaneous equations that make up the global stiffness equation can then be solved using mathematical techniques such as Gauss elimination or Choleski's decomposition techniques. The resulting solutions will give the nodal displacements, from these values the stresses in the structure are calculated.

5.3. Ansys

Ansys (Ansys, USA) is a piece of sophisticated FEA software that is used world-wide by commercial engineering companies as well as academic centres. It has the capability to perform structural, thermal, fluid, electromagnetic and other types of analysis. In terms of structural analysis the software can perform simple linear static analyses that can calculate the stresses and deformations. It can also perform complex transient non-linear phenomena involving dynamic effects and complex behaviours [**89**]. Using the Graphics User Interface (GUI) models can be created and then pre-processed, solved and post-processed all using the same window. There are over 100 different element types available in Ansys including shell, beam and brick types. The academic version of Ansys has a limit of 31,000 nodes. The

software has a range of mathematical models that allow the analysis of non-linear materials and geometries. The Ansys work environment supports neutral format files such as IGES, Parasolid®, ACIS® (SAT) and STEP [**89**]. This means geometry can be imported from a wide range of CAD software. More details can be found about the Ansys software from the user manuals [**90**].

Chapter 6. Literature Review of Measuring the Loads on AFOs

6.1. Introduction to literature review of measuring the loads on AFOs

A lot of the studies undertaken with AFOs are designed to evaluate clinical parameters such as gait velocity; however there are not as many studies that evaluate the mechanical properties of AFOs. There are even less studies investigating the loads acting on AFOs during gait, this is why this review also includes studies that investigate the stresses acting on AFOs

The review is split into two main sections; one section details the studies that measure the loads or stresses acting on AFOs during gait using practical methods, the other section details the studies that investigate the loads or stresses of AFOs using FEA.

6.2. Literature review of measuring the experimental loads on AFOs

There are several studies that use strain gauges to investigate the loads or stresses that act on an AFO during the gait cycle [**18,91,92,93**]

The first series of studies by Robin et. al applied strain gauges to the metal uprights on traditional AFOs [**91,92**]. The first study attached eight strain gauges to uprights (made from duralumin) of seven different types of braces; one had a posterior upright, three had unilateral uprights and three had bilateral uprights [**91**]. Brace is an old fashioned term for an orthosis [**94**]. The strain gauges were positioned in the areas that were considered to be areas of the maximum possible stress but a distance away from the joints to avoid stress concentrations. Measurements were taken during the gait cycle; only one subject was used for the study to avoid gait variations. It was found that the highest stresses occurred with the brace that had the upright in the posterior position, these occurred during swing phase. This was thought to be the case because of the pull of gravity on the foot during swing phase. The lowest stresses occurred with the brace that had both medial and lateral uprights. The highest stress values for the unilateral brace occurred during initial contact and the highest stress values for the bilateral brace occurred during midstance. The most significant forces were found occurring in the

direction of gait for the posterior upright brace and in the lateral direction of the two other types of brace. In the bilateral upright brace the higher stresses were consistently found in the lateral upright. A follow up paper [**92**] tested the bilateral upright braces with four patients who had post-poliomyelitis syndrome. All four subjects had foot drop because of complete paralysis of the dorsiflexor muscles. It was found that the lateral loads were considerably higher than those measured using a normal subject. In contrast the loads in the direction of gait were similar to that of those measured using a normal subject. A third paper by Robin et. al [**93**] used a very similar methodology to the previously mentioned study but it incorporated a brace with polyester uprights. It was concluded that the loads found acting in the plastic braces were similar to those acting in the metal braces.

Work by Chu et. al [**18,95**] involved attaching strain gauges to polypropylene AFOs. In the study eight strain gauges were attached to different positions on five different types of AFOs; which were the flex, standard, moderate, solid and varus models. The gauges were positioned on the neck in the medial, lateral and middle positions. One normal subject conducted different tests including a slow forward walk, a fast forward walk, running, jumping, lifting objects and sitting down and standing up. It was found that for a slow gait the maximum tensile stress was generated during terminal stance and the maximum compressive stress was generated during initial contact. The peak stress concentration was primarily located at the lateral side neck region. There is no verification by the authors of the accuracy of using strain gauges to measure the stresses on the material polypropylene.

There are studies in the literature that document the moments generated by AFOs during gait [**19,96**]. Yamamoto et. al built a novel device, which was an AFO that could be adjusted to achieve different assistive dorsiflexion moments for different subjects [**19**]. The device can be adjusted by inserting into it a number of springs that have different stiffnesses. The AFO device is free to pivot except for the springs which give it the variability in corrective moments that it applies. The moment applied by the AFO was measured by multiplying the spring constant and the moment arm. Force transducers were also situated in the device so the moments could be measured. This device allowed the biomechanics of the AFO to be adjusted to suit an individual's gait. It was found that from a group of fifteen hemiplegic subjects nine subjects experienced a significant decrease in gait cycle

time when the AFO was adjusted to their favoured assistive dorsiflexion moment. It was also reported in the study that the dorsiflexion moment created by the AFO to prevent foot drop during the swing phase is comparatively small to the dorsiflexion moment created by the AFO at initial contact. The same group also demonstrated that the corrective moment generated by the AFO in relation to the total ankle joint moment is very small in the plantarflexion direction [**96**]. The corrective moments generated in the transverse or coronal planes have not been looked into by these studies.

Studies have also shown that novel devices can be built to simulate gait and allow the AFO generated moment around the ankle to be calculated [**5,97**]. Bergman et. al built a novel device [**97**] to test the stiffness and neutral angle of an AFO about two separate joints (one at the ankle and one at the metatarsal-phalangeal) during simulated gait. Stiffness was defined as the moment around the ankle joint exerted by the AFO per degree of ankle joint rotation. The device was built to accommodate different AFO sizes and had six dummy legs with anatomically based joint centres. The AFO is clamped into place and the dummy leg is manually driven to generate an equivalent range of motion to that of normal gait. Force sensors are located in the AFO so that the moment can be continuously calculated. The study found the device to be reliable in measuring the mechanical characteristics of an AFO. A second study [**5**] by Bergman et. al used the same device and calculated the mechanical properties of different types of AFOs which were used by seven subjects with drop foot. The study had the hypothesis that the poor functional effects of the AFO relate to either insufficient contribution of the AFO during swing phase, or unwanted constraining of the ankle during the stance phase. The results showed that the mechanical contribution of the AFO to ankle moment was very low but enough to prevent drop foot occurring. The low stiffness also meant that the ankle was not hampered during stance phase. It was found that for the whole group there was a significant improvement in walking speed and energy cost (12%) when comparing gait with and without an AFO. The AFO had no functional benefit in terms of a reduced energy cost of gait for three patients, who could demonstrate no pathological plantar flexion during swing without their AFO. In conclusion the paper found that AFOs were only successful in meeting their functional requirements when their mechanical characteristics were meeting the patient's mechanical deficiencies.

6.3. Literature review of measuring the theoretical loads on AFOs

In 1987 Cundall's MSc thesis [**23**], which was undertaken at the University of Strathclyde documents the use of FEA for an AFO using simplified geometry such as cylinders, cones and spheres. In this work only moments in the sagittal plane were considered. The results of the finite element analysis were validated using a load/deflection test. The thesis showed the potential for FEA to be a method of predicting the behaviour of an AFO.

Leone et. al [**24**] did a FEA to assess the influence of local flexibility at the ankle area to the overall deformation of a solid ankle foot orthosis. The nodes at the top of the calf section were fixed and the loads applied were consistent with a constant displacement at the metatarsal heads. In this work the flexibility of the AFO was only considered in the sagittal plane.

A study by Chu et. al [**22**] in 1995 did a 3D FEA of the foot, ankle and of an AFO. The model was created with a total of 323 elements and 596 nodes, the orthosis consisted of 128 elements, the soft tissue of 146 elements, bones of 39 elements and ligaments of 10 elements. The upper boundary of the leg was constrained in all planes; this was to simulate the fact that the AFO was attached to the leg using calf straps. There was no space between the soft tissue and the bottom part of the AFO therefore no slip condition was considered at this point. The AFO in the tibia section was only allowed freedom of movement in the vertical direction. For the analysis the soft tissue, bones, ligaments and polypropylene were all assumed to be linear, elastic and isotropic. Forces were applied by the Achilles tendon, flexor and extensor muscles and the external ground reaction forces. Details of these forces are not listed in the journal article. The results showed that in a static analysis the peak tensile stress occurred in the neck regions of the AFO during terminal stance. The peak compressive stress occurred in the heel region of the AFO during initial contact. The study was not validated with practical experiments. Without a validation it is very difficult to draw useful clinical conclusions from FEA results [**98**].

Syngellakis et. al [**21**] produced a paper that documented the non-linear FEA of an AFO. To build the AFO in the FEA software a model of a leg was first inputted and then a shell was built around the geometry. The AFO was then cut out from this shell by using Boolean subtraction. When the model was meshed it had 1708 nodes and 549 elements, the AFO was initially made with a constant thickness of 2mm throughout. The AFO was constrained in the x-direction (the direction of

forward walking) at the calf region where the straps would be attached. Constraints were also applied to all nodes in the heel region so as to simulate the constraint provided by the shoe and the foot. The force applied to the AFO was a uniform pressure of 8.65kPa over the distal part of the foot region. This load was chosen because predicted ankle rotations due to that pressure were similar to the mean values of recorded data for a number of orthoses [**99**]. The FEA was undertaken with both linear material and geometric properties and non-linear material and geometric properties. Results found included the maximum displacement, maximum lateral displacement, rotation angle and maximum Von Mises stress. It was concluded that a linear analysis with a constant Young's modulus leads to an unreliable estimate of AFO stiffness. Another conclusion that was drawn was the fact that the thickness of the AFO model should not be uniform to achieve an accurate assessment of AFO stiffness. A second experiment was done to validate the FEA by comparing the predictions to the experimental data provided by Sumiya et. al [**100,101**]. The experimental data involved measuring the moment at the ankle whilst the AFO was being plantarflexed and dorsiflexed at intervals of 2.5 degrees. Moments were measured by applying a force to an artificial leg which consisted of a pipe and a moulded plaster artificial foot and calf. Results of the FEA showed that the analytical predictions were found to be close to the test measurements done by Sumiya et. al. It should however, be noted that the AFO geometry used in the analysis was only matched to the AFO geometry used in the tests using specimens, therefore there would have been a risk of geometry errors. It should also be noted that for the experimental results errors could have occurred due to manual application of force and friction between the pipe and artificial leg.

Chapter 7. Pressure Measurement Experiments

7.1. Introduction to pressure measurement experiments

To determine the accurate loading conditions that occur during the gait cycle it was decided that the pressures acting on the AFO/skin interface would be measured. Two different types of pressure measurement equipment were used. The first was the F-scan system (Tekscan, USA) which uses force sensitive resistors to measure pressure. The second was the Pedar system (Novel, Germany) which uses capacitors to measure pressure. The methodology and instrumentation, data analysis and results are detailed separately for the two types of sensors. A comparison of the two sensor systems is found at the end of the results section. To conclude the chapter the two sensor systems are discussed individually and also compared.

7.2. Methodology and instrumentation

7.2.1. Experiment one

The F-scan system needed to be calibrated before it could be used to collect data. To do this the six pressure sensors (three at one time) were inserted into a custom built pressure chamber. When the sensors were in position compressed air was then inserted into the chamber at a pressure of 100kPa. The custom built device allowed the pressure sensor tab to extend outside of the chamber so it could be inserted into a hub. The hubs were then wired to a computer laptop so the F-scan software could calibrate the sensors (see Figure 7-1 for the setup).

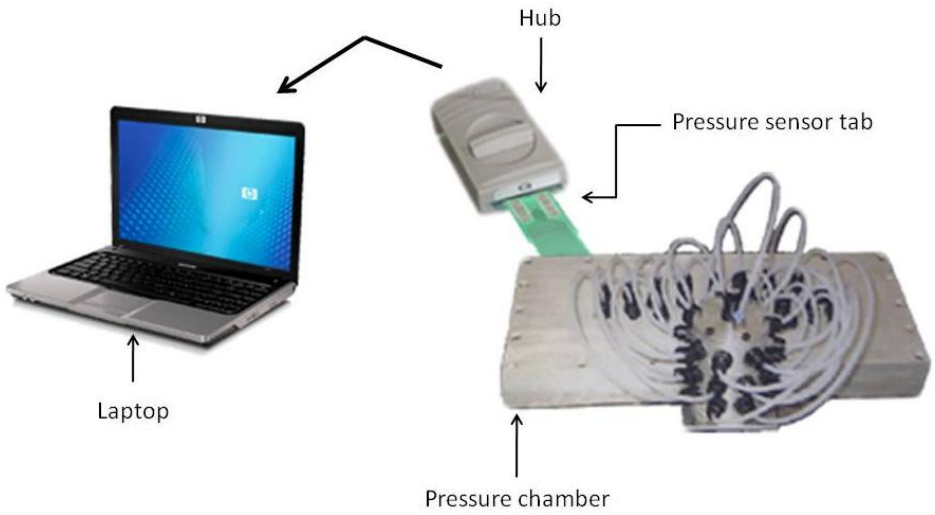

Figure 7-1: Setup of F-scan sensor calibration – (laptop) reproduced from [102**]**

The F-scan pressure sensors were then positioned in six different places inside the AFO. Three sensors were located in the calf position (lateral, central and medial positions), one in achilles tendon position, one on the strap and one beneath the foot (see Figure 7-2 for locations).

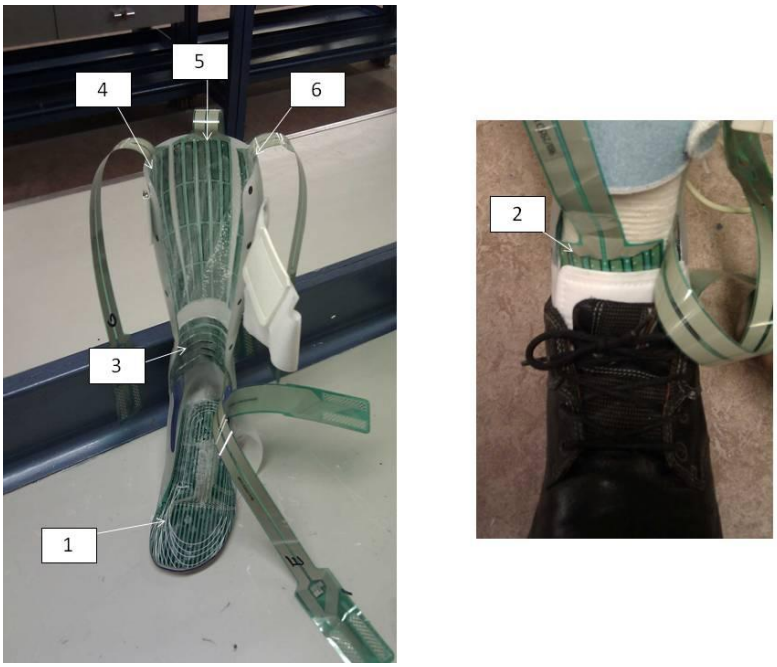

Figure 7-2: Sensor positions: 1 = plantar foot, 2 = strap, 3 = achilles tendon, 4 = medial calf, 5 = central calf, 6 = lateral calf

The sensors were attached to the AFO using a spray on adhesive (Spraymount Adhesive, 3M, UK) The AFO was then worn by the subject (a normal subject with no neurological disorders, weight: 80kg). The tabs from the sensors came outside of the AFO so they could be attached to the hubs. A Velcro cuff was applied over the subject's AFO so that the hubs would remain attached to the subject as they walked. A long cable then attached the hubs to the laptop computer; Figure 7-3 shows the setup. Data was collected as the subject walked with a normal gait for approximately six steps, this was repeated four times.

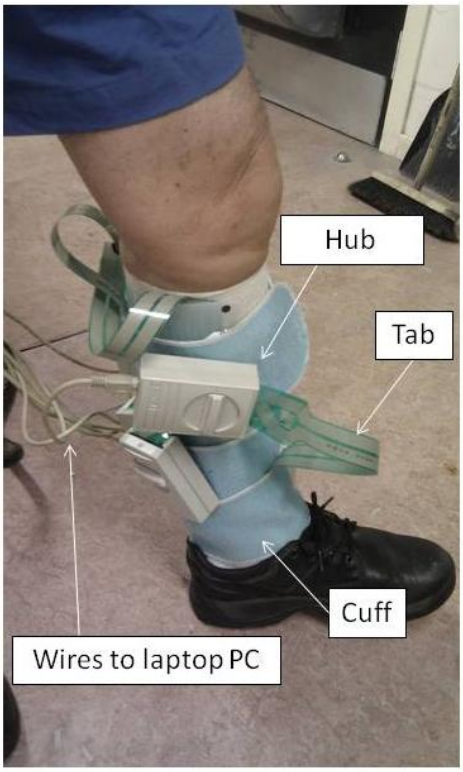

Figure 7-3: The subject wearing the AFO/sensor setup

7.2.2. Experiment one data analysis

The software packages Research Foot (Version 5.24, Tekscan, USA) and Excel (2007, Microsoft, USA) were used to analyse the results from the F-scan tests. The data was split into individual gait cycles by using the plantar force and frame plot as shown in Figure 7-4.

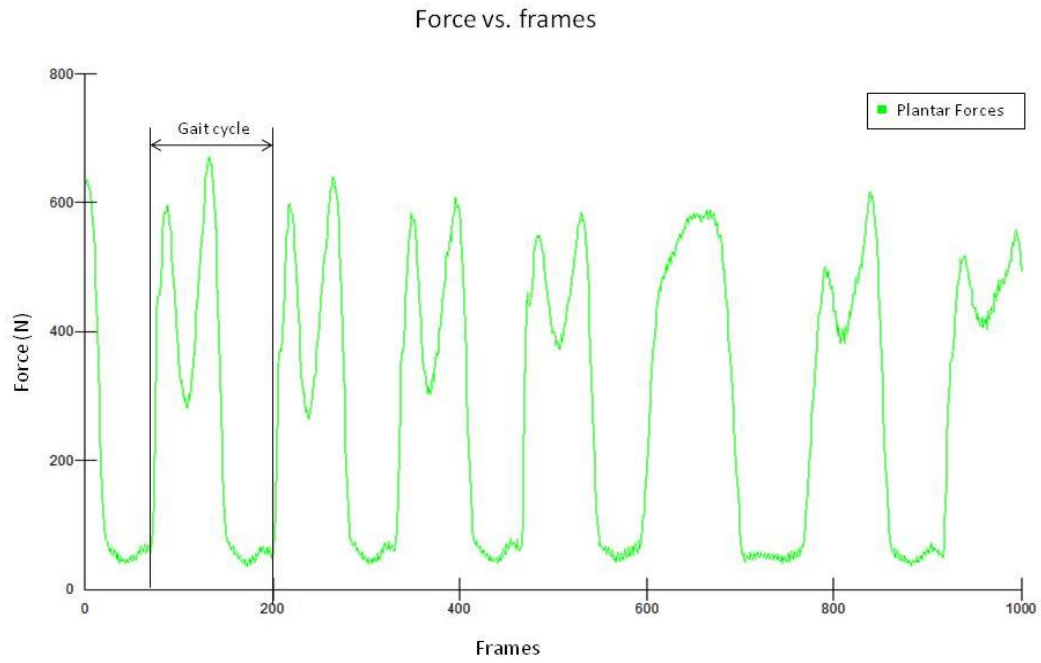

Figure 7-4: A plot of the plantar forces versus the number of frames

At every frame the sensor took a measurement, the frequency of the measurements was 127Hz. This value of frequency was the standard one used by the F-scan system. The sampling frequency was more than adequate for capturing the peaks in the forces during the gait cycle. Initial contact was found by locating the frame of data where the force started to increase significantly. This allowed six gait cycles to be located, the first and last gait cycles were not included because of incomplete data. The six gait cycles chosen for further analysis were from the subject's last walking test, this gave time for the subject to adjust to wearing the AFO. The data for each of the six sensors was split into sections using the Research Foot software (see Figure 7-5). These sections were chosen for the plantar foot sensor because they correspond to the heel, mid-foot and metatarsal/toe sections of the foot. The strap sensor was not split up and the other four sensors were split into three equal sections. The average pressures and maximum pressures for all six sensors were then exported into Excel.

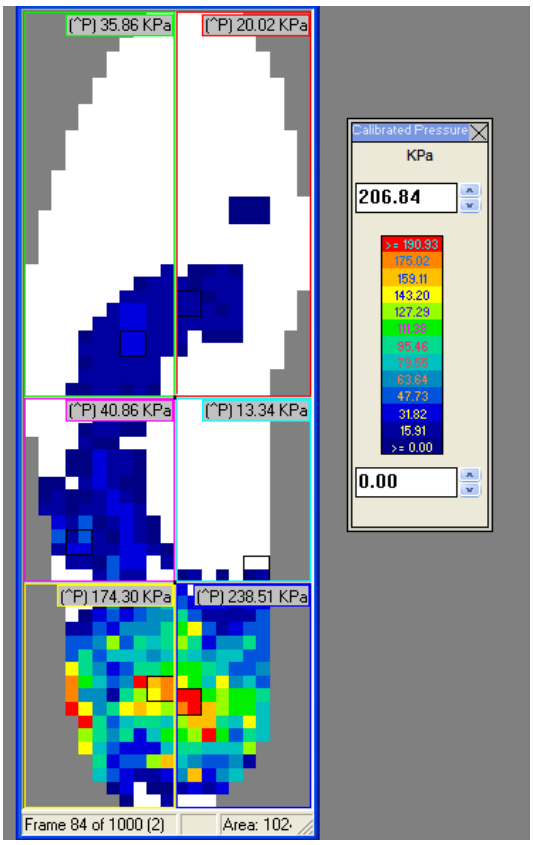

Figure 7-5: Screen shot of the Sensor being split into sections for analysis using Research Foot software

In Excel key points in the gait analysis were found including toe off, mid-stance, heel strike and mid-swing. The gait cycle was split into 60% and 40% sections for the stance and swing phases as documented by Gage et. al [**28**]. Heel strike was deemed to be at 10% of the gait cycle and toe off at 50% of the gait cycle. These were chosen because they were thought to be the times when the maximum pressures would occur. Initial contact and terminal stance were not used because they are instantaneous events at the beginning and end of stance phase [**28**]. This means at these points in the gait cycle the pressures will not have reached their peak values. Mid-stance was at 30% of the gait cycle and mid-swing at 80% of the gait cycle. The points of the gait cycle analysed are shown in Figure 7-6. For each section of each of the six sensors the average and maximum pressures at these time points were then averaged for the six gait cycles analysed. The standard deviation was also taken.

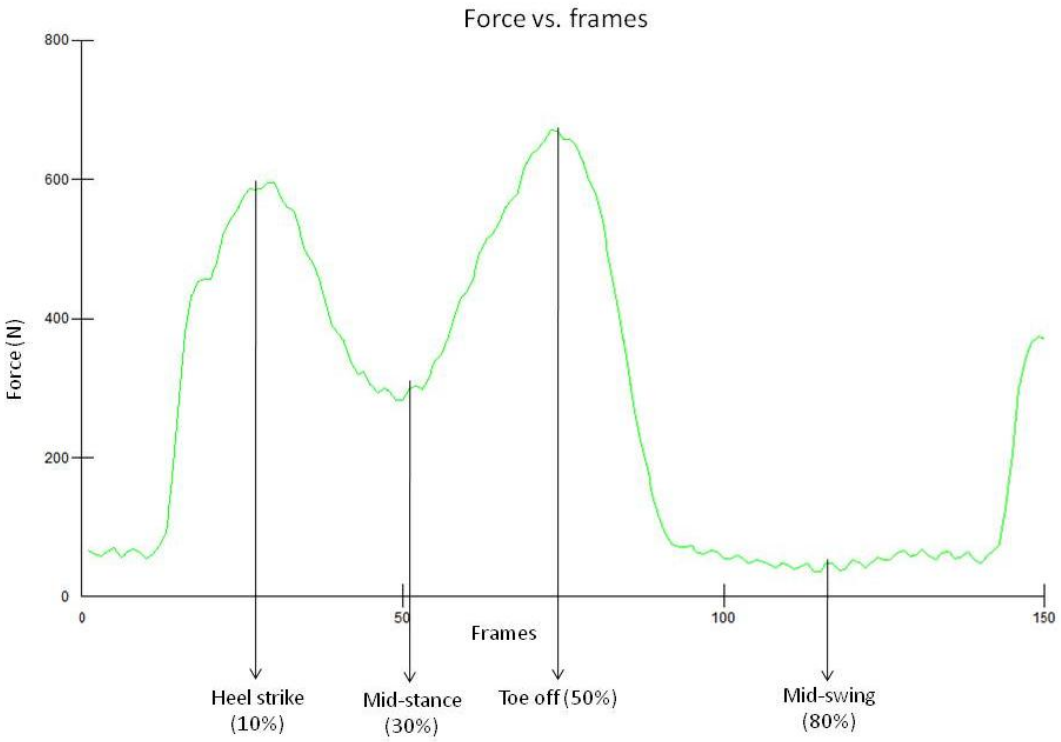

Figure 7-6: The positions in the gait cycle that were analysed

7.2.3. Experiment two

The Pedar system was calibrated previous to the current experiment and did not need to be recalibrated. The Pedar insoles were inserted into the AFO in two different positions (see Figure 7-7). One was positioned at the central calf section and the other in the plantar foot position on the AFO. Each insole contains 99 capacitive sensors.

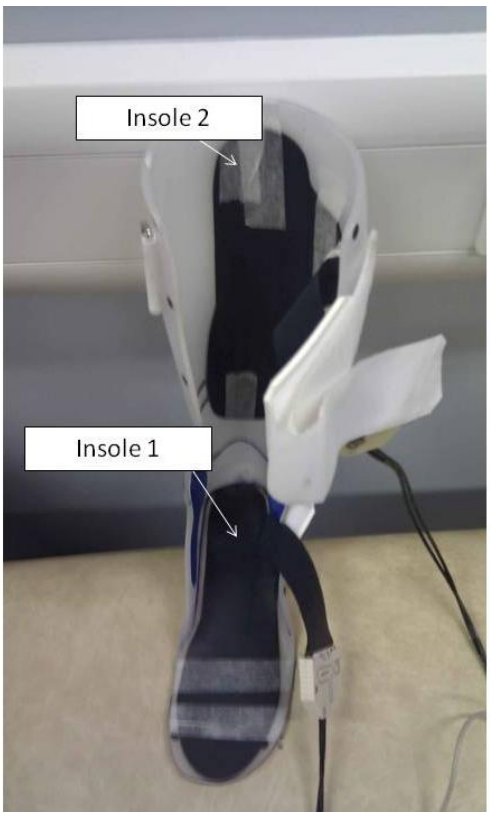

Figure 7-7: Insole positions 1: plantar foot position, 2: calf position

The insole sensors were connected to the Pedar X-box which then sent data to the laptop PC using a Bluetooth TM wireless telemetry system (see Figure 7-8).

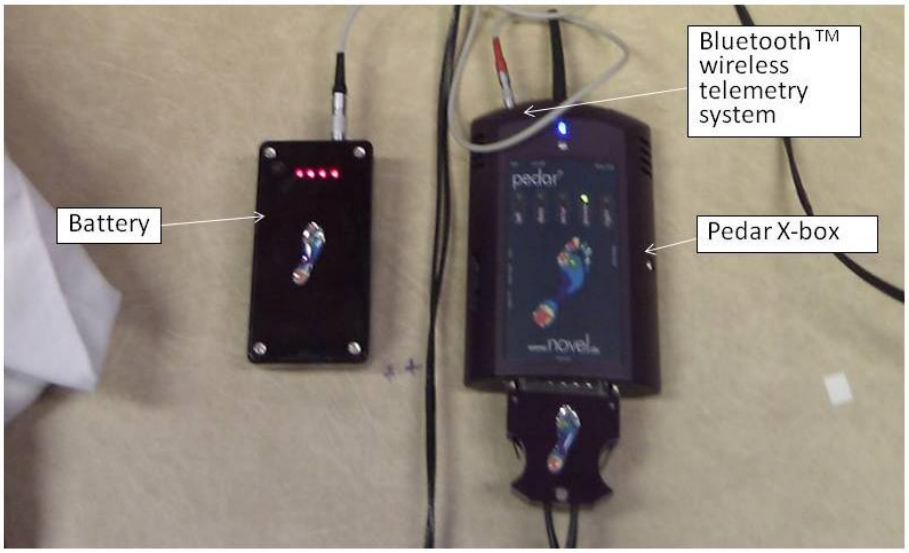

Figure 7-8: Pedar X-box and accessories

The first set of data was taken while the subject was seated, the second while the subject was standing and the third was taken during gait. The subject walked ten steps before needing to turn around, in total 60 steps were completed.

7.2.4. Experiment two data analysis

The data analysis for the pressures taken by the Novel system was similar to that done for the pressures taken by the F-scan system. The software packages Pedar-x Expert (version: 12.1.28, Novel, Germany) and Excel were used. The data was split into gait cycles by cutting the data at intervals dictated by the force versus time graph. Figure 7-9 shows three complete gait cycles, each one starts and ends where the force increases significantly. The Pedar system has a sampling frequency of 50Hz.

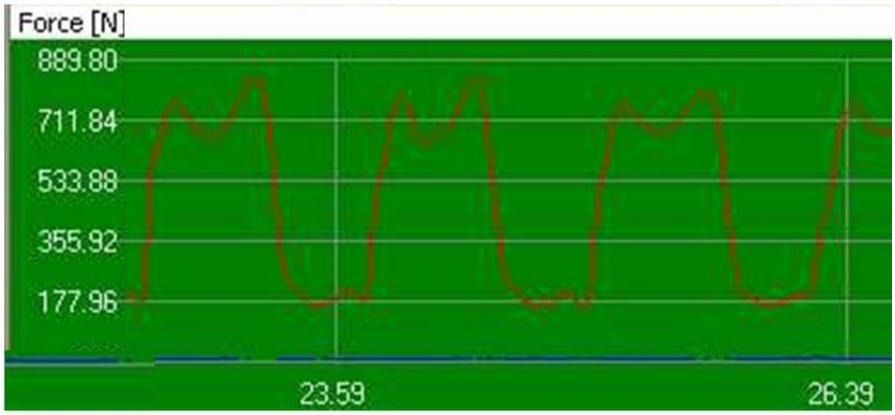

Figure 7-9: Screen shot of the force vs. time graph showing three complete gait cycles

There are 99 sensors located in each of the Pedar insoles and each one takes pressure readings. To make the results comparable to the F-scan system the results were exported to Excel and split into groups that corresponded to the positions that were detailed in the F-scan data analysis section. Figure 7-10 shows how this was done. For each individual gait cycle and each individual section the average pressures and maximum pressures were found. These were then averaged over six gait cycles. The six gait cycles were chosen towards the end of the walking test so that the subject had time to become familiar with the AFO.

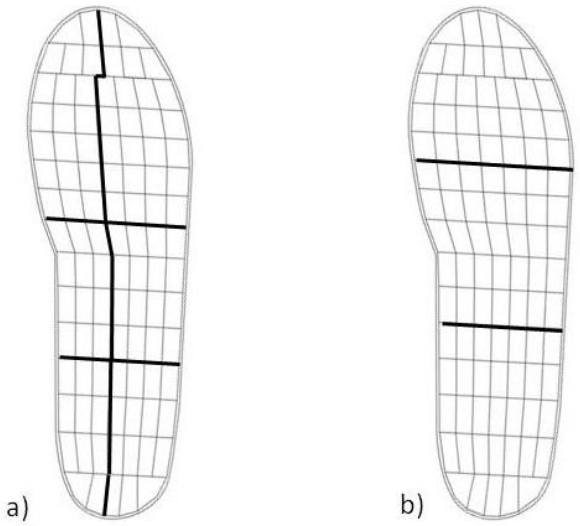

Figure 7-10: The Pedar sensors split into different sections for the plantar insole (a) and the calf insole (b)

7.3. Results

7.3.1. Experiment one

The F-scan system measured the highest pressures during toe off and heel strike. At toe off the highest pressures were measured by the metatarsal sensors and at heel strike the highest pressures were measured by the heel sensors. Both of these results can be seen in Figure 7-11, which shows the maximum pressures at different points of the gait cycle for the different positions measured on the foot. The pressures recorded at midstance are noticeably smaller than the ones measured at heel strike and toe off.

Figure 7-12 shows the maximum pressures measured by the other sensors located on the calf, heel and strap of the AFO. During stance phase the pressures measured on the calf, heel and strap were considerably lower than the ones measured by the foot sensor.

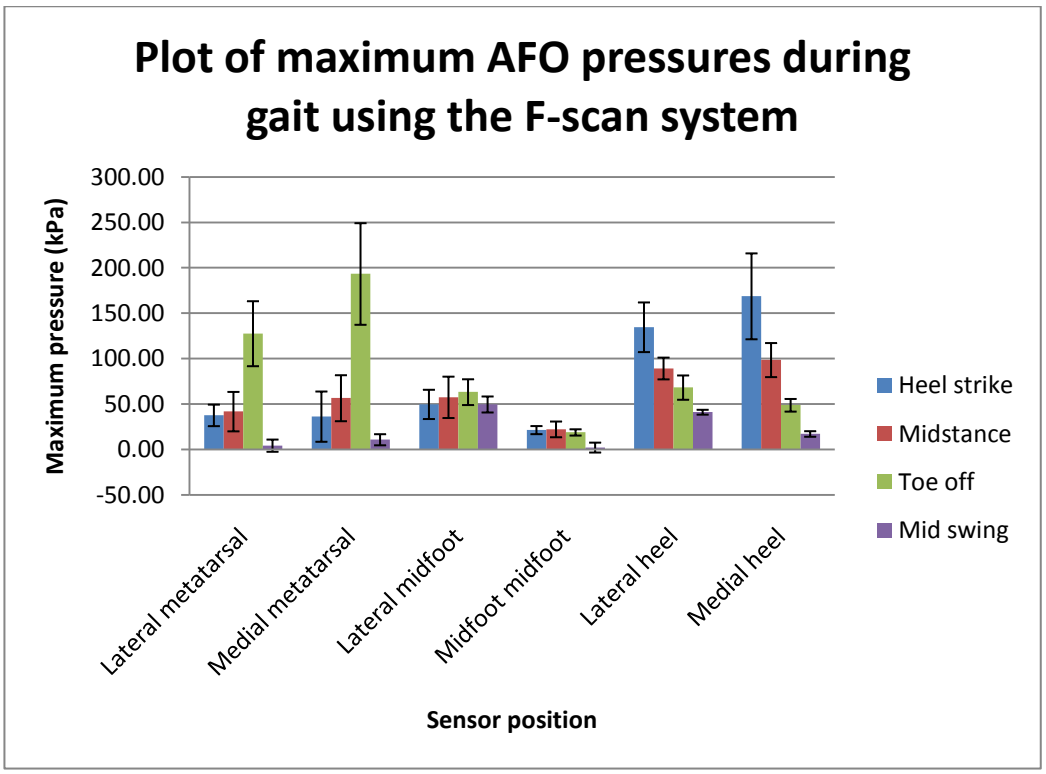

Figure 7-11: Plot of maximum pressures measured by the F-scan system during gait (1)

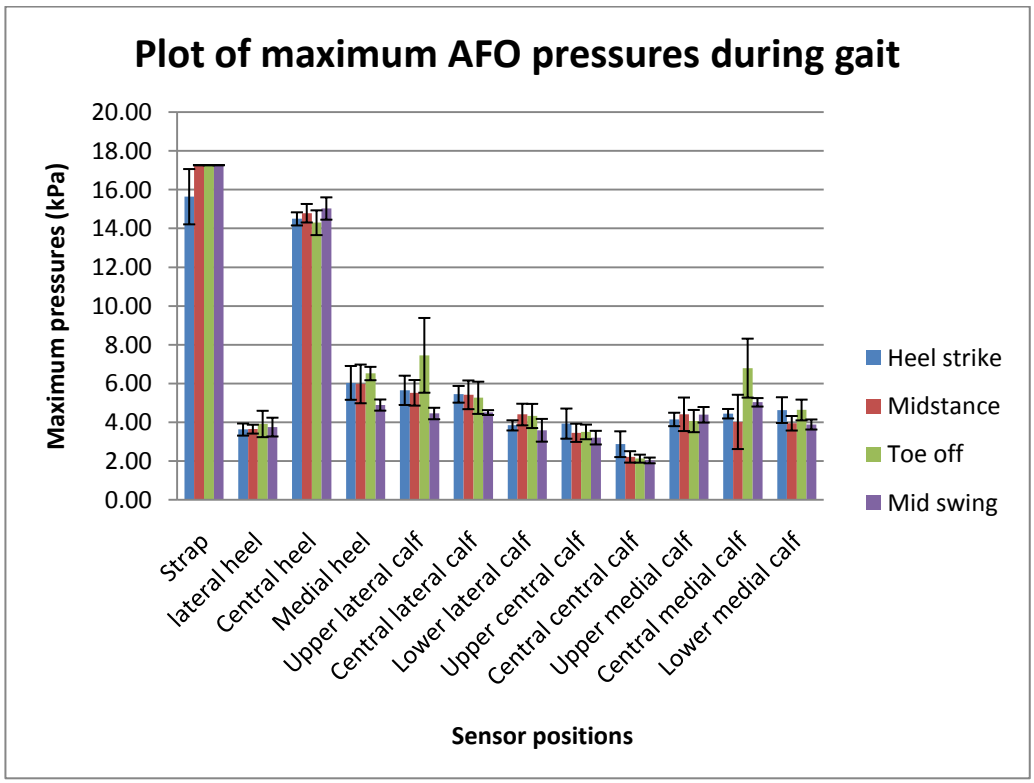

Figure 7-12: Plot of maximum pressures measured by the F-scan system during gait (2)

The maximum pressures measured by the central calf sensor are shown in Figure 7-13. The upper central calf section and central central calf section give an almost constant reading over the different gait cycles (frame 1-1000 is equivalent to six gait cycles). The lower central calf section is very sensitive and is constantly changing.

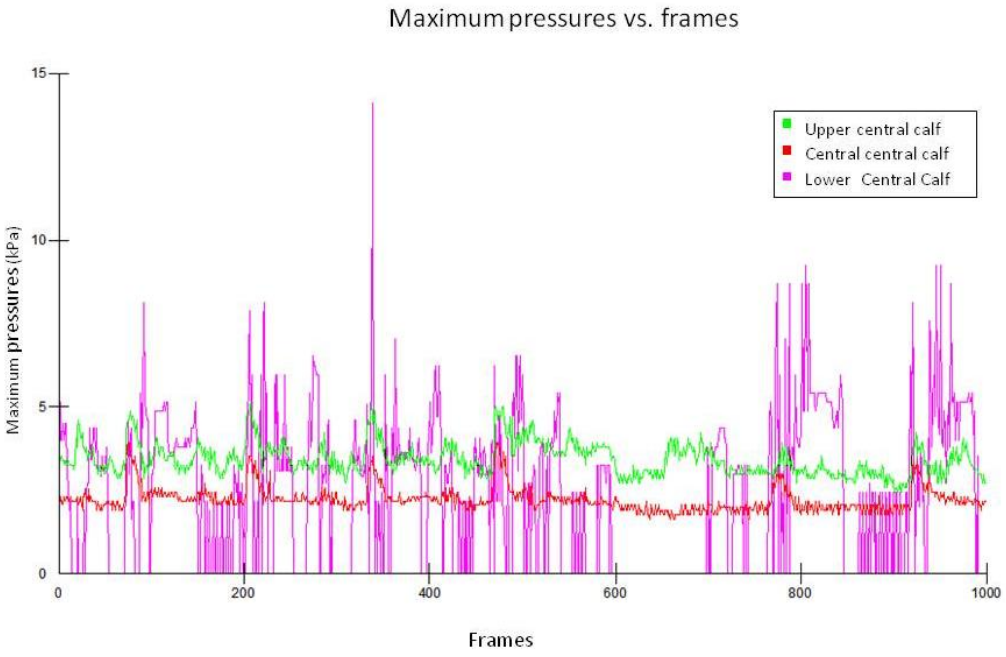

Figure 7-13: Plot of the maximum pressures measured by the F-scan system in the central calf position

The strap sensor measured a very constant pressure throughout the gait cycles; this is shown in Figure 7-14.

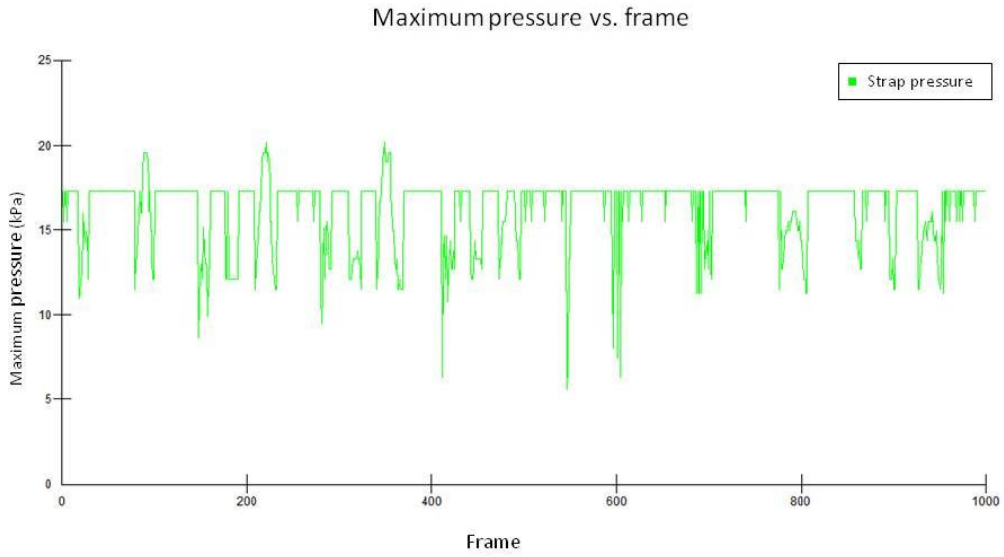

Figure 7-14: Plot of maximum pressures measured by the F-scan system in the lower strap position

7.3.2. Experiment two

After the results were recorded for the Pedar system it was immediately noted that the calf sensor did not record accurate results, this is shown in Figure 7-15. It is clear from the figure that the majority of the sensors were not taking readings.

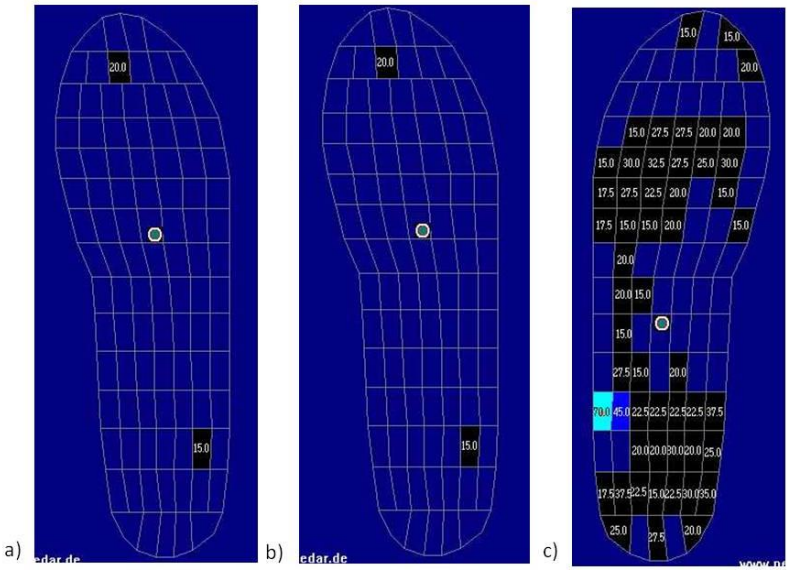

Figure 7-15: The pressure values (kPa) for the calf insole at mid-stance (a) and mid-swing (b) and the pressure values (kPa) for the plantar insole during mid-swing (c)

Figure 7-16 shows the maximum pressures recorded by the Pedar system during different points of the gait cycle and at the different sections of the foot. The highest pressures were recorded at heel strike, mid-stance and toe off. High pressures at the heel sensors were recorded during heel strike. At mid-stance high pressures were also recorded during heel strike. At toe off high pressures were recorded at both the metatarsal sensors and heel sensors. The recorded pressures for all the sensors were low during mid-swing.

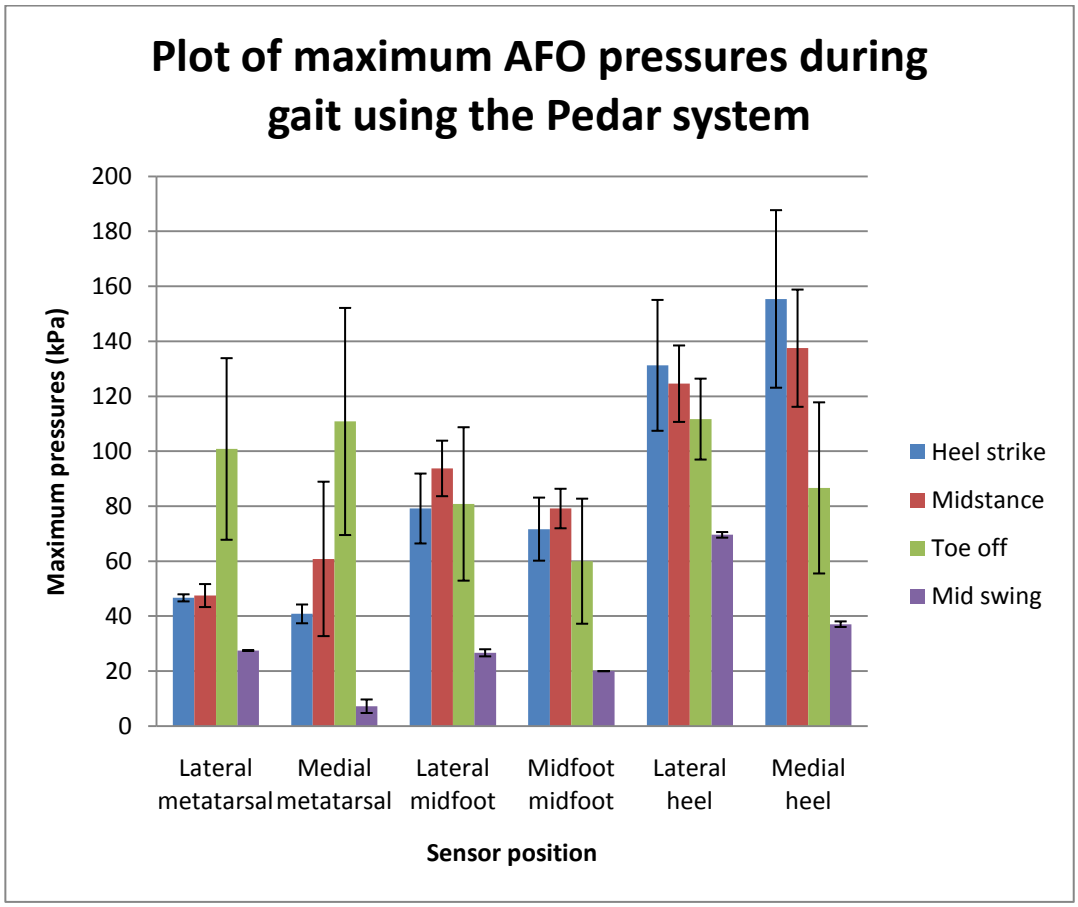

Figure 7-16: Plot of maximum pressures measured by the Pedar system during gait

7.3.3. Comparison between the two sensor systems

Two different types of sensors from two different manufacturers were used with the aim of measuring the same parameter. The data analysis was undertaken in a way that would allow a direct comparison between the two sensors. The only pressures that could be compared were the plantar pressures this was because the Novel calf sensor did not pick up any realistic results

Figure 7-17 shows the average AFO pressures during midstance measured by the F-scan system and the Pedar system. The average pressures measured by both systems at the metatarsal and midfoot sections are comparable, particularly when the standard deviations are taken into account. However, the F-scan system on average measured heel pressures that were 56% as large as the Pedar system values.

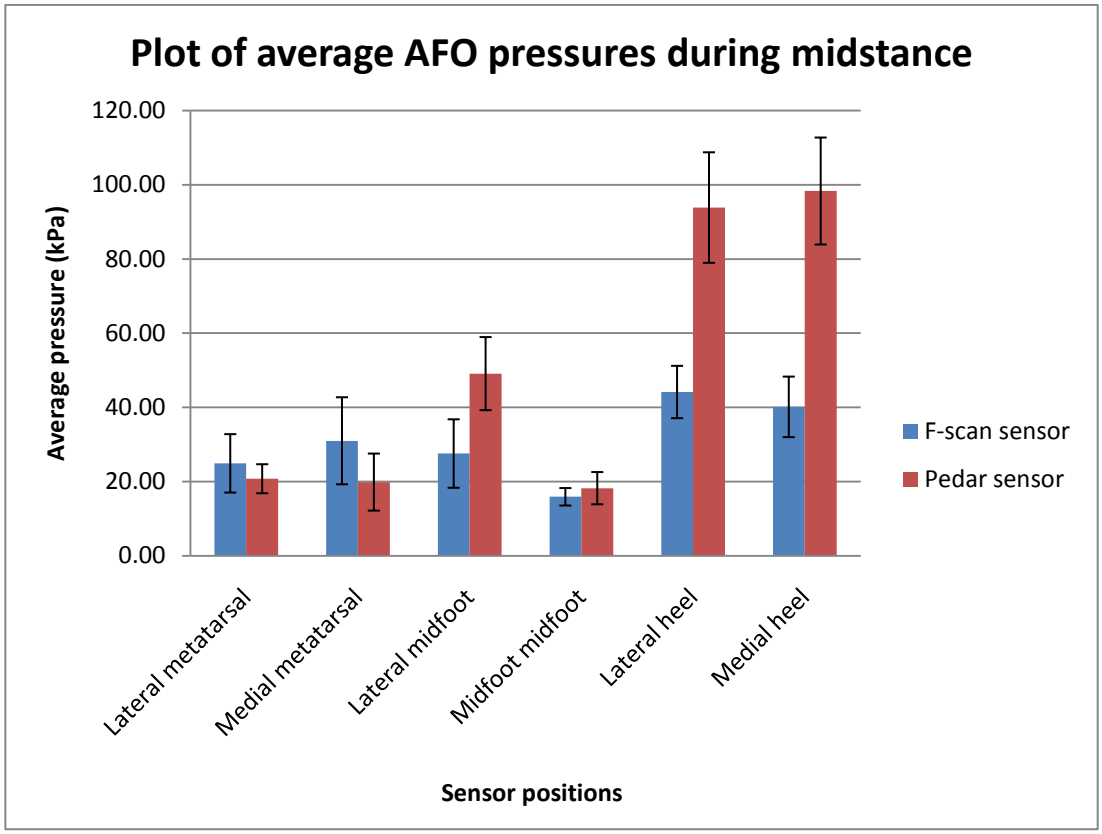

Figure 7-17: Plot of average AFO pressures during midstance for both sensors

Figure 7-18 shows the average pressures measured by both systems during toe off. The results again show that similar pressures were recorded at the metatarsal and midfoot sections. However, the heel pressures for the F-scan system on average were 59% as large as the Pedar system pressures.

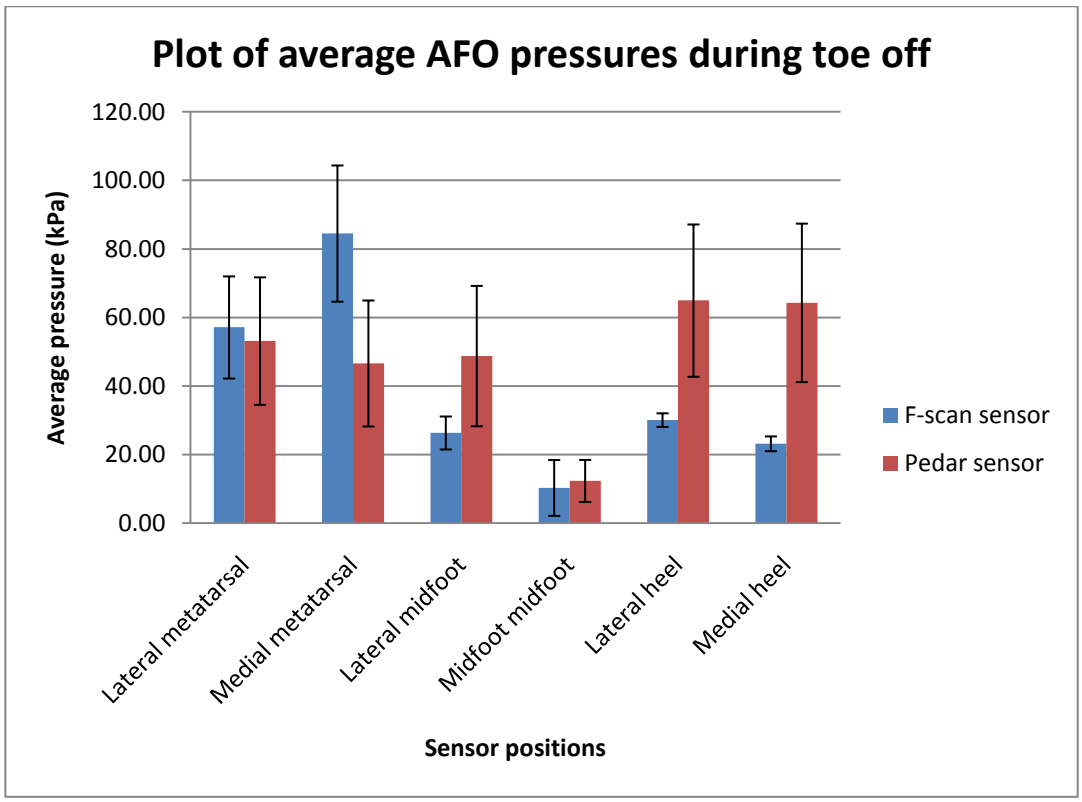

Figure 7-18: Plot of average AFO pressures during toe off for both sensors

7.4. Discussion

The maximum pressure results from the F-scan sensor show that the pressures measured at the calf section are considerably lower than the ones measured at the foot section. In the literature Nowak et. al [**45**] measured 0kPa average pressures at the calf during heel strike, toe off and swing points in the gait cycle, these results are comparable to this study. Not all the results were comparable, at midstance the average pressures found at the calf on average in this study were 13% as large as the ones measured by Nowak et. al. However, some of the results measured at the foot were comparable, including the average pressures at the metatarsals during heel strike for which this study had values within 1.5% of the Nowak et. al study. The fact that some results are very comparable and some are not might be explained by the inaccuracy of the calibration for the F-scan system [**43**]. It is still clear that the overall trend measured of high pressures at the foot area and low pressures at the calf area is in agreement with the literature [**45,47**].

From the results it was found that two of the sensors gave abnormal readings. In Figure 7-13 it is demonstrated that the lower central calf sensor is fluctuating and

not giving any clear readings. There is a possibility that the individual FSRs in one part of the sensor were damaged. In the FEA the pressures measured at this point were not applied, therefore the analysis could not be influenced by the abnormal results.

The F-scan system measured a constant pressure at the lower strap position (see Figure 7-14). From this result it is clear the sensor was measuring the tension in the strap. In the literature it is suggested that there would be a large force acting on the lower strap during swing phase [**103**]. The positions of the forces acting during stance phase would also suggest that smaller forces would act on the lower strap during this phase. Therefore it seems the sensor was not taking accurate readings of the pressure being applied by the subject.

It was found that the Pedar sensor could not be used to measure pressures on the calf section of an AFO (see Figure 7-15). This is thought to be because the sensors have a threshold that needs to be reached before the sensors work. The system is designed for measuring foot pressures which are considerably higher than the pressures acting from the calf [**45**]. If the capacitive technology was applied to a sensor that was designed for measuring lower pressures then more accurate results could be obtained. Another reason for the lack of accurate measurements at the calf could be the shape of the sensor. The Pedar sensor was foot shaped whilst the F-scan sensors used for the calf were a rectangle shape. This made it easier to fit the F-scan sensors to the AFO. The F-scan sensors were also much thinner, which also contributed to the ease of fitting in comparison to the Pedar system.

The results from the two pressure measurement experiments indicate that although the results are similar there are some differences in the accuracy of the two technologies. The main differences occur on the heel sensors (see Figure 7-17 and Figure 7-18). One reason for this could be that in the data analysis the number of sensors that made up the selected heel area was larger for the Pedar analysis than the F-scan analysis. The literature suggests that the Pedar system is the more accurate and reliable of the two sensor systems [**50**]; this is why the pressures from the Pedar system were used on the foot section of the AFO in the FEA. Ideally results from the Pedar system would also be used for the calf section but because of problems with the system there were no results to use.

Differences in the heel pressure measurements could have occurred because of a difference in the subjects walking. Steps were taken to minimise this problem by analysing the last set of gait cycles for each experiment. However, the experiments were still conducted four days apart and the fact that one set of equipment (the F-scan system) was wired to the computer might have also affected the subject's gait.

A limitation with both the F-scan sensor and Pedar sensor technology is that they both involve measuring a parameter that is inversely proportional to the distance between two surfaces. If the sensor is applied across a curved surface then as a consequence the two surfaces risk becoming closer together at certain points. This will mean a load will be measured even though one has not been applied. Consequently the pressures recorded by the F-scan sensor in the calf and achilles tendon positions have to be viewed with caution.

Although there were potential error sources in the measurement of the pressures, results were successfully obtained and could be used to apply loads to the AFO FE model that accurately represent the loads acting during gait.

Chapter 8. Digital Scanning

8.1. Introduction to digital scanning

Before any analysis of the AFO can begin there needs to be an accurate digital geometric model of it. One way of re-creating the geometry is to use a digital scanner, this was thought to be a fast and accurate method.

8.2. Methodology and Instrumentation

The AFO that was used in this study was custom made for a healthy individual by the National Centre of Prosthetics and Orthotics (University of Strathclyde, Glasgow, UK). The AFO is a solid AFO made from polypropylene with two straps. The digital scanner (Konica Minolta, Japan) was set up to take four step scans; at 90° intervals. Before the scanning took place the AFO was attached to a turntable (see Figure 8-1 and Figure 8-2). Metallic clips were used to attach the AFO (not shown in the figures) and these did appear in the digital scans of the geometry.

Figure 8-1: Digital scanner setup

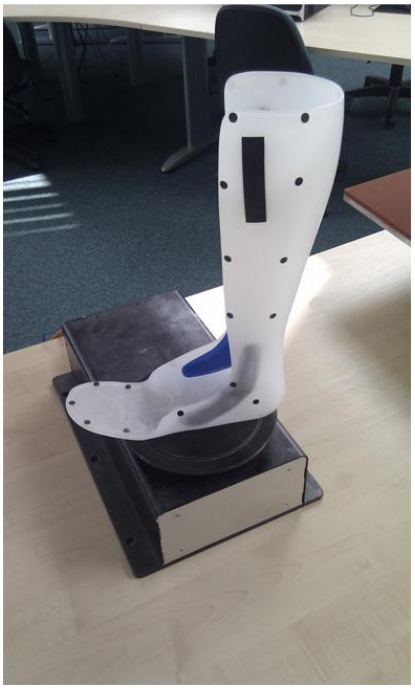

Figure 8-2: AFO and turntable

The images were sent from the laser scanner to the PC and were loaded into the Polygon Editing Tool software (Konica Minolta, Japan). It was clear from the information of the scans that detail was missing from the foot section of the AFO, therefore a fifth scan was taken. The fifth scan was taken by rotating the AFO so that the foot section was perpendicular to the digital scanner lens.

The information from the five scans was then exported into Geomagic Studio 10 (Version 10, Geomagic Inc, USA). In this software program the excess data from the scan was deleted. The scans were then merged together using a process that involved registering common points to all the scans. To do this, easy to find points were used for example the top corners of the AFO. After the scans were merged editing took place to smooth out any rough edges, fill any holes in the data and to remove any excess data from the merging of the scans. At this stage of the process the model is made up of polygons; these needed to be converted into NURBS (non-uniform rational b-spline) surfaces to allow the file to be exported to FEA software [**104**]. A combination of automatic and manual tools in Geomagic were used to do this. The software detected the contours of the geometry and used lines to define different regions of the geometry. These regions were then subdivided into patches. The number of patches was specified to be approximately 1000; this was determined through a process of trial and error. It was discovered that a model made up of 1000 patches allowed a sufficient amount of geometric information to be exported so the FEA software could accurately create the geometry. It was also discovered a higher number of patches would have caused computation problems in the FEA software because of the high number of nodes needed. The model was then exported into the FEA software Ansys (Ansys, USA) as an IGES file.

8.3. Results

Figure 8-3 shows the data from a single scan in the Polygon Tool Editing software. It is clear the amount of data that needs to be deleted.

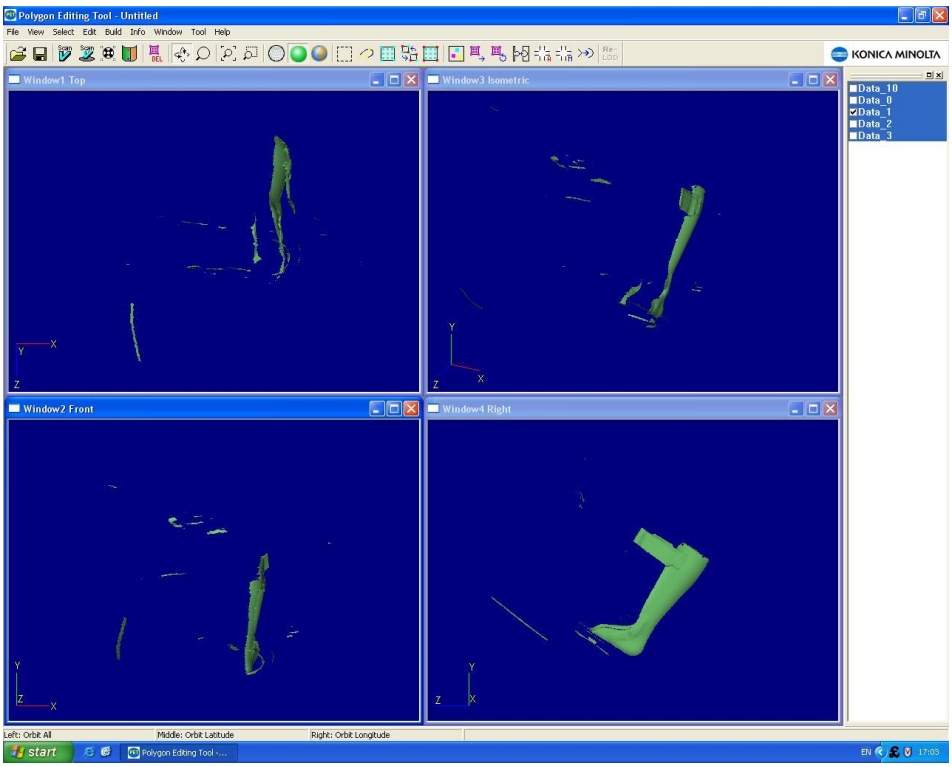

Figure 8-3: Data from a single scan of the AFO

The steps taken in the Geomagic software can be seen in Figure 8-4. In the figure (a) shows the initial merging of the first four scans and (b) shows the addition of the 5th scan. In the image (c) shows the filling of the holes and the smoothing of any rough edges. Finally in the image (d) shows the geometry split into patches. Figure 8-5 shows the geometry after it was imported into Ansys. The meshing of the geometry shown in Figure 8-5 is discussed in section 9.2.

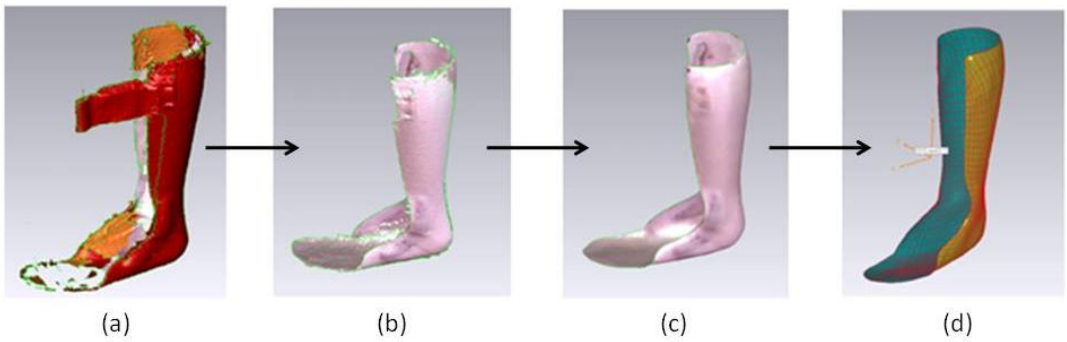

Figure 8-4: The progressive editing steps made in the Geomagic software

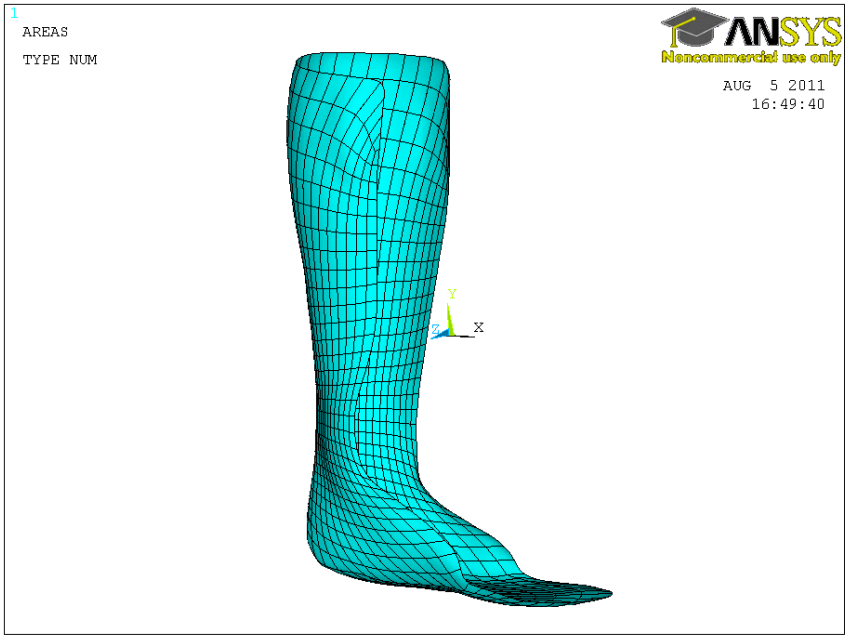

Figure 8-5: The AFO geometry inside the FEA software (before being meshed)

8.4. Discussion

There are possible sources of errors when capturing the geometries of physical objects using a digital scanner. In this study a particular source of errors was the fifth scan which captured the bottom of the AFO foot. Care was taken to ensure the AFO foot section was positioned so it was perpendicular to the digital scanner viewing angle. However, when the scan was completed the profile of the digital AFO foot was not as uniform as the geometry of the actual AFO foot. Several scans were taken to achieve the best result, but there still remained errors in the geometry.

Another possible source of errors is the merging of the scans. To merge two scans together approximate locations were chosen that appeared in both of the scans. This gave the Geomagic software points to align the two scans so that the data could be merged together. As the locations were approximate this will have lead to errors in the geometry of the AFO.

Nevertheless the digital scanning method used was considered to be the most accurate method of capturing the AFO geometry and creating an FE model. Even

though errors are associated with the method, it is still thought to create superior geometries to other methods, for example using CAD modelling from the physical object.

Chapter 9. Finite Element Analysis of the AFO

9.1. Introduction to the finite element analysis of the AFO

In the previous two chapters the pressures acting on the AFO have been determined and the geometry of the AFO also determined. The results of these experiments will now be combined to analyse the loads acting on an AFO in FE software. This chapter begins with a section that details the methodology and instrumentation of the work done prior to the start of the analyses. The next section of the chapter describes each analysis individually. An iterative approach was taken to using the FE software, therefore changes to the methodology had to be made and these are detailed in the individual analysis sections. Each analysis was designed to build on the accuracy of the last analysis. The individual analysis sections also contain results and a short discussion. At the end of the chapter is a summary of the analyses and their results. The next chapter discusses the results further.

9.2. FE model development and analysis

To do the FEA the software Ansys (version 12, Ansys, USA) was used, the steps described in section 5.2 were followed.

9.2.1. Element type

As mentioned in section 5.2 the field variable in a stress analysis is displacement. The element type used for this analysis was an eight noded shell (SHELL281). SHELL281 has eight nodes with six degrees of freedom at each node; translations in the x, y and z axes and rotations about the x, y and z axes [**105**]. This shell element was chosen because it is suitable for analysing thin to moderately-thick shell structures [**105**] and the AFO is considered to be a shell structure. It is also well suited for large strain nonlinear applications and has a special feature of being able to compute plasticity analyses [**105**]. Non-linear analyses were attempted in this study and therefore this was an appropriate element type. With this type of element there are certain interpolation functions that are applied within Ansys.

9.2.2. Geometry

When the geometry of the AFO was imported into Ansys the next stage was to generate a mesh so that Ansys could determine where the nodes and elements were located (step 2 of FEA: discritise the continua). The meshing options used were the default settings chosen by Ansys and the meshing was done from the areas (the patches defined in the Geomagic software) that made up the FE model. The mesh size chosen was one with 18530 nodes and 6153 elements (see Figure 9-1). A check was done to see if this mesh resolution allowed adequate convergence of the stresses in the model (see section 9.3).

Figure 9-1: The meshed geometry with 18530 nodes and 6153 elements

The program Ansys allows analyses to be done with linear geometry or non-linear geometry. Non-linear analyses are achieved by activating large displacement effects. When large displacement effects are active it means that Ansys accounts for the change of stiffness due to geometric changes during deformation [**21**]. The analyses were initially undertaken with linear geometry (the large displacement effects inactive).

9.2.3. Material properties

The next stage of the FEA was to define the material properties. Two types of analysis were attempted to be undertaken; one with linear material properties and one with non-linear material properties. For the linear material analysis the Young's modulus of homopolymer polypropylene was assumed to be 1300 MPa and the poisons ratio 0.35; values found in the literature [**21,106**]. The material properties were also assumed to be elastic and isotropic. Details of how the non-linear material properties were defined are listed in section 9.10.

9.2.4. AFO Thickness

Two more analyses that were undertaken include a model with a constant AFO thickness and one with a variable thickness. The thickness of the AFO was inputted to the FE after results were taken from a practical experiment (see Figure 9-2). This involved using a thickness gauge and a vernier to measure the distance from one side of the AFO to the other.

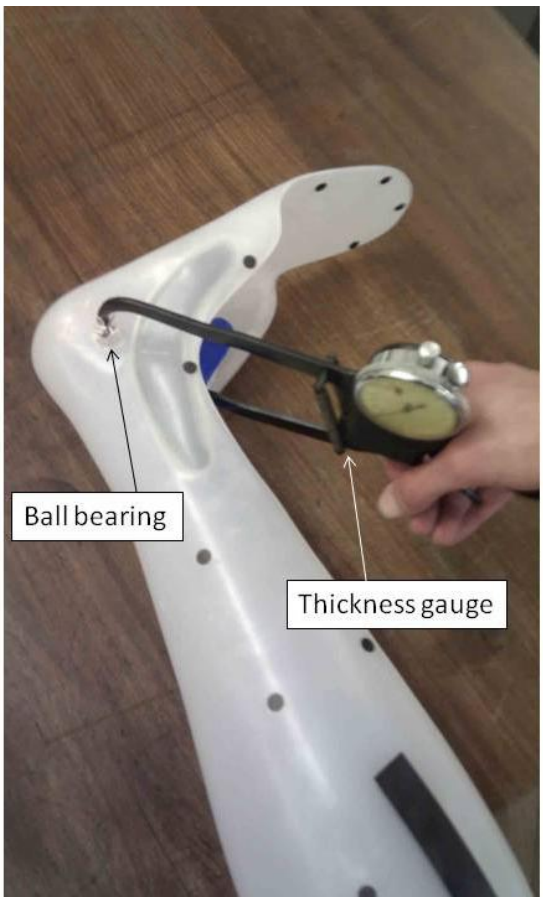

Figure 9-2: The setup for measuring the thickness of the AFO (using the thickness gauge)

To make measurements with the thickness gauge, ball bearings were attached with white tack to either side of the AFO. To calculate the AFO thickness the diameter of the two ball bearings was subtracted from the total value displayed by the thickness gauge. This allowed for a more accurate measurement because the surface of an AFO is not flat. There were nineteen measurements taken on the calf section of the AFO (eight on the lateral side, eight on the medial side and three on the posterior side). Eight measurements were taken on the plantar foot section of the AFO and four measurements taken on the ankle section of the AFO (two on the lateral side and two on the medial). Each measurement position was marked with a black dot (see Figure 9-2). The measurements were taken three times and an average of these results was taken. The measurements at the edges of the AFO were taken using the vernier and the measurements towards the middle of the AFO were taken using the thickness gauge. Some locations on the AFO were impossible to reach with the range of the thickness gauge. The FE model was split up into

corresponding sections that matched the location of the measurements. The average thickness value for that section was then inputted into the model. In total there were thirteen sections. Thickness values found at the heel were 49% of those found at the lower medial calf section (the location of the maximum thickness). The thickness values found at the ankle trim were 90% of those found at the lower medial calf section. These values are similar to those found in the literature [**21**]. See appendix A for all the measurement values, positions of the measurements and the positions of the sections the AFO was split into.

For the analyses with a constant thickness (analyses 1-3) the average of all the thickness values was taken and this was determined to be 3.76mm.

9.2.5. Boundary conditions - loads

The next stage in setting up the analysis was to insert the loads into the FE model. Average pressures from the Pedar system were applied to the foot position of the AFO. The average pressures from the F-scan system were applied to the calf section of the AFO. Pressure was only applied in the sections of the AFO where the sensors were positioned during the practical experiments. It was decided to take the average pressures from the point of time 50% into the gait cycle, which represents toe off. Toe off (at 50%) was chosen as a point in the gait cycle to analyse because it is where the largest ankle moments are generated (see section 2.3.1)

Analytical calculations were undertaken to calculate the loads acting on the straps. A free body diagram (see Figure 9-3) shows the loads acting on the AFO. The ground reaction force was taken from a previous experiment done by Solomonidis et. al. [**107**]. This experiment involved using the force platform in the University of Strathclyde's Bioengineering Unit laboratory to calculate the forces and moments acting on a subject wearing an AFO during gait. The same AFO and the same subject were used as in the pressure measurement experiments. From the data collected by the force platform the centre of pressure (COP) could also be calculated. This is shown by G in Figure 9-3 and it is where the ground reaction force is acting. The same experiment also used the Vicon system in the University of Strathclyde's Bioengineering Unit laboratory to calculate the knee and ankle joint

centres as the subject walked over the force platform. This information allowed the calculation of the angle between the ground and the AFO.

Both the ground reaction force and the ground to AFO angle were calculated at a point 50% into the gait cycle (at toe off). This point in time could be calculated using a similar method as used in the pressure measurement experiments. The force in the y direction was found to increase significantly at initial contact. Two points were found in the data where this happened and this was deemed to be one complete gait cycle. A point 50% into the data was then found. Both the force platform and Vicon system sampled data at 100Hz.

The foot force was a value calculated by the F-scan software that was used to measure the pressures. To be consistent the force was acting at a time point 50% into the gait cycle. This force is acting at point O in Figure 9-3, which is the COP on the AFO foot area as calculated by the F-scan software. Moments were taken about the ankle centre (where the lower strap connects to the AFO) to calculate the force that acts at the strap at the top of the AFO. The forces in the horizontal and vertical directions were then summed to find the force acting at the lower strap. Full calculations and results are documented in appendix B. The strap loads were added to the Ansys model as point loads acting at position A and C (see Figure 9-3). To position the loads at the correct angles two sets of local coordinate systems were created in the Ansys model. The angles are documented in appendix B.

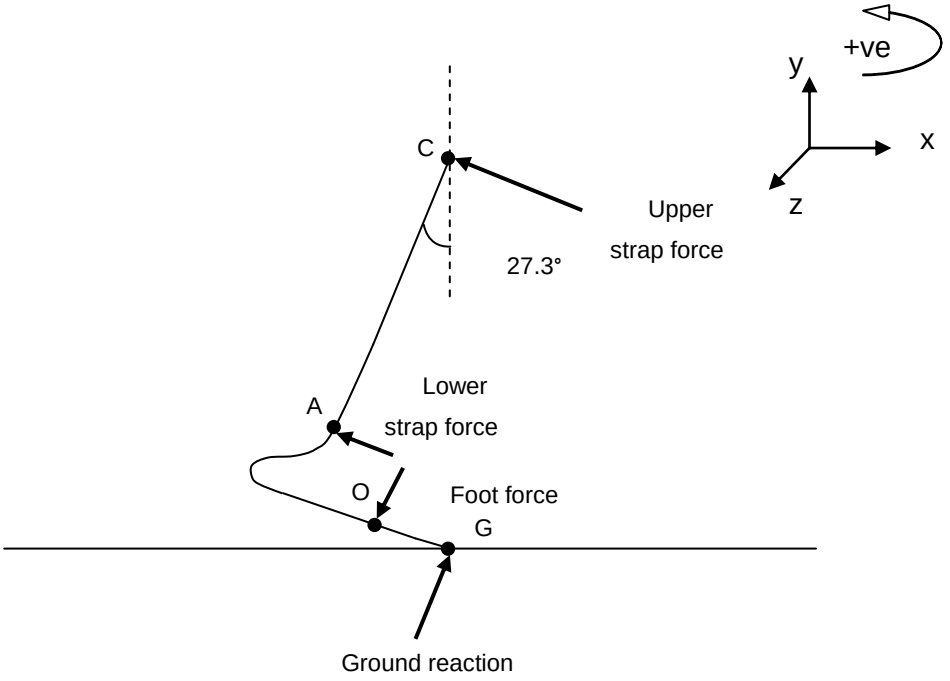

Figure 9-3: A free body diagram showing the forces acting on an AFO during toe off

The loads were halved so that they could be applied to both the medial and lateral sides of the AFO. Figure 9-4 shows all the loads being applied to the model in Ansys.

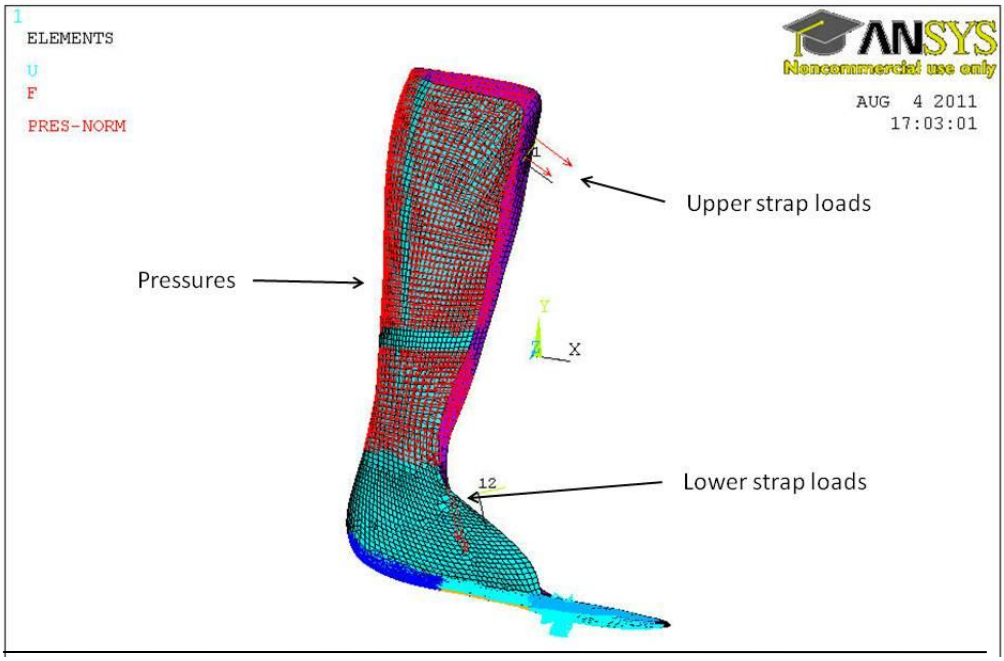

Figure 9-4: A screenshot of Ansys indicating the loads being applied to the AFO

9.2.6. Boundary conditions - displacement constraints

The displacement constraints that were applied to the model were applied to simulate toe off. The initial displacement constraints that were applied to the model were a line of nodes across the bottom of the AFO foot section. They were positioned at the approximate COP (as calculated by the force platform experiment and detailed in appendix B). The nodes were then constrained in the translational x,y and z directions. At the same nodes the AFO was free to rotate in any direction. Figure 9-5 shows where the constraints were applied.

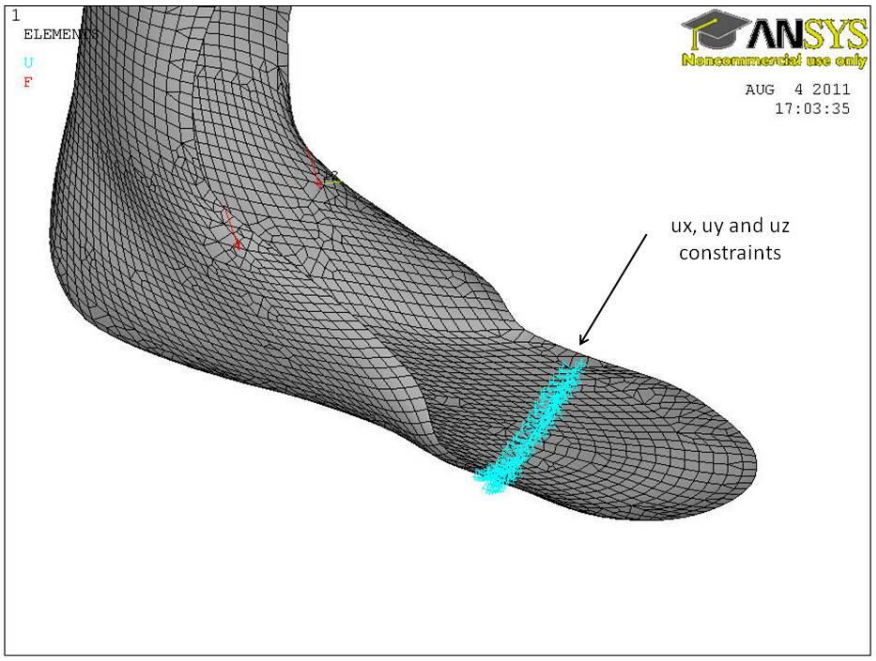

Figure 9-5: A screenshot of Ansys that depicts the displacement constraints at toe off

9.3. Mesh sensitivity study

Before any analyses were started, a mesh sensitivity study was undertaken. The following section is referenced from an online FE tutorial [**108**]. A mesh sensitivity study establishes how fine a mesh needs to be for a particular model. An important parameter is chosen for example Von Mises stress and then an analysis is performed with a nominal size of mesh. The analysis is then repeated with a coarser mesh and the results are compared. If the results are comparable then the coarser mesh is adequate for that problem.

For this mesh sensitivity study the parameter Von Mises stress was chosen. This was because it is a widely accepted predictor of yielding for problems such as this one, where a multi-axial state of stress exists [**109**]. For the mesh sensitivity the material properties were linear and the thickness of the shell elements was kept constant (see section 9.2.3 and 9.2.4 for details). The loads were simplified to two force point loads of 90N each acting at the top of the calf section of the AFO (see Figure 9-6). The displacement constraints applied were a region of nodes in the midfoot section of the AFO (see Figure 9-6). The element edge length was then specified to be different values and the Von Mises stresses calculated for each

element size. All other properties of the analysis were kept constant. Table 1 shows the results.

The results from analyses one to four show that a change in element length between 9mm and 6mm makes negligible difference to the maximum Von Mises stress. There is however, a 7.41% difference in the maximum Von Mises stress between having a mesh with element edge lengths of 6mm and 5mm. This suggests that having a mesh with element edges length of 5mm would give more accurate results. However, a finer mesh (one with an element edge length of 4mm) could not be analysed because of the node limit of 31,000 in the academic version of Ansys. This meant that the further convergence of the maximum Von Mises stress values could not be confirmed. The analysis with an element edge length of 5mm gave the greatest computational time. If the computation time was too great then it would have impacted on the number of analyses that could have been conducted in the project time. Therefore to achieve a balance between accuracy and appropriate computation time it was decided to choose the element edge length of 6mm. This created a model with approximately 18000 nodes and 6000 elements.

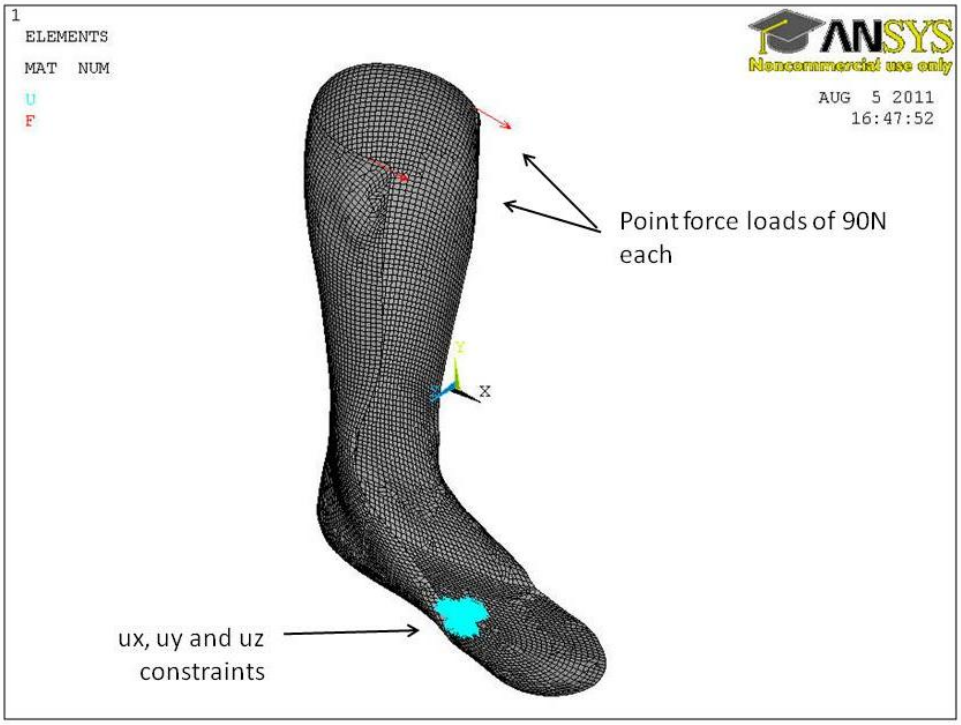

Figure 9-6: The boundary conditions applied to the AFO for the mesh sensitivity analysis

Table 1: The mesh sensitivity results

Mesh sensitivity analysis number	Analysis parameters			Results	
	Element edge length (mm)	Nodes	Elements	Maximum Von-Mises stress (MPa)	% difference of max Von-Mises stress between analyses and analysis 1
1	5	24727	8206	390.60	-
2	6	18530	6153	361.65	7.41%
3	7	14082	4681	361.67	7.41%
4	8	11366	3773	361.73	7.39%
5	9	9720	3231	366.05	6.29%

9.4. AFO analysis one

The first analysis was conducted with a model that had a constant thickness, linear material properties and only small displacements active. From the results of the analysis it was clear that the boundary conditions that were applied to the model did not constrain the model in an accurate way. The displacement at the top of the AFO was 431mm, which is too large to be accurate (see Figure 9-7). The model needed more constraints to prevent this large displacement from happening. The leg would provide a constraint at various places on the AFO. It was decided to constrain the AFO at the top in the y and z directions. This would allow the AFO to move forwards with the movement of the leg but would stop the movement in the lateral and longitudinal directions. Syngellakis et. al [**21**] used a similar technique, in addition to the original constraints that they applied to their FE model they added an extra constraint in the z direction to reduce rigid body rotation. Figure 9-8 shows the boundary conditions that were applied to analysis two.

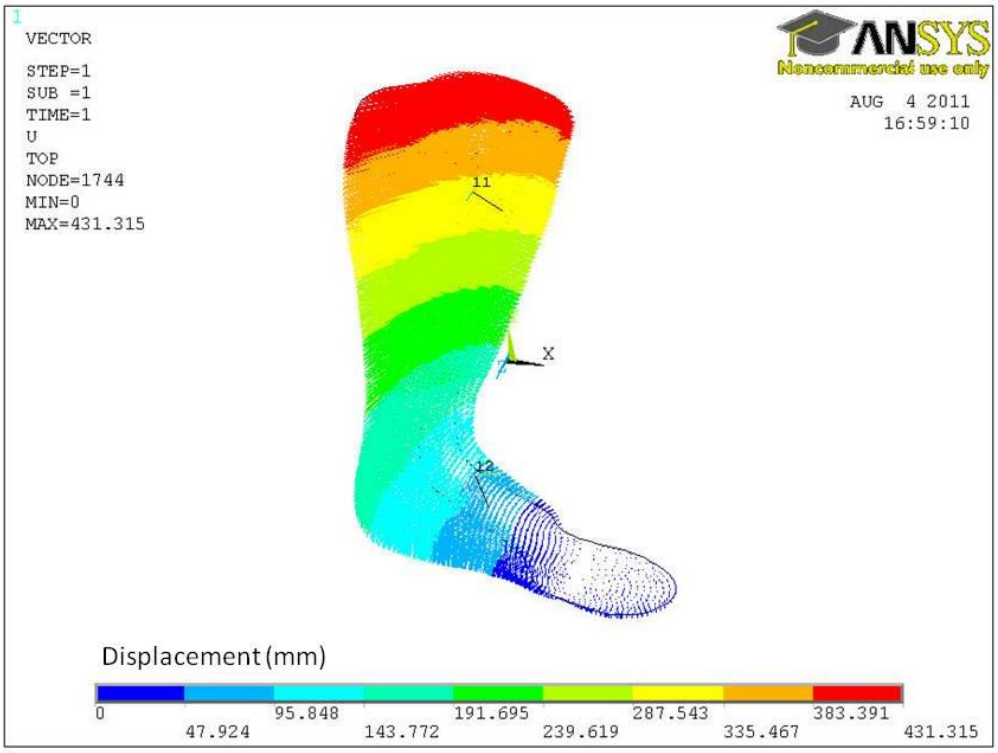

Figure 9-7: A vector plot of the displacements for analysis one

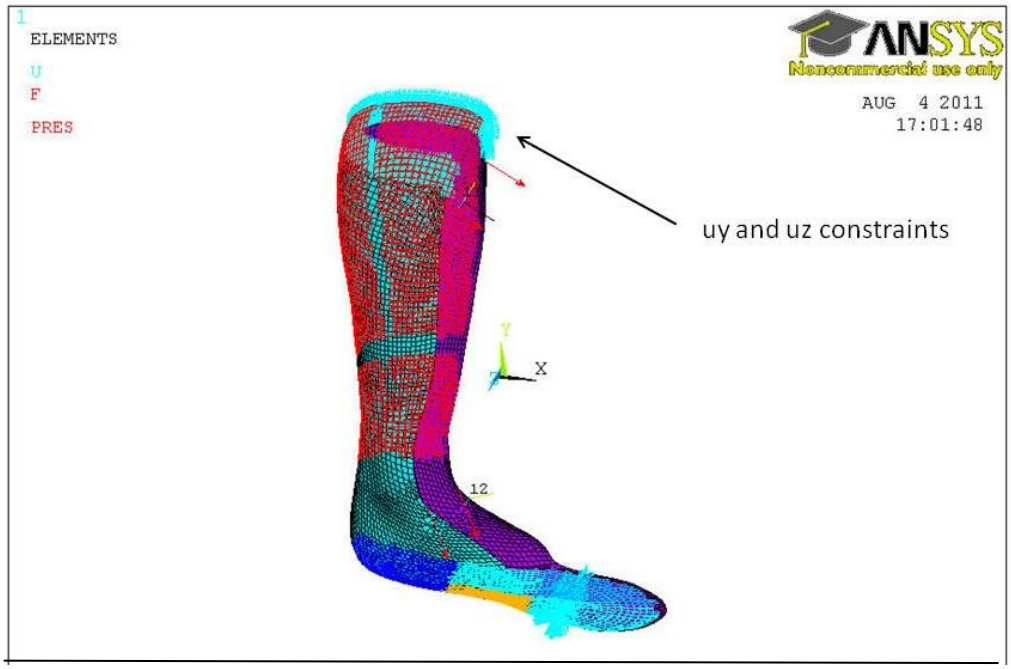

Figure 9-8: The extra boundary conditions that were applied to analysis two

9.5. AFO analysis two

In the second analysis the properties of the model were exactly the same as analysis one, the only difference was the increase in the number of constraints. The results from the analysis show that the new constraints made a large difference to the amount of displacement at the top of the AFO (see Figure 9-9). A much reduced displacement of approximately 4mm was found. At the toe region of the AFO a displacement of 13.76mm was found.

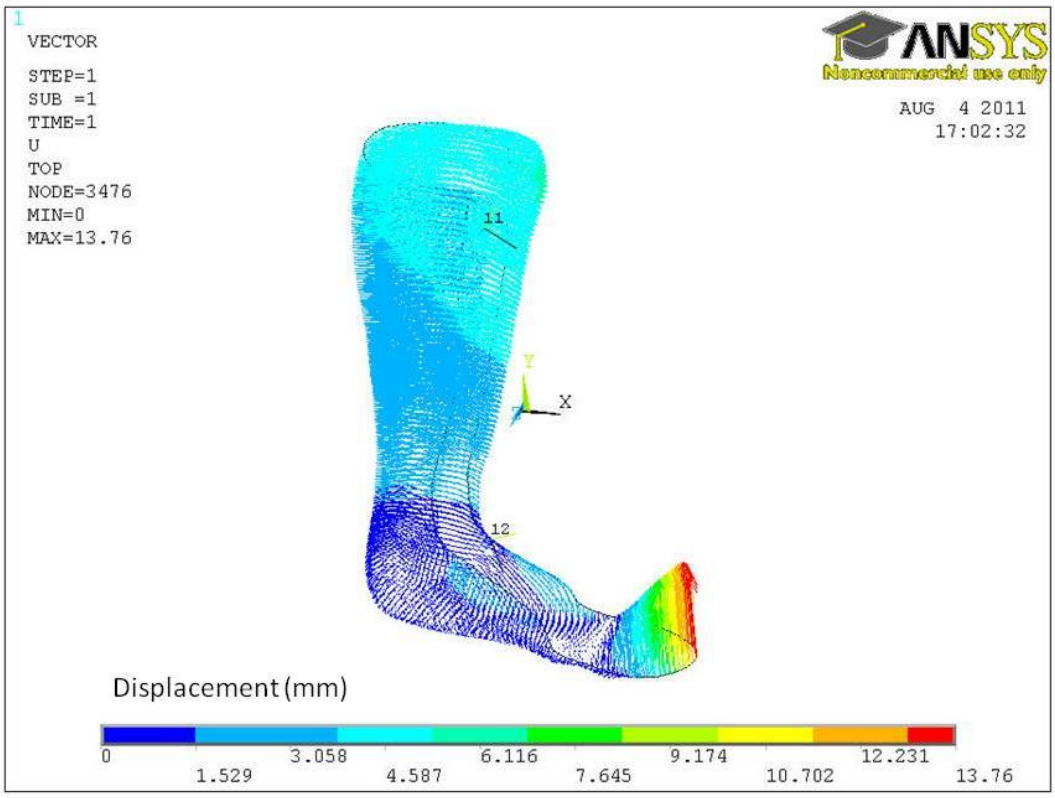

Figure 9-9: A vector plot of the displacements for analysis two

It was thought that at toe off the toe section of the AFO would remain relatively flat to the ground and the rest of the AFO would displace, therefore for analysis three the constraints at the toe section of the AFO were increased (see Figure 9-10).

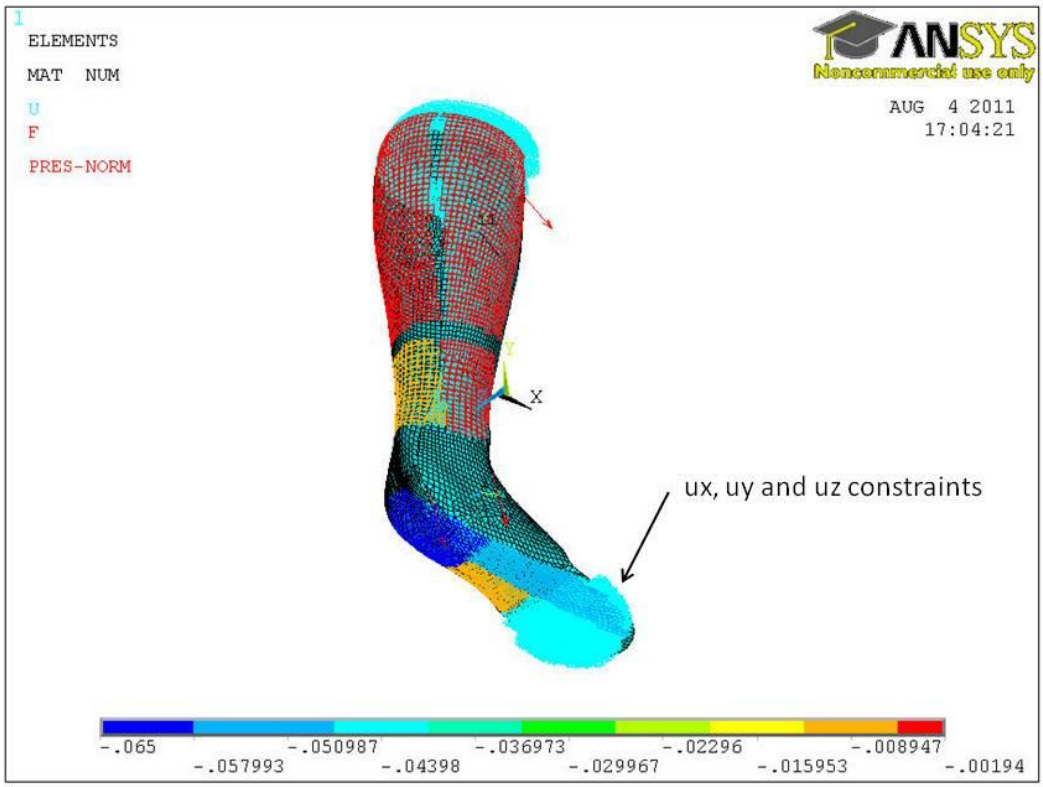

Figure 9-10: The extra boundary conditions that were applied to analysis three

9.6. AFO analysis three (part one)

In analysis three the same properties were used as in analysis one and two, the only difference was the extra boundary conditions on the toe area of the AFO. The displacement results (see Figure 9-11) show that the toe area is not displaced but the rest of the AFO shows a small displacement. At the toe off point in the gait cycle the expected result was that the toe area would remain flat to the ground and Figure 9-11 shows this. Before conducting additional analyses it was decided to undertake a validation to see if the results of the simulation were accurate.

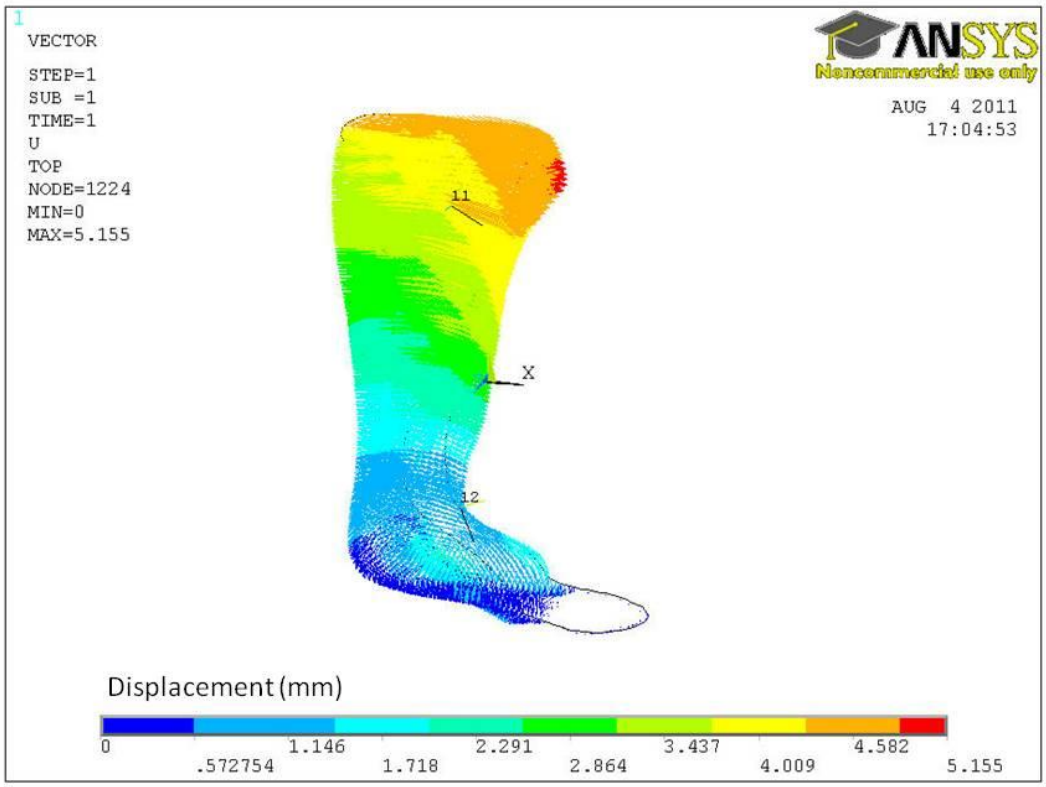

Figure 9-11: A vector plot of the displacements for analysis three

9.7. Validation

To check the results of the simulation they were compared to the results from a practical experiment where strain gauges were attached to the AFO. Previously, the strains have been measured in an AFO using strain gauges attached to polypropylene [**110**]. The results found that the accuracy of the strain gauges were not comparable to the accuracy of using strain gauges on aluminium. The work did suggest methods of improving the accuracy and current work by Solomondis et. al [**107**] has improved the accuracy further. The experiment described here is an outcome of the improved work.

In the same experiment that provided kinetic and kinematic data to calculate the strap loads (see section 9.2.5) there was also a strain gauge attached to the AFO. It was attached using adhesive to the lower calf region of the AFO (see Figure 9-12). The strain gauge was a rosette and therefore could calculate strains in the y-direction, the 45° to the vertical direction and the -45° to the vertical direction. The values that were recorded from the strain gauge were at a sampling frequency that

corresponded to the sampling frequency of the force platform and Vicon system (100Hz). This meant it was straight forward to find the corresponding strain at a time point 50% into the gait cycle (at toe off). The strain data was in volts and had to be converted into microstrain, equation 2 shows how this was done.

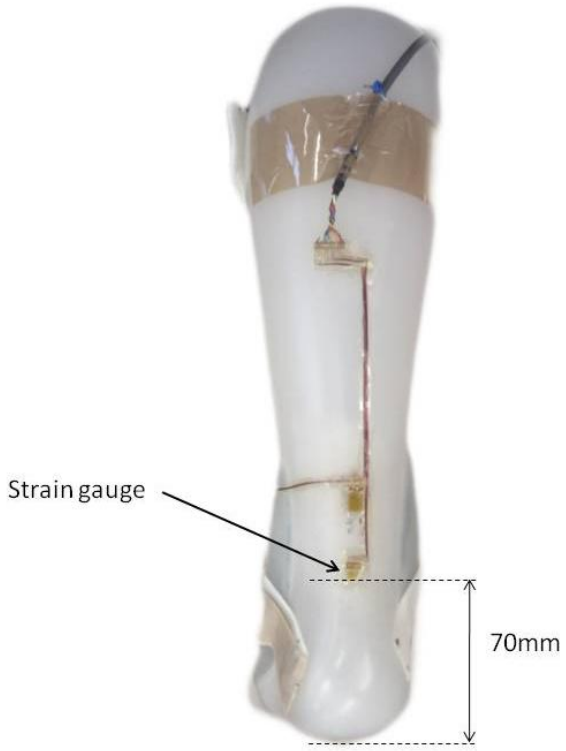

Figure 9-12: Posterior view of the AFO with strain gauge attached

$$e_o = \frac{E}{4} K_s \varepsilon_o \qquad \text{Equation 2}$$

Where e_o is the output voltage, E is the bridge voltage, K_s is the gauge factor and ε_o is the strain. There was also a gain value of 500 that the value had to be divided by. To convert from strain to microstrain the answer was multiplied by $10x10^6$. The microstrain calculated in the y-direction at toe was -2310 (microstrain), this value could then be compared to the solutions from the FEA.

9.8. AFO analysis three (part two)

After the validation, the strains calculated from the experiment could be compared to the strains from analysis three (see Figure 9-13).

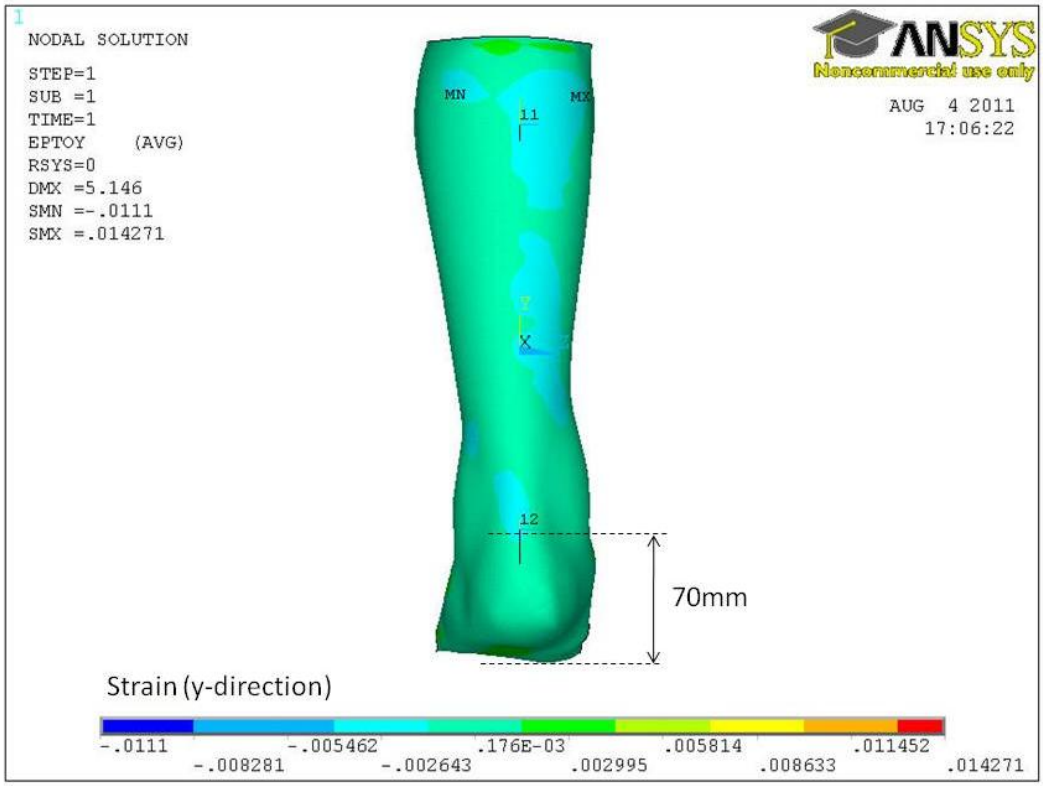

Figure 9-13: A contour plot of the strains in the y-direction for analysis three

The strain in the y-direction at the position where the strain gauge was attached (as indicated in Figure 9-13) was -0.02642 (-2642 microstrain). There is a 14.4% difference between the experimental strain and the predicted strain, this is considered a close agreement. However, the predicted strain is averaged over a certain area as depicted by the colour scheme in Figure 9-13. There was a more precise way to find the strains at the corresponding area to where the strain gauge was positioned in the experiment, which is detailed in the analysis summary section of this chapter. One way to improve the accuracy further may be to introduce a variable AFO thickness.

9.9. AFO analysis four

In analysis four variable thicknesses were applied to the AFO, it is detailed how this was done in section 9.2.4. The element type and boundary conditions were kept the same as analysis four. The strains in the y-direction will be documented in the summary table at the end of this chapter. The principal stresses in the first principal axis are shown in Figure 9-14 and Figure 9-15.

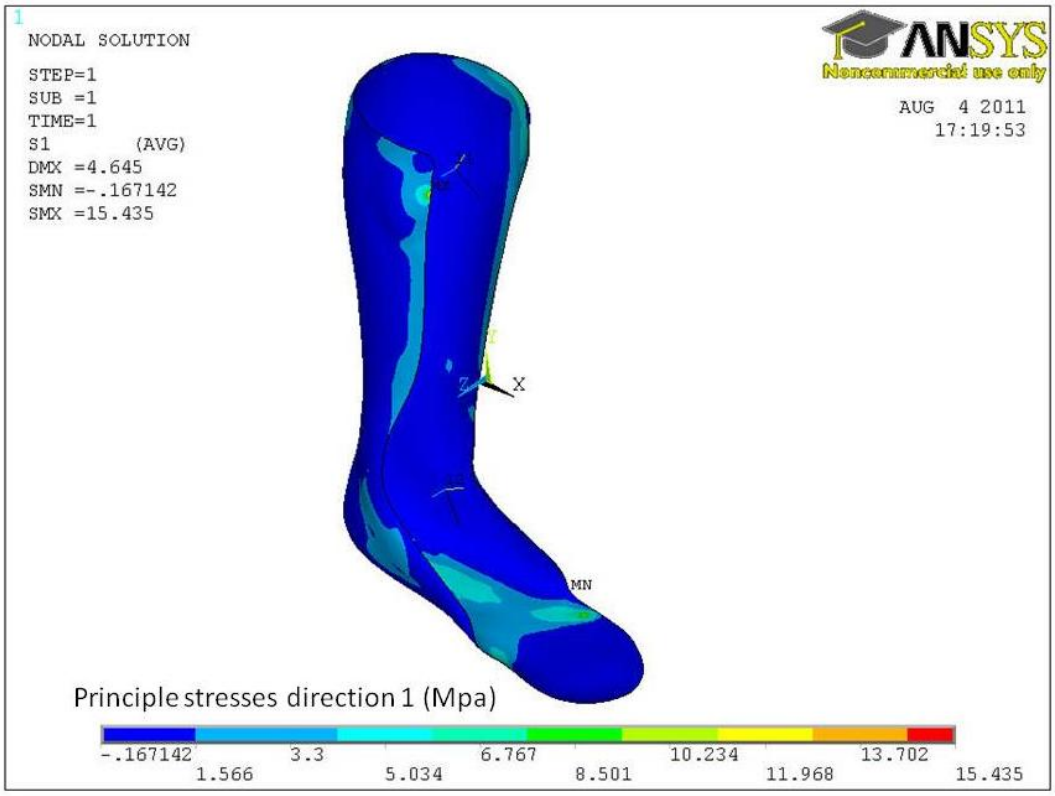

Figure 9-14: A contour plot of the principal stresses (direction 1) for analysis four (1)

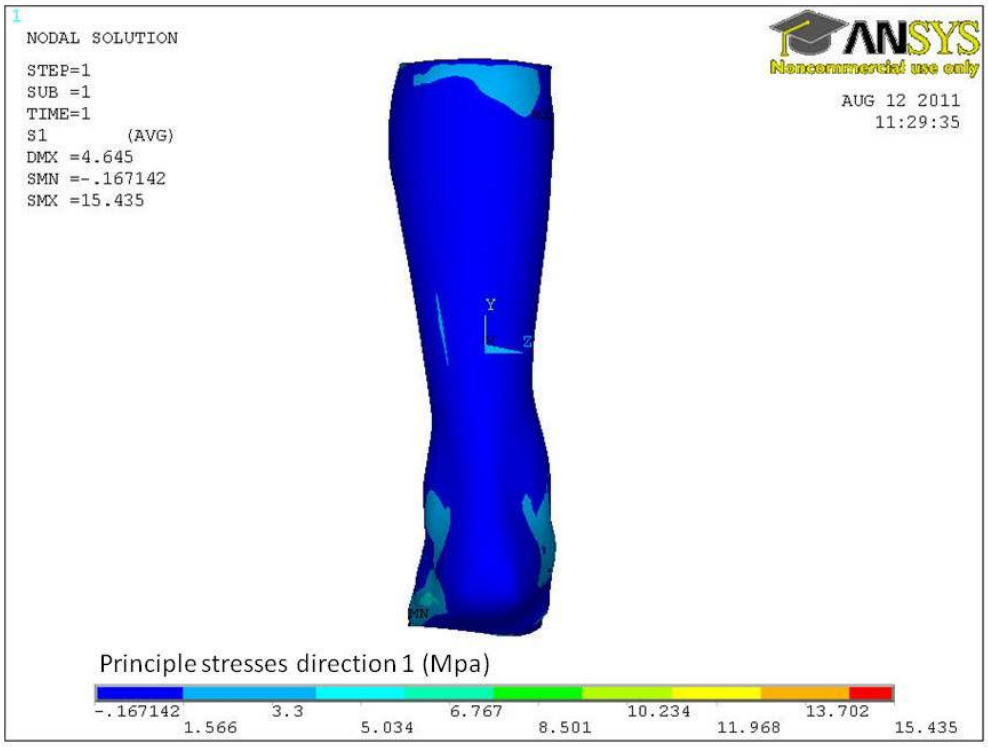

Figure 9-15: A contour plot of the principal stresses (direction 1) for analysis four (2)

Figure 9-14 and Figure 9-15 indicate that the stresses that act on the AFO at toe off are very low. The maximum stresses are positioned where the top strap would connect to the AFO. Apart from the small areas of stress concentration at the straps and constraint locations, the stresses are approximately -0.17Mpa. The next step in attempting to improve the accuracy of the analysis was to introduce non-linear material properties.

9.10. AFO analysis five

Polypropylene is a non-linear material [**76**] and therefore in analysis five it was attempted to input non-linear material properties into the FE model.

These properties were taken from a tensile test on a homopolymer specimen of polypropylene conducted by Solomonidis et. al [**107**] at the Bioengineering Unit (University of Strathclyde). The stress and strain values (see Figure 9-16) were inputted into Ansys and therefore the non-linear stiffness could be calculated.

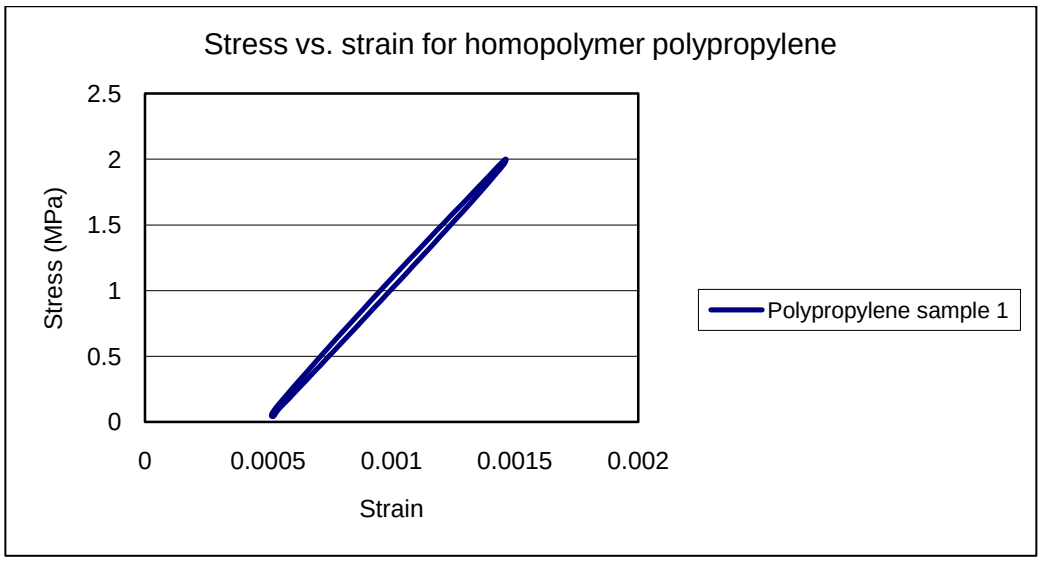

Figure 9-16: Plot of stress vs. strain for a sample of polypropylene sample loaded by a tensile test.

Only the loading values were applied to the FE model. When the non-linear stress and strain values were initially applied to the FE model and the analysis was ran, errors occurred.

It was found that the SHELL 281 element was unsuitable for an analysis with a material that exhibited plasticity. Figure 9-16 shows the data that was put into the model showed the material was displaying elasticity properties and not plasticity properties. However, it is thought that Ansys cannot differentiate between data that shows elasticity and data that shows plasticity therefore it automatically assumes plasticity might occur. SHELL 281 was then replaced with SHELL 93. SHELL 93 was chosen through a process of trial and error; the model was ran with different element types until it began to solve. The reason for this process was that SHELL281 was listed as having a special feature of being able to solve models with plasticity [**105**] and therefore the reason why it did not work was unknown. This meant the logical step of finding an alternative element with plasticity listed as a special feature could not be applied.

Another error occurred because the initial Young's modulus was not set correctly. The values of stress and strain from the tensile test had been inputted to Ansys but the initial Young's modulus was still set at a value found from the literature. To solve this problem a calculation was done to find the initial gradient of the curve

defined by the stress and strain values. This value was then set as the initial Young's modulus value.

After solving these problems the analysis ran but the problem would not converge. It was decided as a compromise that the linear gradient of the data would be found and this would be used as the Young's modulus. Figure 9-17 shows the Young's modulus being equal to 2038.1 MPa. It is clear from Figure 9-16 and Figure 9-17 that the experimental data is very close to being linear data, therefore the gradient of the best fit line would provide an accurate Young's modulus value. Analysis five was then conducted with the new Young's modulus and because the material properties were changed back to being linear, the element type was also changed back to SHELL281. Variable thicknesses were applied, the boundary conditions kept the same and small displacements were active in the model, the results are documented in table 3.

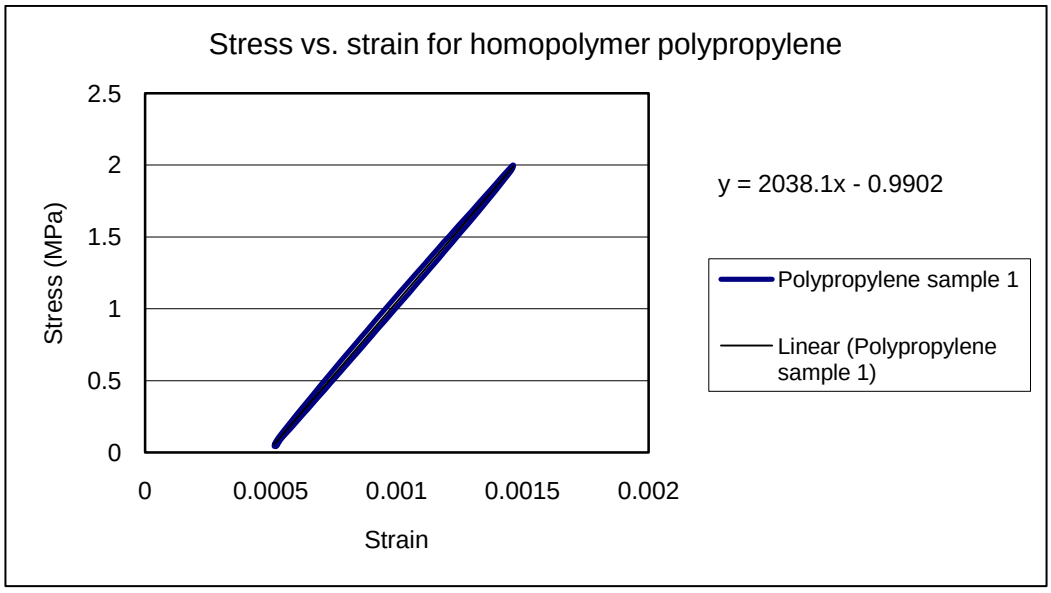

Figure 9-17: Plot of stress vs. strain for a sample of polypropylene sample loaded by a tensile test including line of best fit and equation

9.11. AFO analysis six

The literature suggests that conducting models with large displacements activated improves the accuracy of the FE solutions [**21**]. Therefore an analysis was conducted with large displacements active. All boundary conditions were kept the

same, variable thicknesses were applied and the Young's modulus was inputted as the same value as used in analysis five. For a non-linear analysis Ansys performs iterative steps until the answer converges, Figure 9-18 shows a plot of how the analysis converged.

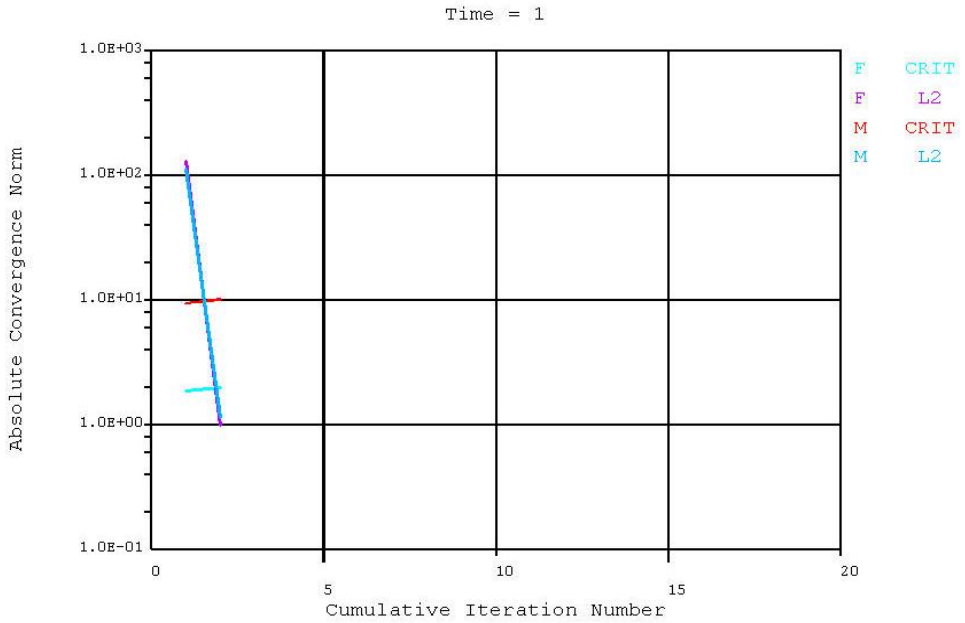

Figure 9-18: A plot to show the convergence of analysis six

It is clear from Figure 9-18 that the solution converged quickly. The results from the analysis are shown in table 3.

9.12. Summary of the analyses

Table 2 documents the six different analyses that Ansys conducted and their individual properties.

Table 2: The different type analyses that were conducted (X indicates property is selected)

Analysis Number	Analysis property					
	Constant thickness	Variable thickness	E^1 = 1300 MPa	E^2 = 2038.1 Mpa	Small displacements	Large displacements
1,2,3	X		X		X	
4		X	X		X	
5		X		X	X	
6		X		X		X

Table 3 compares the stresses, strains and loads for the four main analyses. The maximum principal stresses were chosen not to study how the AFO might fail but as a benchmark that could be compared between the analyses. It was also chosen because it could be calculated from the strain gauge data from the validation study, results could then be compared. Principal stresses act in three directions and direction one was chosen because it indicates the largest stresses. In all the analyses the stresses were found to be low.

The strain in the y-direction was chosen to be compared between the analyses because then each analysis could be directly compared with the validation study. The analysis with the closest result to the validation study was analysis four; there was a percentage difference of 33% between the strains. The strains at element 5014 were chosen because its position corresponded to the location where the strain gauge was attached to the AFO. The strain value is an average of the strain values at all of the nodes in that element.

Columns 4-7 in table 3 present the total loads acting on the AFO. It is clear from the results that the total forces in the y-direction were all close to the subject's weight (784N).

[1] = modulus value obtained from literature

[2] = modulus value obtained from experiment

The values in this table are discussed further in the next chapter.

Table 3: Comparison of different stresses, strains and loads for all of the analyses

Analysis Number	Parameters					
	Maximum principal stress in direction 1 (MPa)	Maximum y-direction strain at element -5014 (microstrain)	Total forces in the x-direction (N)	Total forces in the y-direction (N)	Total forces in the z-direction (N)	Total moments (about the z axis) at the ankle joint (Nm)
(validation)	n/a	-2310	n/a	n/a	n/a	n/a
3	19.93	-1160	171.9	752.9	10.88	34.61
4	15.44	-1540	178.8	810.1	29.46	40.01
5	15.45	-983	178.8	810.1	29.46	40.01
6	15.49	-1030	178.6	812.6	26.92	40.03

The total forces that were acting in the y-direction (vertical direction) were summed to be approximately 810N. This can be compared to the ground reaction force 828N (in the y-direction) recorded by Solomonidis et al. [**107**] in the force platform experiment (detailed in the 9.2.5). The ground reaction force is acting on both the AFO and leg combined. The force calculated by Ansys is the total forces acting on the leg by the AFO. It is a positive value because it is resisting the negative y-direction forces being applied by the leg. Using Newton's third law (see equation 3) it can be asserted that total of the ground reaction force that is transmitted by the AFO alone is 18N.

$$F_{TOT} = F_{AFO} + F_{LEG} \qquad \text{equation 3}$$

Where F_{TOT} is the ground reaction force, F_{LEG} is the force transmitted by the leg alone (or the force acting on the AFO by the leg) and F_{AFO} is the force transmitted by the AFO alone. The same equation can be applied to the moments (see equation 4).

The total forces in the x-direction and the z-direction (at toe off) measured by the force platform experiment were 117N and -55.7N respectively. The loads transmitted through the leg were 178N and 29N respectively. This means both the leg loads are higher than the total loads.

$$M_{TOT} = M_{AFO} + M_{LEG} \qquad \text{equation 4}$$

In the above equation M_{TOT} is the moment generated by the ground reaction force, M_{LEG} is the moment generated by the leg alone and M_{AFO} is the moment generated by the AFO alone. All moments are acting about the ankle joint centre (see Figure 9-19). The ankle joint centre was approximated by choosing a z coordinate that was positioned halfway between where the two lower strap loads were acting. The other coordinate values were estimated using the data from the kinematic and kinetic experiments done by Solomonidis et. al. The total moment acting on the AFO and leg due to the ground reaction force was a dorsiflexion moment of 120Nm (see appendix C). The total moment calculated by Ansys was approximately 40Nm, it was positive and therefore a dorsiflexion moment. This is the moment being applied on the leg by the AFO. As a result the leg needs to generate a plantarflexion (negative) moment of 40Nm to resist the stiffness of the AFO and 120Nm to resist the ground reaction force. Using equation 4 it can be determined that the moment generated by the leg is of a 160Nm value acting in the negative direction (tending to plantarflex the ankle). This means that the AFO is not generating an assistive moment but is in fact causing the leg to waste muscle power in order to generate a larger moment than would normally be required.

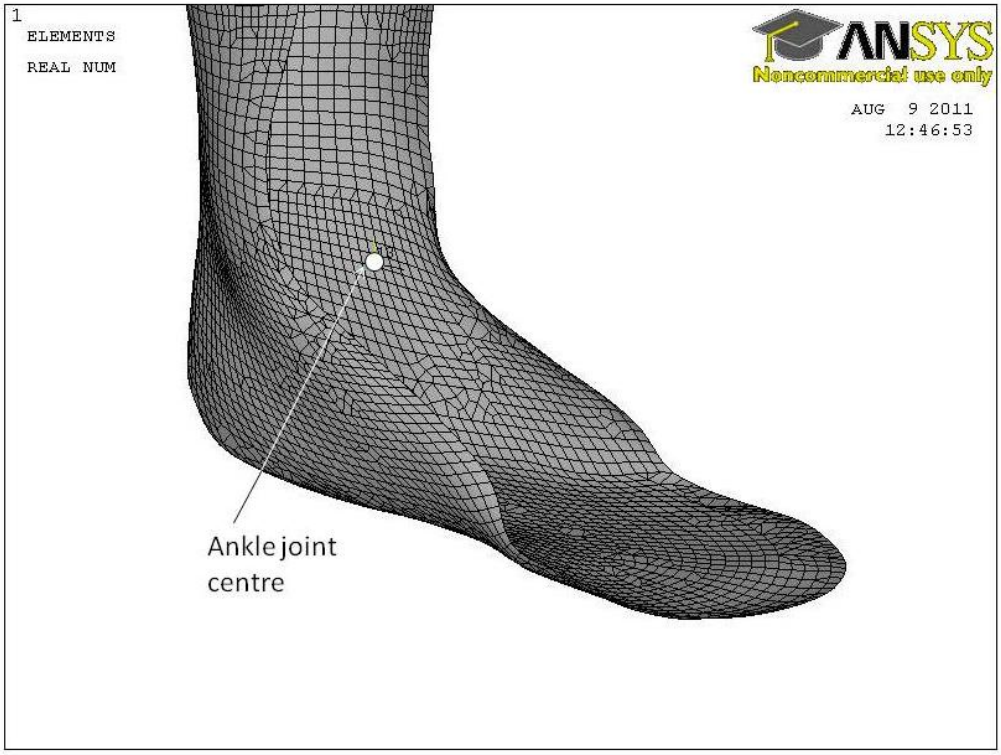

Figure 9-19: Location of the ankle joint centre

Both the force and moment values taken from Ansys that were used for the above calculations were from analysis four as it was deemed to be the most accurate. Table 4 summarises the loads.

Table 4: Summary of the important load results from analysis four

Force Direction	Force type			Moment direction	Moment type		
	F_{tot}(N)	F_{leg} (N)	F_{AFO} (N)		M_{tot} (N)	M_{leg} (N)	M_{AFO} (N)
Y direction	830	-810	-18.0	About z axis	120	-40.0	160

.

Only the forces in the y-directions and moments in the sagittal plane were investigated because these were the largest values.

Chapter 10. Discussion

10.1. Introduction

In this chapter the results of chapter 9 will be discussed in more detail. The results from the digital scanning of the AFO and pressure measurement experiment chapters will also be linked into the discussion.

10.2. FEA

The validation study gave a strain value of -2310 microstrain. The best match to this value was achieved in analysis four, with a percentage difference of 33%. Between analysis three and four there was an increase in accuracy. This was because of the introduction of variable thicknesses to the model. This corresponds with what has been reported in the literature by Syngellakis et. al [**21**]. However, there were assumptions made in the application of the different thicknesses to the FE model; for example the thicknesses were applied to approximated sections of the AFO. This means the accuracy of the model could still be improved further. One way to do this would be to export the geometry from the digital scanning software as a 3D model with thicknesses as opposed to a surface. However, it is not possible to achieve this using the academic version of Ansys because the number of nodes that would be required to mesh the model is greater than the software limit.

Analysis five was initially conducted with non-linear material properties but it was unsuccessful because the analysis did not converge. This was thought to be because the data inputted was very close to being linear and therefore the software might have been unable to compute the data as being non-linear. In future work, there should be another tensile test undertaken that puts the polypropylene specimen under a larger stress so that it exhibits greater non-linear properties. The stresses and strains from this test could then be inputted into Ansys and the solver ran again.

After the unsuccessful convergence of the solution for analysis five, the material properties were changed back to a linear value and the analysis conducted for a second time. The Young's modulus was increased in analysis five (compared to analysis four) because the Young's modulus was calculated from the stress/strain

curve taken from experimental data [**107**] and was found to be greater than the value taken from the literature. Consequently, it was expected that analysis five would be a closer match to the validation, however this was not the case. The type of polypropylene used to make the AFO in this study has been tested in previous work [**110**]. It has been shown to display viscoelastic properties because it demonstrated a linear stress/strain relationship at low stresses and a non-linear stress/strain relationship at high stresses. In the literature [**111**] it states that the Young's modulus of viscoelastic materials is affected by the strain rate, loading history and temperature. This means that because the loading conditions are different between a uniaxial tensile test and the loads experienced during gait it is unlikely that the Young's modulus calculated from the tensile test data will be an accurate value to use in the FEA.

Analysis six was conducted with large displacements activated and improved the accuracy of the model (in comparison to analysis five). This again corresponds with what was reported in the literature by Syngellakis et. al [**21**]. The difference made was very small; this is assumed to be because the displacements in the model are small.

The results show that small stresses were found acting on the AFO in all of the analyses. The overall majority of the stresses were compressive and <1Mpa in magnitude. The magnitude is supported by experimental work done by Chu et. al [**18**] but the direction is not. They measured a peak tensile stress of 0.39Mpa at the upper calf section in a solid AFO at toe off. This is thought to be in the wrong direction because there is a plantarflex moment at the ankle during toe off and this is thought to apply a compressive stress to the back section of the AFO. The loads applied in the FEA resulted from a normal subject wearing the AFO and the work by Chu et. al also used a normal subject, this is a possible reason for the low magnitudes of the stresses that were recorded . The AFOs were designed to resist forces that would be applied by a subject with a neurological disorder. When a normal subject walks with an AFO and applies smaller force values, large stresses will not be generated.

The FEA results indicate that the AFO is offloading the leg by 18N. This is a small percentage of the total load; only 2.2%. It indicates that the AFO is providing minimal support to the muscles in the leg. This is thought to be because the friction acting between the AFO and the leg is quite low and therefore the forces aren't

being transmitted to the AFO. This result also links to the pressure measurement experiment results because low pressures were found at the calf section. If higher pressures were found it would be expected that more forces would be transmitted through the AFO. It is thought that to improve the biomechanics of gait for an AFO wearer with some paralysed leg muscles; it would be beneficial for the AFO to take a larger percentage of the load. This would have its own problems including a higher chance of skin irritation at the AFO/skin interface.

The results given by Ansys of the total AFO moment (in the sagittal plane) indicate that the AFO applies an additional dorsiflexion moment that the ankle moment generated by the leg has to overcome. This does not match the results found by Yamamoto et. al [**19**]; they found that during toe off the AFO did apply a very small assistive plantarflexion ankle moment. It should be taken into account that the custom made AFO used by the study is being worn by hemiplegic subjects and therefore the total ankle moment is much less than the one in this study. This would affect the size and possibly the direction of the moment taken by the AFO.

It is thought unlikely that the muscles in the leg would be able to generate such a large moment of 160Nm to resist both the stiffness of the AFO and the ground reaction force. Therefore it is possible an error might be the cause of the large dorsiflexion AFO moment. One possible error is the position of the ankle joint centre; this was only estimated and could be calculated more precisely. However, a trial and error process was undertaken to investigate the chance of this error being the cause of the unexpected result. From this process only small differences in the total moments were achieved. In future work the moment value from this study will have to be investigated to verify the accuracy.

The AFO in this study was made by R. Bowers, a prosthetist at the National Centre of Prosthetics and Orthotics at the University of Strathclyde. He also wrote a document explaining some of the biomechanical issues with this AFO [**4**]. The main purpose of this particular type of AFO is to prevent plantarflexion during swing phase and to realign the ground reaction force during stance phase [**112**]. The AFO used in this study is relatively stiff and is also designed to block dorsiflexion and plantarflexion [**4**]. This would cause a dorsiflexion moment to be created in the AFO when the external forces are trying to plantarflex it (this occurs at toe off) and therefore might explain the unexpected large dorsiflexion moment found in the analysis.

10.3. Possible FEA errors

The results from pressure measurement experiment one showed that there was inaccuracy in the pressure value measured at the strap. To overcome this problem the strap forces were calculated analytically and were applied to the model as point loads. This is an assumption and the forces would not be acting at just a single point. A way to improve this in future work would be to use transducers that can measure the tension in a strap experimentally.

When the AFO geometry was captured by the digital scanner there will have been some errors introduced. Other geometry errors will have occurred from the measurements of the thickness of the AFO. Approximate measurements for several areas of the AFO were conducted but ideally the geometry would be more accurate. Differences in the AFO geometry between the model and the real object will have lead to errors in the FEA. However, it is thought these errors will have been small because improvements to the geometry could only be small.

In this work 18530 nodes were used to mesh the model of the AFO (corresponding to an element edge length of 6mm). The mesh sensitivity study indicated that the Von-Mises stresses may be more accurate with a finer mesh (one with an element edge of length of 5mm), but this lead to a greater computation time. Therefore it is possible that the compromise in the mesh size could have caused inaccurate results. With the full version of Ansys (no node limit) it would have been possible to investigate this further.

In Ansys it was necessary to have two different models to conduct solutions on; one with a uniform thickness and one with a variable thickness. A possible error might have occurred because of applying the loads in different places between models. Care was taken to ensure the point loads were selected at the exact same nodes between different models. In terms of applying the pressure to areas of elements it was more difficult to specify the exact same area. Points in the mesh were singled out and this allowed the approximate positioning of the pressures in the same places.

Another possible cause of errors is the fact that the average pressures were applied to the model rather than the actual pressures. This means that higher pressures should have been applied to the AFO in certain locations. A way to improve the accuracy would be to insert the pressure values measured at each

individual sensor rather than taking average values. The pressures should also be measured all over the AFO surface instead of just at certain positions.

The results show that the forces determined by Ansys acting in the x and z directions are greater than the forces that were recorded by the force platform experiment. This suggests that the results determined by Ansys are erroneous. A possible reason for this is the fact that the force strap calculations were only made and applied in the sagittal plane. The forces in reality would not be solely acting in the sagittal plane and therefore errors will have been introduced into the model. The expected result would be if the strap forces were calculated in 3-dimensions, that the x and z-direction forces calculated by Ansys would be a small percentage of the forces given by the force platform experiment.

The constraints applied in analyses might be a cause of errors. In reality the AFO would be partially constrained by the leg at several different areas. Some movement would be allowed against the soft tissue of the leg but there would still be some constraints as well. There would be complete constraint in the y-direction at the COP and partial constraints at the other areas of metatarsal area. One way to provide the sort of partial constraints that would accurately recreate the constraints between the leg and the AFO; would be to model the leg in Ansys. Chu et. al [**22**] have done an analysis with the foot and AFO both modelled, but no validation of the results was provided so the accuracy of their results cannot be determined.

One more cause of error could be the assumption made that the shoe the subject was wearing over the AFO was not an extra part of the analysis. It was assumed that the shoe did not provide any additional boundary conditions to the AFO, even though this might not have been the case. This is something that would need to be investigated.

The FE simulation was found at best to give results within 33% of the validation study. This indicates the potential of the FE model to provide accurate and therefore useful clinical information. Errors were possibly caused by inaccuracies in the AFO geometry, the mesh size (not being fine enough) and assumptions made in calculating the material properties and the boundary conditions.

Chapter 11. Conclusion and Future Work

The main aim of this thesis was to calculate the loads that an AFO experiences during gait. To do this, six objectives identified in the introduction were achieved.

- The pressures acting on an AFO during normal gait were successfully measured using two different pressure measurement systems.
- Using the information from the pressure measurement equipment, the location and the magnitude of the pressures on the AFO were then calculated so they could be applied to the FE model.
- The geometry of the AFO was successfully captured using a digital scanner. The results were then exported into Ansys as an accurate surface model.
- An FE model of the AFO was developed and the stresses, strains and loads acting on the AFO were predicted.
- The results from the FEA were then validated using experimental strain data.
- The analysis of the stress, strain and load results was then undertaken and discussed.

The results indicate that during toe off the forces in the y-direction (vertical direction) transmitted through the AFO were 2.2% of the forces in the y-direction (vertical direction) that are transmitted through the leg. This suggests that the AFO is not providing much support in terms of taking load away from muscles.

The results also show that the AFO provided a dorsiflexion moment of 40Nm that the subject had to overcome. This result would suggest that the AFO is making it harder to walk for someone with healthy plantarflexor muscles. It is thought however that if the plantarflexors were not healthy, then the AFO would provide a plantarflexion moment to resist dorsiflexion. The moment would be quite large because of the AFO's stiffness and it would reduce the moment required to be produced by the muscles in the leg. This would mean that the biomechanical function of a patient could potentially be improved with this type of AFO. Further work needs to be undertaken to confirm this. A similar study could be done using a subject with a gait deficiency.

At the beginning of this thesis it was found that although the importing of geometry using digital scanning technology was a relatively quick process it was not

without errors. It is thought however, that improvements to the accuracy could be made in future scans.

The two pressure measurement experiments gave similar results for the pressures acting on the foot section of an AFO. Out of the two sets of results the Pedar system was thought to be more reliable. Loads at the calf section and achilles heel section of the AFO were low in comparison to the loads acting at the foot section. This is a result that might explain why there are such low forces in the y-direction (vertical direction) being transmitted through the AFO.

The validation study demonstrated that the strains calculated by the analyses gave at best a 33% difference between those recorded in a practical experiment. This is a good indication that the FE model is accurate, although it is thought that errors still remain in the model. Some future work to address the errors is detailed below.

To improve the accuracy of the FE model in this study a number of steps could be taken. One way would be to improve the accuracy of the applied loads. This could be achieved by using different equipment to monitor the pressures. One suggestion would be to use capacitive sensors (as used in the Pedar system) that are designed for lower pressures. These could then be placed at other positions inside the AFO and not just on the heel section.

Another way to improve the accuracy would be to do the analysis on a different version of Ansys. If the full commercial version of Ansys was used, this would remove the maximum node limit. This would be useful for investigating the mesh sensitivity study further. It needs to be checked whether the stresses converge at a level greater than 18000 nodes or not.

Future work could include doing the analyses of different time points in the gait cycle for example heel strike, midstance and mid-swing. Another possibility would be to do a dynamic analysis that monitors the loads continuously throughout the gait cycle.

The whole study could be repeated using a subject with a gait deficiency. The results would indicate whether the AFO would take a percentage of the total moment away from the subject. This would inform whether AFOs are helping to meet their biomechanical requirements. The result could also lead to determining

whether the AFO is over engineered. If the stresses calculated by the FEA were still low then it could be suggested that the AFO could be made thinner. However the other biomechanical requirements would still need to be taken into account. For example would the thinner AFO still provide an adequate moment resisting the patient's plantarflexion during swing phase. This information could also be calculated from a FEA study. This shows the potential of using FEA and how it can provide beneficial biomechanical data for an orthotist. The FE model would need to be thoroughly validated beforehand, to prove its accuracy.

This study investigated the loads acting on an AFO during gait, by conducting a simulation in FE software. Measurements of the pressures acting on an AFO were experimentally found and then used in the FE model to simulate the loading conditions. The loads at toe off predicted by the FE software indicated that the AFO takes only 2.2% of the total vertical forces. It was also indicated that the AFO created a 40Nm resistive dorsiflexion moment to the plantarflexion moment generated by the leg at toe off. This suggests that the AFO is making it more difficult to walk for someone with healthy plantarflexor muscles. This indicates the potential of the FE model to provide useful clinical data to orthotists.

Bibliography

1 International Organisation for Standardisation ISO 8549-1: Prosthetics and orthotics-vocabulary, part 1: General terms for external limb prostheses and external orthoses (1989).

2 W. H. Henderson, L. W. Lamoreux. "The orthotic prescription derived from a concept of basic orthotic functions". *Bulletin of Prosthetics Research* (1969), 89-96.

3 J. C. Tan. *Practical manual of physical medicine and rehabilitation*. Elsevier Mosby, Philadelphia, USA, 2006.

4 R. Bowers, K. Ross. "Best practice statement: use of ankle-foot orthoses following stroke". *NHS Quality Improvement Scotland* (2009).

5 D. J. J. Bergman, V. De Groot, P. van Diggele, H. Meulman, H. Houdijk, J. Harlaar. "Polypropylene ankle foot orthoses to overcome drop-foot gait in central neurological patients: a mechanical and functional evaluation". *Prosthetics and Orthotics International*, 34, 3 (2010), 293-304.

6 D. C. M. de Wit, J. H. Buurke, J. M. M. Nijlant, M. J. I. Jzerman, H. J. Hermens. "The effect of an ankle-foot orthosis on walking ability in chronic stroke patients: a randomized controlled trial". *Clinical Rehabilitation*, 18 (2004), 550-557.

7 H. Gok, A. Kucukdeveci, H Altinkaynak, G. Yavuzer, S Ergin. "Effects of ankle-foot orthoses on hemiparetic gait". *Clinical Rehabilitation*, 17 (2003), 137-139.

8 C. Chen, K. Yeung, C. Wang, H. Chu, C. Yeh. "Anterior Ankle-Foot Orthosis Effects on Postural Stability in Hemiplegic Patients". *Archives of Physical Medicine and Rehabilitation*, 80 (1999), 1587-1592.

9 S. F. Tyson, H. A. Thorton. "The effect of a hinged ankle foot orthosis

hemiplegic gait: objective measures and opinions". *Clinical Rehabilitation*, 15 (2001), 53-58.

10 S. A. Radtka, S. R. Skinner, D. M. Dixon, M. E. Johanson. "A comparison of solid, dynamic and no ankle foot orthoses in children with spastic cerebral palsy". *Physical Therapy*, 77, 4 (1997), 395-409.

11 B. Balaban, E. Yasar, U. Dal, K. Yazicioglu, H. Mohur, T. A. Kalyon. "The effect of hinged ankle-foot orthosis on gait and energy expenditure in spastic hemiplegic cerebral palsy". *Disability and Rehabilitation*, 29, 2 (2007), 139-144.

12 S. Ounpuu, K. Bell, R. B. Davis. "An evaluation of the posterior leaf spring orthosis using joint kinematics and kinetics". *Journal of Pediatric Orthopaedics*, 16, 3 (1996), 378-384.

13 P. R. G. Lucareli, M. Lima, J. G. Lucarelli, F. P. S. Lima. "Changes in joint kinematics in children with cerebral palsy while walking with and without a floor reaction ankle-foot orthosis". *Clinics*, 62, 1 (2007), 63-68.

14 P. A. Burtner, M. H. Woollacot, C. Qualls. "Stance balance control with orthoses in a group of children with spastic cerebral palsy". *Development Medicine and Child Neurology*, 41 (1999), 748-757.

15 J. Leung, A. Mosely. "Impact of ankle-foot orthoses on gait and leg muscle activity in adults with hemiplegia". *Physiotherapy*, 89, 1 (2003), 39-55.

16 R. Ofir, H. Sell. "Orthoses and ambulation in hemiplegia: a ten year retrospective study". *Archive of Physical Medicine and Rehabilitation*, 61, 5 (1980), 216-220.

17 J. A. Shamp, A. Klope. Ankle foot orthoses - metal vs. plastic. *Clinical Prosthetics and Orthotics*, 7, 1 (1983), 1-3.

18 T. Chu, R. Feng. "Determination of stress distribution in various ankle-foot orthoses: experimental stress analysis". *Journal of Prosthetics and*

Orthotics, 10, 1 (1998), 11-16.

19 S. Yamatomo, S. Miyazaki, T. Kubota. "Quantification of the effect of the mechanical property of ankle-foot orthoses on hemiplegic gait". *Gait & Posture*, 1 (1993), 27-34.

20 M. Lord, D. Jones. "Issues and themes in computer aided design for external prosthetics and orthotics". *Journal of Biomedical Engineering*, 10 (1988), 491-498.

21 S. Syngellakis, M. A. Arnold, H. Rassoulian. "Assessment of the non-linear behaviour of plastic foot orthoses by the finite element method". *Proceedings of the Institution of Mechanical Engineers H*, 214 (2000), 527-539.

22 T. M. Chu, N.P. Reddy, J. Padovan. "Three-dimensional finite element stress analysis of the polypropylene, ankle-foot orthosis: static analysis". *Archive of Physical Medicine and Rehabilitation*, 17, 5 (1995), 372-279.

23 J. Cundil. "A method of determining the characteristics of an ankle-foot orthosis using finite element analysis". *University of Strathclyde MSc Thesis* (1987).

24 D. Leone, S. Diemente, S. Gustave, M. Lopez-Isa. "Structural analysis of solid ankle-foot orthoses". (Durham, New Hampshire 1988), Proceedings of the 14th Annual Northeast Bioengineering Conference, 26-28.

25 C. L. Vaughan, B. L. Davis, J. C. O'Conner. *"Dynamics of Human Gait"*. Kiboho Publishers, Western Cape, South Africa, 1992.

26 B. H. Brown, P. V. Lawford, R. H. Smallwood, D. R. Hose, D. C. Barber. *"Medical physics and biomedical engineering"*. Taylor and Francis, Oxon, UK, 1999.

27 M. W. Whittle. *"Gait analysis an introduction"*. Butterworth-Heinemann, Elsevier, Philadelphia, USA, 2003.

28 J. R. Gage, P. A. Deluca, T. S. Reshaw. "Gait analysis: principles and applications". *The Journal of Bone and Joint Surgery*, 77, 1607-1623.

29 J. Perry. *"Atlas of limb prosthetics: surgical, prosthetic and rehabilitation principles"*. Mosby - Year Book, 1992.

30 J. Perry. "Kinesiology of lower extremity bracing". *Clinical Orthopaedics and Related Research*, 102 (1974), 18-31.

31 http://moon.ouhsc.edu/dthompso/gait/epow/jtmom.htm (Accessed: 20/06/2011).

32 B. J. Hafner, J. E. Sanders, J. M. Czerniecki, J. Fergason. "Transtibial energy-storage-and-return prosthetic devices: a review of energy concepts and a proposed nomenclature". *Journal of Rehabiliation Research and Development*, 39, 1 (2002), 1-11.

33 J. D. Hsu, J. W. Michael, J. R. Fisk. *"AAOS atlas of orthotics: biomechanical principles and application"*. 2nd edition The C. V. Mosby Company, St Louis, USA, 1985.

34 D. H. Sutherland. "The evolution of clinical gait analysis part I: kinesiological EMG". *Gait & Posture*, 14, 1 (2001), 61-70.

35 D. H. Sutherland. "The evolution of clinical gait analysis part II - kinematics". *Gait & Posture*, 16 (2001), 159-179.

36 D. H. Sutherland. "The evolution of clinical gait analysis part III - kinetics and energy assessment". *Gait & Posture*, 21 (2005), 447-461.

37 M. R. Pitkin. *"Biomechanics of lower limb prosthetics"*. Springer, London, UK, 2006.

38 R. B. Davis, S. Ounpuu, D. Tyburski, J. R. Gage. "A Gait Analysis Data Collection and Reduction Technique". *Human Movement Science*, 10 (1991), 575-587.

39 I. W. Griffiths. *"Principles of biomechanics and motion analysis"*.

Lippincott Williams & Wilkins, Baltimore, USA, 2006.

40 D. Gordon E. Robertson, G. E. Caldwell, J. Hamill, G. Kamen, S. N. Whittlesey. *"Research Methods in Biomechanics"*. Human Kinetics, Champaign, USA, 2004.

41 P. R. Cavanagh, F. G. Hewitt Jr, J. E. Perry. "In-shoe plantar pressure measurement: a review". *Foot*, 2 (1992), 185-194.

42 N. Maalej, H. Zhu, J. G. Webster, W. J. Tompkins, J. J. Wertsch, P. Bach-y-Rita. "A conductive polymer pressure sensor". (New Orleans, LA, USA 1988), IEEE Engineering in Medicine & Biology Society 10th Annual International Conference.

43 J. Woodburn, P. S. Helliwell. Observations on the F-Scan In-shoe Pressure Measuring System. *Clinical Biomechanics*, 5 (1996), 301-304.

44 P. Convery, A. W. P. Buis. "Conventional patellar-tendon-bearing (PTB) socket/stump interface dynamic pressure distributions recorded during the prosthetic stance phase of gait of a trans-tibial amputee". *Prosthetic and Orthotics International*, 22 (1998), 193-198.

45 M. D. Nowak, K. S. Abu-Hasaballah, P. S. Cooper. "Design enhancement of a solid ankle-foot orthosis: Real-time contact pressures evaluation". *Journal of Rehabilitation Research and Development*, 37, 3 (2000), 273-281.

46 A. Sakamoto, B. McHugh, P. McClachlan. "Stance phase force/pressure patterns in ankle foot orthosis". (Hong Kong 2004), International Society for Prosthetics and Orthotics 11th World Congress.

47 C. Gant, A. Chase, D. Harris. The Cherwell ankle-foot orthosis. *Annual report, Oxford Orthopaedic Engineering Centre, University of Oxford*, 11 (1984), 82-83 (As quoted by P. Bowker et. al in "Biomechanical basis of orthotic management").

48 M. Lord. Foot pressure measurement: a review of methodology.

Journal of Biomedical Engineering, 3, 2 (1981), 91-99.

49 L. A. Boyd, E. L. Bontrager, S. J. Mulroy, J. Perry. The reliability and validity of the novel pedar system of in-shoe pressure measurement during free ambulation. *Gait & Posture*, 5, 2 (1997), 165.

50 P. M. Quesada, G. S. Rash, N. Jarboe. Assessment of pedar and F-scan revisted. *Clinical Biomechanics*, 12, 3 (1997), S15.

51 A. B. Putti, G. P. Arnold, L. Cochrane, R. J. Abboud. The Pedar in-shoe system: repeatability and normal pressure values. *Gait and Posture*, 25 (2007), 401-405.

52 J. D. Hsu, J. W. Michael, J. R. Fisk. *"AAOS atlas of orthoses and assistive devices"*. 4th edition Mosby Elsevier, Philadelphia, USA, 2008.

53 http://www.oandp.org/olc/lessons/html/SSC_07/ (Accessed: 14.06.2011).

54 B. B. Bhakta. Management of spasticity in stroke. *British Medical Bulletin*, 56, 2 (2000), 476-485.

55 S. J. Olney, C. Richards. "Hemiparetic gait following stroke. Part I: Characteristics". *Gait & Posture*, 4 (1996), 136-148.

56 E. Ann Hurley. "Use of KAFOs for Patients with Cerebral Vascular Accident, Traumatic Brain Injury and Spinal Cord Injury". *Journal of Prosthetics and Orthotics*, 18, 3 (2006), 199-201.

57 N. B. Alexander, A. Goldberg. "Gait disorders: Search for muliple causes". *Cleveland Clincal Journal of Medicine*, 72, 7 (2005), 586-600.

58 G. Cobeljic, M. Bumbasirevic, A. Lesicm, Z. Bajin. "The management of spastic equinus in cerebral palsy". *Orthopaedics and Trauma*, 23, 3 (2009), 201-209.

59 http://moon.ouhsc.edu/dtompso/namics/valgus.htm (Accessed: 20.06.2011).

60 F. H. Martini. *"Anatomy and Physiology"*. Pearson Education, San Francisco, 2006.

61 J. R. Gage, T. F. Novacheck. "An update on the treatment of gait problems in cerebral palsy". *Journal of Pediatric Orthopaedics Part B*, 10 (2001), 265-274.

62 J. Perry, J. M. Burnfield. *"Gait analysis: normal and pathological function"*. Slack Incorporated, Thorofare, USA, 2010.

63 G. C. Bennet, M. Rang, D. Jones. "Varus and Valgus Deformities of the Foot in Cerebral Palsy". *Developmental Medicine Child Neurology*, 24 (1982), 499-503.

64 N. J. Holland, T. J. Murray, S. C. Reingold. *"Multiple Sclerosis: a Guide for the Newly Diagnosed"*. Demos Medical Publishing, New York, 2007.

65 J. S. Hebert. Ambulatory KAFOs: A Physiatry Perspective. *Journal of Prosthetics and Orthotics*, 18, 3 (2006), 169-174.

66 A. Beelen, F. Nollet, M. de Visser, B. A. de Jong, G. J. Lankhorst, A. J. Sargeant. "Quadriceps muscle strength and volutary activation after polio". *Muscle and Nerve*, 28 (2003), 218-226.

67 A. E. H. Emery. *"Muscular Dystrophy"*. Oxford University Press, New York, USA, 2008.

68 M. Benson, J. Fixsen, M. Macnicol, K. Parsch. *"Children's Orthopaedics and Fractures"*. Springer, New York, USA, 2010.

69 M. M. Agha, J. I. Williams, L. Marrett, T. To, A. Zipursky, L. Dodds. "Congenital abnormalities and childhood cancer". *Cancer*, 103, 9 (2005), 1939-1948.

70 E. M. Gutierrez, A. Bartonek, Y. Haglund-Akerlind, H. Saraste. "Characteristics gait kinematics in persons with lumbosacral myelomeningocele". *Gait & Posture*, 18 (2003), 170-177.

71 R. J. Abboud. "(i) Relevant Foot Biomechanics". *Current Orthopaedics*, 16 (2002), 165-179.

72 S. R. Whiteside, M. J. Allen, W. J. Barringer, W. D. Beiswenger, M. D. Brncick, T. D. Bulgarelli, C. J. Henges, R. S. Lin. "Practice Analysis of Certified Practitioners in the Disciplines of Orthotics and Prosthetics". *American Board for Certification in Orthotics, Prosthetics and Pedorthics, Inc* (2007).

73 D. N. Condie. "The modern era of orthotics". *Prosthetics and Orthotics International*, 32, 3 (2008), 313-323.

74 W. Clover Jr. "Lower extremity thermoplastics: an overview". *Journal of Prosthetics and Orthotics*, 3, 1 (1990), 9-13.

75 W. D. Callister. *"Materials science and engineering"*. Joh Wiley and Sons, New York, USA, 2007.

76 J. G. Williams. *"Stress analysis of polymers"*. Ellis Horwood Limited, Chichester, UK, 1980.

77 J. E. Edelstein, J. Bruckner. *"Orthotics A Comprehensive Clinical Approach"*. Slack, Thorofare, USA, 2002.

78 G.S. Kulkarni. *"Textbook of Orthopedics and Trauma"*. Jaypee Brothers Medical Publishers Ltd, New Delhi, India, 2008.

79 http://www.langergrp.com (Accessed: 03.07.2011).

80 http://www.mobilelimbandbrace.com. Accessed: 07/08/2011.

81 http://www.surefitlab.com/products//orthopedic-appliances/afos-custom/ (Accessed: 03.07.2011).

82 http://www.beckerorthopedic.com/cenfab/cfp.htm (Accessed: 03.07.2011).

83 G. Rubin, M. Dixon. "The modern ankle-foot orthoses (AFOs)". *Bulletin*

of Prosthetics Research (1973), 20-41.

84 http://www.cc-mfg.com/mpSPIRAL.html (Accessed: 03.07.2011).

85 P. Bowker, D. N. Condie, D. L. Bader, D. J. Pratt. *"Biomechanical basis of orthotic management"*. Butterworth-Heinemann, Oxford, UK, 1993.

86 T. T. Chu. Biomechanics of Ankle-Foot Orthoses: Past, Present and Future. *Topics in Stroke Rehabilitation*, 7, 4 (2001), 19-28.

87 G. Pelosi. The Finite Element Method, Part 1: R. L. Courant. *IEEE Antennas and Propagation Magazine*, 49, 2 (2007), 180-182.

88 S. S. Bhavikati. *"Finite Element Analysis"*. New Age International, Dehli, India, 2005.

89 http://www.ansys.com/Products/Simulation+Technology/Structural+Mechanics (Accessed: 26.06.2011).

90 http://www.ansys.com/Support/Documentation (Accessed: 26.06.2011).

91 G. C. Robin, A. Magora, E. Adler, J. Saltiel. "Dynamic stress analysis of below-knee drop foot braces". *Medical and Biological Engineering Computing*, 6 (1968), 533-546.

92 G. C. Robin, A. Magora. "Dynamic stress analysis of below-knee drop foot braces; studies on patients with paralysis of the lower limb". *Medical and Biological Engineering Computing*, 7 (1969), 221-226.

93 G. C. Robin, A. Magora, J. Saltiel, E. Adler. "Dynamic analysis of plastic below-knee drop foot braces". *Medical and Biological Engineering Computing*, 9 (1971), 631-636.

94 http://www.ispo.ca/lexicon/ (Accessed: 16.04.2011).

95 R. Feng. Determination and studying of stress distribution in various ankle-foot orthoses: experimental stress analysis. *New Jersey Institute of*

Technology MSc Thesis (1997).

96 S. Yamamoto, M. Ebina, S. Kubo, H. Kawai, T. Hayashi, M. Iwaski, T. Kubota, S. Miyazaki. Quantification of the Effect of Dorsi-/ Plantarflexibility of Ankle-Foot Orthoses on Hemiplegic Gait: A Preliminary Report. *Journal of Prosthetics and Orthotics*, 5, 3 (1993), 88-94.

97 D. J. J. Bergman, A. Rozumalski, D. Koops, V. de Groot, M. Schwartz, J. Harlaar. "A new method for evaluating ankle foot orthosis characteristics: BRUCE". *Gait & Posture*, 30 (2009), 144-149.

98 M. Viceconti, S. Olsen, K. Burton. Extracting clinically relevant data from finite element simulators. *Clincial Biomechanics*, 20 (2005), 451-454.

99 J. F. Lehmann, P. C. Esselman, M. J. Ko, J. C. Smith, B. J. Delateur, A. J. Dralle. "Plastic ankle-foot orthoses: evaluation of function". *Archives of Physical Medicine and Rehabilitation*, 64, 9 (1983), 402-407.

100 T. Sumiya, Y. Suzuki, T. Kasahara. "Stiffness control on posterior-type plastic ankle-foot orthoses: effect of ankle trimline Part 1: a device for measuring ankle moment". *Prosthetics and Orthotics International*, 20, 2 (1996), 129-131.

101 T. Sumiya, Y. Suzuki, T. Kasahara. "Stiffness control on posterior-type plastic ankle-foot orthoses: effect of ankle trimline Part 2: orthosis characteristics and orthosis/patient matching". *Prosthetics and Orthotics International*, 20, 2 (1996), 132-137.

102 http://www.small-laptop-s.com/laptop-ratings.htm (Accessed: 06/08/2011).

103 B. McHugh. Analysis of body-device interface forces in the sagittal plane for patients wearing ankle-foot orthoses. *Prosthetics and Orthotics International*, 23 (1999), 75-81.

104 Geomagic Studio 12 tutorial "Point Cloud to Exact Surface output" accessed from http://support1.geomagic.com/ics/support/default.asp?deptID=5668

(accessed 13.08.2011).

105 http://www.kxcad.net/ansys/ANSYS/ansyshelp/Hlp_E_SHELL281.html (Accessed: 06.07.2011).

106 http://www.northseaplastics.com/support.asp (Accessed: 29/07/2011).

107 S. Solomonidis, E. Papi. *Experiments (kinematic gait, kinetic gait, strain gauging an AFO and strain gauging a polypropylene sample experiments) at the Bioengineering Unit, University of Strathclyde* (unpublished 2011).

108 http://www.mece.ualberta.ca/tutorials/ansys/AU/Converge/Converge.html (Accessed: 07/08/2011).

109 K. L. Lawrence. *Anys workbench tutorial - structural and thermal analysis using the ansys workbench release 12.1 environment*. SDC Publications, Mission, USA, 2010.

110 E. Papi. "Investigate the use of strain gauge technology for the determination of the mechanical characteristics of polypropylene ankle-foot orthoses". *University of Strathclyde MSc Thesis* (2008).

111 R. J. Crawford. *Plastic Engineering*. Elsevier Butterworth-Heinemann, Oxford, UK, 2004 (3rd edition).

112 Communication with S. Solomonidis (09.08.2011).

Appendices

Appendix A: Thickness measurements

Table 5: All the thickness measurements, the averages and standard deviations

Thickness Point (see Figure A-1 for location)	Measurement 1 (mm)	Measurement 2 (mm)	Measurement 3 (mm)	Average thickness (mm)
1	4.15	4.00	4.07	4.07 ± 0.08
2	3.99	3.93	3.90	3.94 ± 0.05
3	3.99	4.01	3.98	3.99 ± 0.02
4	4.09	4.12	4.14	4.12 ± 0.03
5	4.01	3.88	4.08	3.99 ± 0.10
6	4.16	4.09	4.16	4.14 ± 0.04
7	3.01	3.55	3.60	3.39 ± 0.33
8	2.36	2.23	2.30	2.30 ± 0.07
9	4.54	4.52	4.54	4.53 ± 0.01
10	4.14	4.17	4.20	4.17 ± 0.03
11	4.30	4.31	4.27	4.29 ± 0.02
12	4.14	4.17	4.20	3.96 ± 0.00
13	3.96	3.96	3.96	4.17 ± 0.03
14	4.44	4.44	4.47	4.45 ± 0.02
15	4.13	4.18	4.16	4.16 ± 0.03
16	3.56	3.56	3.69	3.60 ± 0.08
17	4.06	4.06	4.06	4.06 ± 0.00
18	4.13	4.16	3.76	4.02 ± 0.22
19	2.56	2.78	2.56	2.63 ± 0.13
20	4.06	4.06	3.96	4.03 ± 0.06
21	4.16	4.56	4.16	4.29 ± 0.23
22	4.09	4.09	4.10	4.09 ± 0.01
23	3.86	4.16	4.36	4.13 ± 0.25
24	4.70	4.56	4.36	4.54 ± 0.17
25	4.70	4.90	4.56	4.72 ± 0.17
26	2.56	2.78	2.56	2.63 ± 0.13
27	4.14	4.15	4.16	4.15 ± 0.01
28	4.19	4.18	4.19	4.19 ± 0.01
29	4.45	4.45	4.46	4.45 ± 0.01
30	4.57	4.65	4.63	4.62 ± 0.04
31	4.44	4.44	4.47	4.45 ± 0.02
32	3.99	3.99	3.90	3.90 ±0.05

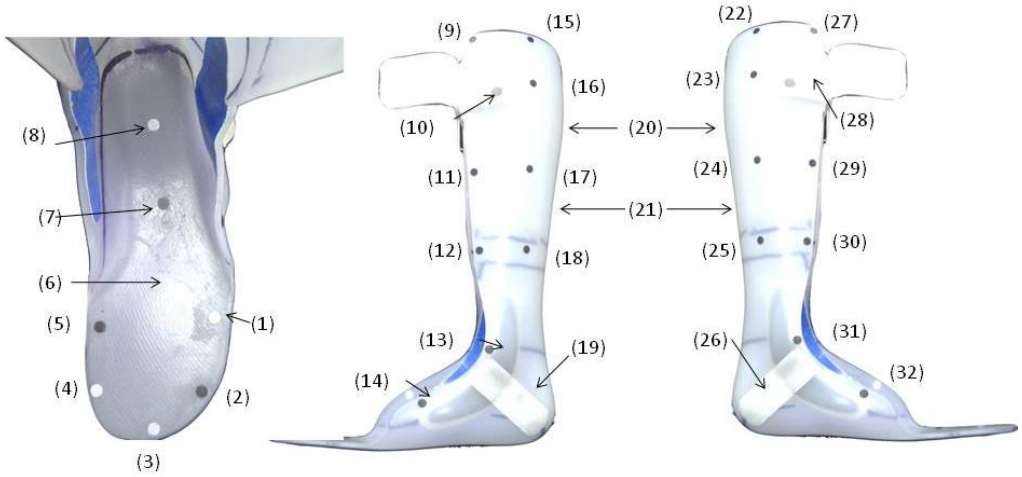

Figure A-1: Positions of the thickness measurement points

Table 6: Average thicknesses for different sections of the AFO

AFO geometry groups	Average thickness (mm)
1. Plantar edge	4.02 ± 0.07
2. Plantar centre	4.14 ± 0.00
3. Midfoot	3.39 ± 0.00
4. Heel	2.30 ±0.00
5. Lateral calf edge	4.29 ± 0.17
6. Lateral ankle trim	4.21 ± 0.35
7. Lateral calf centre	3.96 ± 0.24
8. Lateral malleous	2.63 ± 0.00
9. Central calf centre	4.16 ± 0.19
10. Medial calf centre	4.37 ± 0.31
11. Medial malleous	2.63 ± 0.00
12. Medial calf edge	4.35 ± 0.22
13. Medial ankle trim	4.21 ± 0.35

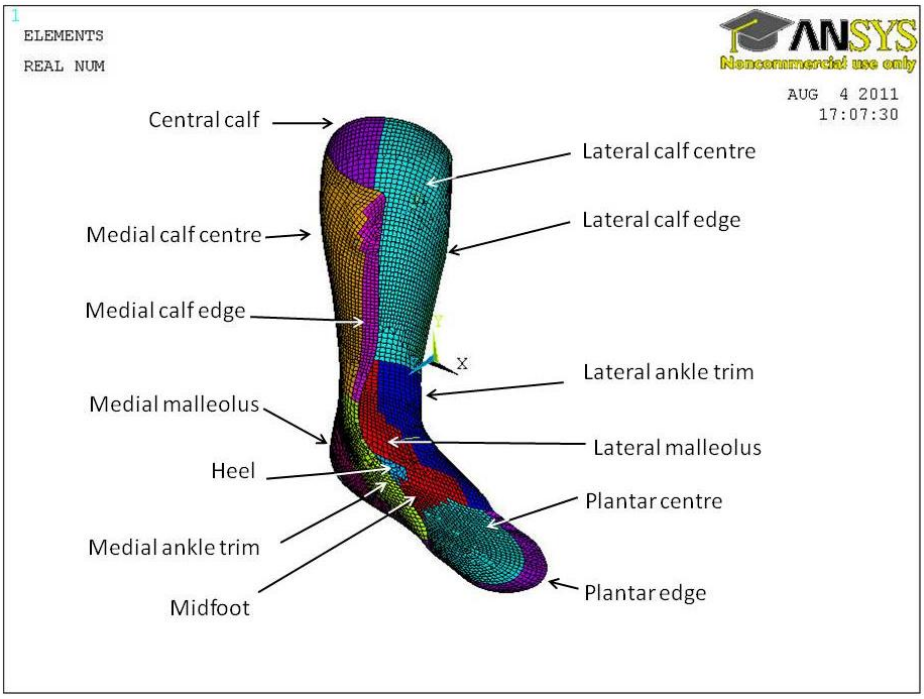

Figure A-2: The locations of the AFO geometry groups used to apply various thicknesses to the model

The value that was inserted into the uniform thickness analyses was 3.76mm, this was calculated by taking the average from the values in the second column of table 4.

Appendix B: Strap force calculations

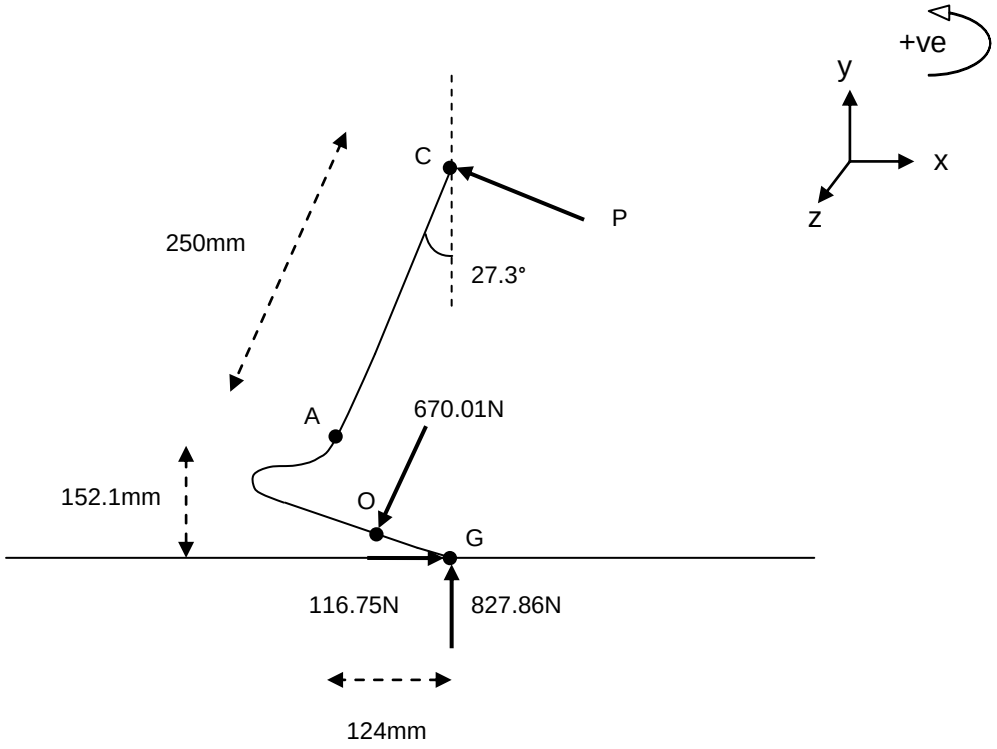

Figure B-1: Force diagram for AFO at toe off, C = top of AFO, A = ankle centre, O = COP for pressure acting on AFO, G = COP of ground reaction force.

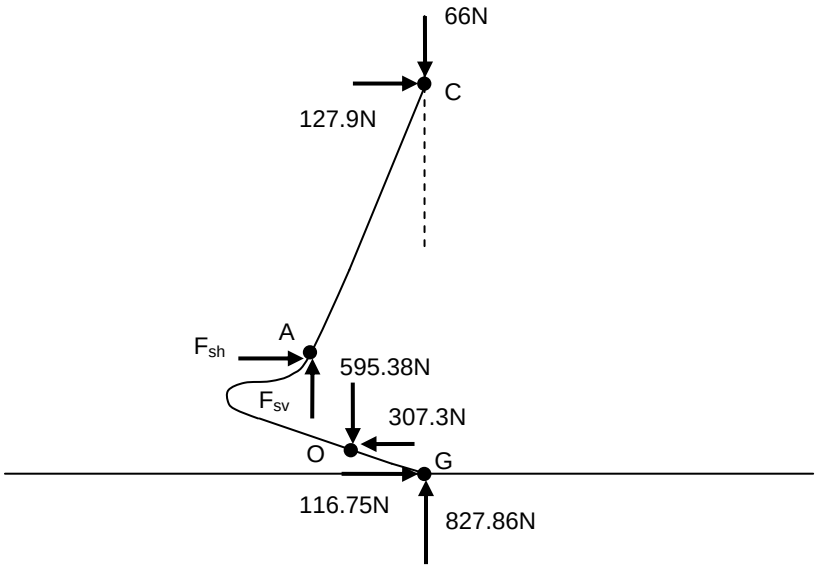

Figure B-2: Force diagram for AFO at toe off, C = top of AFO, A = ankle centre, O = COP for pressure acting on AFO, G = COP of ground reaction force.

$\Sigma M_A = 0 = (P \times 0.250) + (827.86 \times 0.124) + (116.75 \times 0.152) -$

(670.01×0.126)

$\therefore P = -143.9N$

$P\ acts\ at\ an\ angle\ of\ 27.3°\ to\ the\ positive\ horizontal\ (x) direction$

$\Sigma F_V = -66 + F_{SV} + 827.86 - 595.38$

$\therefore F_{SV} = -166.48N$

$\Sigma F_H = 127.9 + F_{SH} + 116.75 - 307.3$

$\therefore F_{SH} = 62.65N$

$\theta = tan^{-1}\left(\frac{62.64}{166.48}\right) = 20.6°$

$F_S\ acts\ at\ an\ angle\ of\ 69.4°\ to\ the\ positive\ horizontal\ (x) direction$

Appendix C: Moment created by the ground reaction force at the ankle

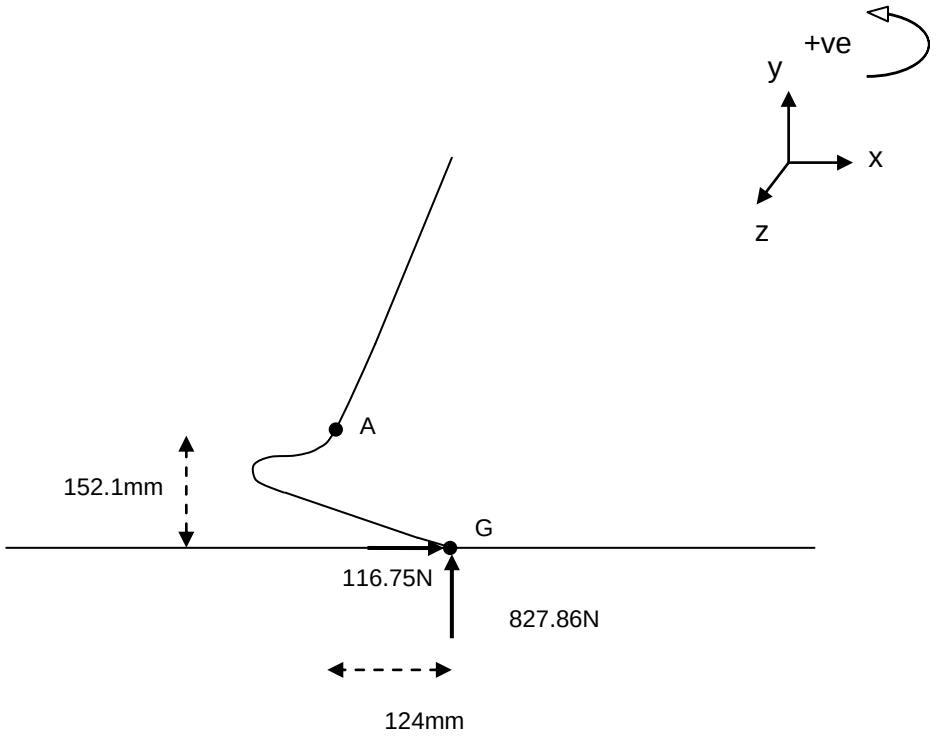

Figure C-1: Diagram of the calculation of the moments about the ankle

$$M_A = (827.86 \times 0.124) + (116.75 \times 0.152) = -120.4Nm$$

Moment at ankle acting by AFO and leg on ground